Metrology for Ambient

Mass Spectrometry

Tara La Roche Salter

National Physical Laboratory and

University of Nottingham

Thesis submitted to the University of Nottingham for

the degree of Doctor of Philosophy

July 2015

Abstract

Ambient mass spectrometry (AMS) is a new and versatile method for analysing a multitude of different sample types with the benefit of analysis at ambient pressure and the many other advantages that this entails. However, as these techniques are still in their infancy, metrological development of the techniques is essential. This is a critical step before AMS can be used reliably in the application areas in which it has shown great promise. The research in this thesis addresses the development of AMS sources, in particular plasma-assisted desorption-ionisation, PADI. Optimisation and characterisation is fundamental to understanding and developing the technique.

Optimisation of PADI is addressed; this includes understanding the effects of different parameters to maximise signal intensities. The power, and temperature, of the plasma is shown to have a significant effect on the fragmentation observed in the mass spectra. This is an important result that is further explored with the use of thermal desorption to aid the analysis of low volatility molecules. The form of the analyte is also an important consideration for analysis by PADI; characteristic ions from powders are easily detected, whereas for thin film samples an analyte vapour pressure of greater than 10^{-4} Pa is needed. This result provides an indication of the limitations of PADI and what classes of analyte it will be successful at analysing. It is also shown that we can improve signal intensities using a heated sample stage allowing the analytes to be thermally desorbed before being ionised by the plasma. This is

an important result for future work, where ambient plasma sources can be implemented as an ionisation source in conjunction with another mechanism, such as thermal or laser desorption, to generate gas-phase ions.

A comparison of different ambient methods for personal care products shows the usefulness and also complementarities of PADI with desorption electrospray ionisation, DESI, one of the most established AMS techniques which utilises a different mechanism for desorption and ionisation. This also demonstrates the chemical information that can quickly be gained from these techniques, with minimal sample preparation. DESI is also compared to secondary ion mass spectrometry, SIMS. Vacuum-based techniques such as SIMS are much more established than ambient techniques; it is insightful to understand the advantages that each source can offer, for the analysis of different types of molecule as well as the mass spectral information that can be gained from SIMS and DESI.

List of publications

Salter, T.L., Green, F.M., Gilmore, I.S., Seah, M.P., and Stokes, P. A comparison of SIMS and DESI and their complementarities. *Surf. Interface Anal.,* 2011. **43**(1-2): p. 294-297.

Green, F.M., Seah, M.P., Gilmore, I.S., Salter, T.L., and Spencer, S.J., Analysis of thin films and molecular orientation using cluster SIMS. *Surf. Interface Anal.,* 2011. **43**(9): p. 1224-1230.

Salter, T.L., Green, F.M., Faruqui, N., and Gilmore, I.S., Analysis of personal care products on model skin surfaces using DESI and PADI ambient mass spectrometry. *Analyst,* 2011. **136**(16): p. 3274-3280.

Bowfield, A., Barrett, D.A., Alexander, M.R., Ortori, C.A., Rutten, F.M., Salter, T.L., Gilmore, I.S., and Bradley, J.W., Surface analysis using a new plasma assisted desorption/ionisation source for mass spectrometry in ambient air. *Rev. Sci. Instrum.,* 2012. **83**(6): p. 063503.

Salter, T.L., Gilmore, I.S., Bowfield, A., Olabanji, O.T., and Bradley, J.W., Ambient Surface Mass Spectrometry Using Plasma-Assisted Desorption Ionization: Effects and Optimization of Analytical Parameters for Signal Intensities of Molecules and Polymers. *Analytical Chemistry*, 2013. **85**(3): p. 1675-1682.

Bowfield, A., Bunch, J., Salter, T.L., Steven, R.T., Gilmore, I.S., Barrett, D.A., Alexander, M.R., McKay, K., and Bradley, J.W., Characterisation of a micro-plasma for ambient mass spectrometry imaging. *Analyst*, 2014. **139**(21): p. 5430-5438.

Salter, T.L.R., Bunch, J., and Gilmore, I.S., Importance of Sample Form and Surface Temperature for Analysis by Ambient Plasma Mass Spectrometry (PADI). *Analytical Chemistry,* 2014. **86**(18): p. 9264-9270.

McKay, K., Salter, T.L., Bowfield, A., Walsh, J.L., Gilmore, I.S., and Bradley, J.W., Comparison of Three Plasma Sources for Ambient Desorption/Ionization Mass Spectrometry. *J. Am. Soc. Mass Spectrom.*, 2014. **25**(9): p. 1528-1537.

Gurdak, E., Green, F.M., Rakowska, P.D., Seah, M.P., Salter, T.L., and Gilmore, I.S., VAMAS Interlaboratory Study for Desorption Electrospray Ionization Mass Spectrometry (DESI MS) Intensity Repeatability and Constancy. *Analytical Chemistry,* 2014. **86**(19): p. 9603-9611.

Acknowledgments

Table of Contents

List of figures

List of tables

Glossary

AGC	Automatic gain control
AMS	Ambient mass spectrometry
APCI	Atmospheric pressure chemical ionisation
APGD	Atmospheric pressure glow discharge
ASAP	Atmospheric solids analysis probe
DAPCI	Desorption atmospheric pressure chemical ionisation
DART	Direct analysis in real time
DBD	Dielectric barrier discharge
DBDI	Dielectric barrier discharge ionisation
DCBI	Desorption corona beam ionisation
DESI	Desorption electrospray ionisation
ELDI	Electrospray-assisted laser desorption/ionisation
ESI	Electrospray ionisation
FA-APGD	Flowing afterglow atmospheric pressure glow discharge
FAPA	Flowing atmospheric-pressure afterglow
FTICR	Fourier transform ion cyclotron resonance
GC-MS	Gas chromatography mass spectrometry
HDFa	Human dermal fibroblasts
ICP-MS	Inductively coupled plasma mass spectrometry
LAESI	Laser ablation electrospray ionisation
LC-MS	Liquid chromatography mass spectrometry
LOD	Limit of detection
LPTD	Leidenfrost phenomenon-assisted thermal desorption
LTP	Low temperature plasma
MALDI	Matrix-assisted desorption ionisation

MHCD	Microhollow cathode discharge
MIPDI	Microwave-induced plasma desorption ionisation
MS	Mass spectrometry
MS/MS	Tandem mass spectrometry
PADI	Plasma-assisted desorption ionisation
PALDI	Plasma-assisted laser desorption ionisation
PAMLDI	Plasma-assisted multiwavelength laser desorption ionisation
PCP	Personal care products
PET	Poly (ethylene terephthalate)
PLA	Poly (lactic acid)
PMMA	Poly (methyl methacrylate)
PPAMS	Plasma pencil atmospheric mass spectrometry
PTFE	Polytetrafluoroethylene
PVC	Polyvinyl chloride
QTOF	Quadrupole/time-of-flight
SIMS	Secondary ion mass spectrometry
SRM	Selected reaction monitoring
TLC	Thin layer chromatography
TOF	Time-of-flight

Chapter 1

Plasma sources for ambient surface mass spectrometry

1.1 Ambient mass spectrometry

Ambient mass spectrometry (AMS) techniques are an exciting area in analytical science, offering quick sample analysis at atmospheric pressure. A subset of this diverse field, ambient plasma techniques, have taken off in the last 7 years with several different variants emerging. Here, we examine the range of these techniques, the research that is being undertaken to fundamentally characterise and optimise them, as well as the wide range of fields that they have so far been applied to.

Traditional surface mass spectrometry is dominated by matrix-assisted laser desorption ionisation (MALDI) [1-4] and secondary ion mass spectrometry (SIMS) [5, 6]. These techniques have been around for over 20 years but one of their main limitations is that they are confined to vacuum. In 2004 the first ambient mass spectrometry technique was developed, desorption electrospray ionisation (DESI) [7]. This has become one of the most popular ambient ionisation techniques with over 400 publications in 8 years and a commercial source manufactured by Prosolia, Inc.. Since 2004 there has been an explosion

in this new field with the development of many different sources [8]. The second ambient technique developed in 2005, and the first that utilised a plasma, was termed direct analysis in real time (DART) [9].

Although there are many, over 30, variants in the field, there have been attempts [10] to categorise these techniques into three main sections based on their desorption and ionisation processes: spray-based, laser-based and plasma-based. There are other techniques that are not covered by these three categories such as acoustic desorption methods.
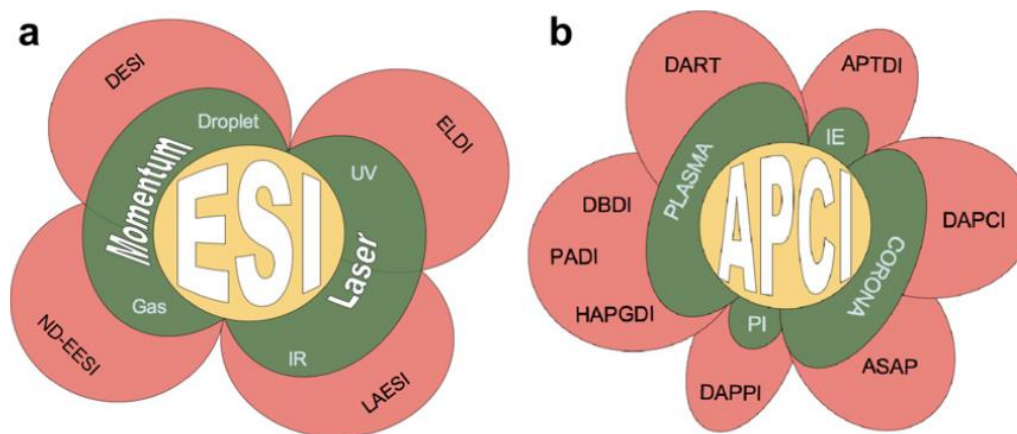
Figure 1.1. Flowergrams summarizing ambient desorption ionization methods. (a) The techniques (Red) where ESI mechanisms (Yellow) are predominantly responsible for ionization. Both laser and momentum desorption (Green) have been demonstrated. (b) The methods where chemical ionization (Yellow) is responsible for ionization. The chemical reagents are produced by various methods (Green), such as photoionization (PI), ion evaporation (IE) and electrical discharge. Figure and caption reproduced from [11].

Ambient mass spectrometry techniques have many advantages especially for surface analysis. The ability to analyse at atmospheric pressure enables samples to be analysed with minimal or no preparation and the possibility

exists for *in vivo* analysis. Quick sample introduction and analysis times lead to the capability for high-throughput analysis. Many different substrates and types of molecules can be analysed although the majority of AMS has been limited to small molecule applications. Due to the versatility of the techniques they can be coupled to current state-of-the-art mass spectrometers such as the Orbitrap™ [12] as well as novel hand-held mass spectrometers [13].

As the majority of this thesis is concerned with the development of the metrology for plasma-assisted desorption ionisation (PADI), this review revolves around this source and other plasma sources used for ambient mass spectrometry.

1.2   Plasma-based ambient mass spectrometry techniques

1.2.1 Introduction

Within the large domain of ambient mass spectrometry [10], plasma-based desorption and ionisation techniques [14, 15] have developed as one of the leading variants, with several different types of operation and source design. Plasmas are attractive as an ambient mass spectrometry source due to the absence of solvents and high voltages; although there are significant voltages and gas supplies that need to be used. A more detailed description of the generation and physics behind plasmas is given in Chapter 2.3.

1.2.2 Types of plasma sources

The development of plasma sources for ambient mass spectrometry started with direct analysis in real time, DART, in 2005 [9]. This was followed in 2006 by the development of a glow discharge confined within a cell at atmospheric pressure [16]. The afterglow of this discharge was subsequently used as an ionisation source for mass spectrometry [17], that was originally termed flowing afterglow atmospheric pressure glow discharge, FA-APGD, later shortened to flowing atmospheric-pressure afterglow, FAPA. The first paper utilising a dielectric barrier discharge, DBD, for ambient mass spectrometry was by Na [18] in 2007. In the same year, the first PADI paper was published [19], followed in 2008 by the low temperature plasma probe, LTP [20].

As with all ambient mass spectrometry techniques there are a multitude of different acronyms for the plasma sources and this list is constantly growing. However, these can be roughly divided due to their type of discharge, method of generation and part of the plasma effluent they utilise. Table 1.1 summarises the main plasma sources, and below a brief description is given for each source.

Table 1.1. Summary of atmospheric pressure plasmas used as mass spectrometry sources.

Technique	Type of discharge	Power supply	Year of first publication and reference
DART	Corona to glow discharge	DC	2005 [9]
DBDI	Dielectric barrier discharge	AC	2007 [18]
FAPA	Glow to arc discharge	DC	2006 [17]
LTP	Dielectric barrier discharge	AC	2008 [20]
PADI	RF corona to glow discharge	RF/AC	2007 [19]
MHCD	Glow discharge	DC	2010 [21]

Direct analysis in real time, DART

In DART, a DC high voltage power supply, with voltages in the kV range [9] produces a corona-to-glow transitional discharge [22] between a needle and perforated disk electrode. Figure 1.2 shows a cutaway view of the DART source [9]. The plasma species are partially filtered by grid electrodes at the exit of the source so that the cations, anions and electrons are removed leaving only the metastables to interact with the sample. Typically helium is used as the discharge gas, at a rate of around 3.5 litres per minute. The gas stream is often heated, up to maximum of 550 °C, to assist in desorbing analytes as the temperature of the gas prior to this heating is between 50 and 60 °C [22].
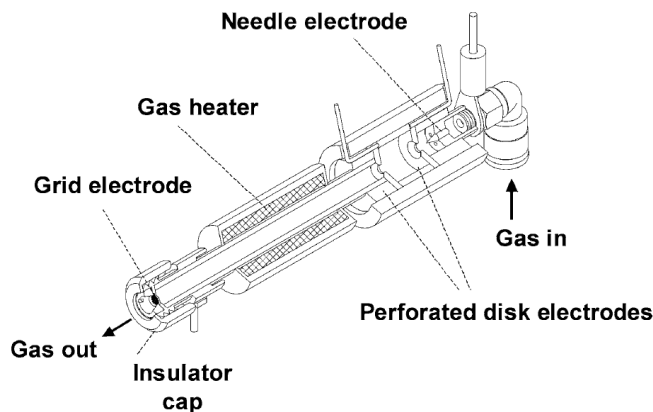
Figure 1.2. Cutaway view of the direct analysis in real time, DART, source. Figure and caption reproduced from [9].

Flowing atmospheric-pressure afterglow, FAPA

In FAPA, the glow-to-arc discharge (GD) is generated between a pin cathode and plate anode using a DC high voltage power supply, with hundreds of volts used. The ions, electrons and excited species generated by the GD exit the chamber through a small hole. The gas from the FAPA plasma is hotter, around 235 °C [22], than that of other plasmas used for ambient mass spectrometry so no additional heating of the gas is used. Other configurations of this plasma source have been developed, such as a more sensitive pin-to-capillary configuration [23], shown in Figure 1.3 (b), and the halo-FAPA [24], a source consisting of two concentric electrodes forming a ring-shaped plasma through which the sample can be passed.
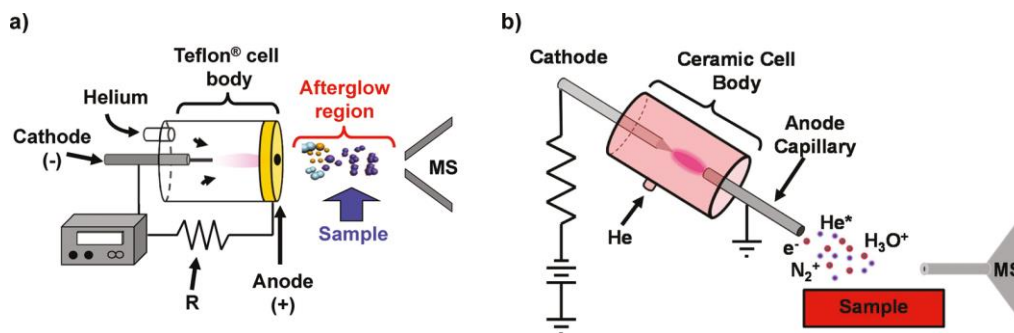
Figure 1.3. Diagram of (a) pin-to-plate FAPA configuration and (b) modified pin-to-capillary FAPA. Figure and caption reproduced from [23].

Plasma-assisted desorption/ionisation, PADI

This technique uses a voltage at radio frequency (13.56 MHz) to generate a plasma, again with helium as the discharge gas [19]. This produces a pink-purple glow that can be seen in Figure 1.4 which directly interacts with the sample. The design is based upon a plasma needle designed by Stoffels *et al.* [25] and discussed in more detail in the next chapter. PADI is the subject of the majority of the research in this thesis and is discussed in further detail in the results chapters.
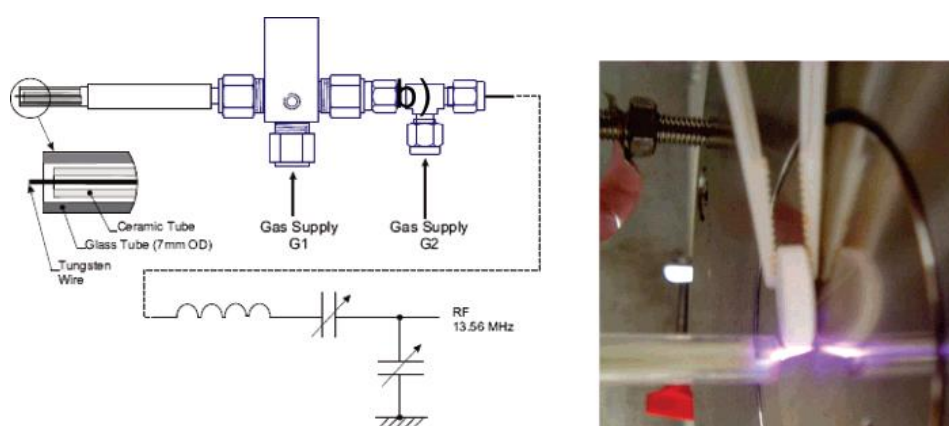
Figure 1.4. Schematic of the PADI source and a photograph of the source in operation analysing a tablet sample. Figure and caption reproduced from [19].

Dielectric barrier discharge, DBD, and low temperature plasma, LTP

There are several different ambient plasma sources that utilise a DBD. The first of these to be developed, termed dielectric barrier discharge ionisation DBDI [18], used a high voltage (3.5 – 4.5 kV) AC circuit, with frequency 20.3 kHz. The discharge electrode was a hollow stainless steel needle and the counter electrode a copper sheet placed under the glass slide sample, which also acted as the discharge barrier. Again, helium was used as the discharge gas.

Another variant that uses a DBD is the low temperature plasma, LTP, probe. This also operates using an AC kilohertz voltage with a power consumption of typically less than 2 W [20]. Generally helium is the preferred discharge gas although argon, nitrogen and ambient air have also been successfully used [20]. As with PADI, the afterglow of the LTP directly interacts with the sample, Figure 1.5 (b).
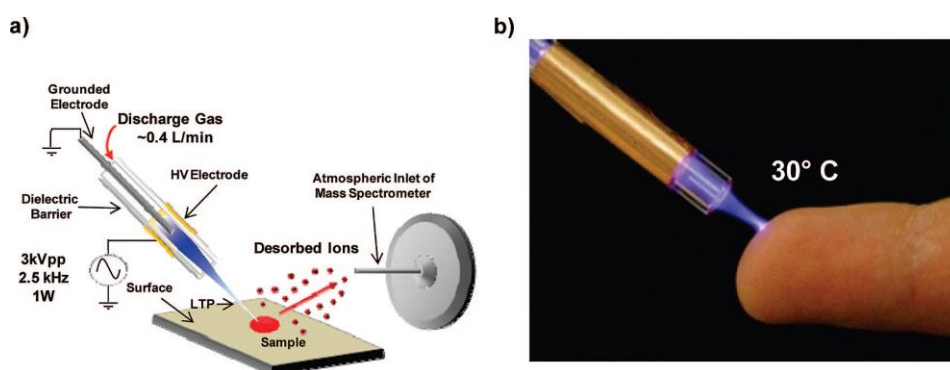
Figure 1.5. (a) Low temperature plasma probe schematic and (b) photograph of the plasma being used to sample compounds on a human finger. Figure and caption reproduced from [20].

Alternative versions of the LTP have been constructed, such as a probe with a pencil graphite as the central electrode [26], and a capillary source where the sample flows through the plasma [27].

Microhollow cathode discharge, MHCD

Microhollow cathode discharges (MHCD) are currently the smallest plasmas that have been developed for ambient mass spectrometry [21]. Here, a plasma discharge hole of 200 µm wide was used but this dimension could be made smaller. The drawback for this system is that the plasma sputters the electrodes leading to device failure, and in this study the device failed after 10 hours of use.

1.2.3 Ionisation and desorption mechanisms

As discussed in the previous section, there are many different ways of generating an atmospheric pressure plasma for use as an ionisation and/or desorption source for mass spectrometry. How the plasma species then desorb and ionise the sample is the topic of this section.

The desorption mechanisms for plasmas are thought to come from thermal, momentum or sputtering processes [9], with thermal desorption being the main process to liberate analytes from the surface into the gas phase [28]. Subsequent ionisation is thought to occur directly or indirectly from species created in the discharge.

Although the majority of research into ionisation mechanisms has been carried out with DART [9, 29, 30], it is not unrealistic to extend these findings to other plasma sources. Different mechanisms are proposed for the formation of positively and negatively charged ions. For positive ion formation with helium used as the discharge gas, helium metastables leaving the plasma source interact with gaseous atmospheric constituents and gas-phase analytes causing Penning ionisation [31] that ultimately, if not initially, lead to transfer of charge to the analyte. In Penning ionisation, a gas-phase excited-state atom or molecule, in this case helium He^*, interacts with a molecule M with lower ionisation energy than He^*, resulting in the formation of a radical molecular cation $M^{+\bullet}$, an electron e^-, as well as a neutral gas molecule, here He [9, 30].

$$He^* + M \ \rightarrow \ M^{+\cdot} + \ He + e^- \qquad (1.1)$$

Helium is most commonly used as the discharge gas in ambient plasmas due to the properties of the metastables; their energy is high enough to ionise virtually any molecule, and the non-radiative lifetime is of the order of several seconds [17, 32]. The (2^3S) excited electronic state of helium has an energy of 19.8 eV, which is larger than the ionisation energy of most atmospheric gases, see Figure 1.6, hence this excited state reacts with nitrogen, either from the laboratory air or from impurities in the gas supply:

$$He^* + N_2 \ \rightarrow \ N_2^+ + \ He + e^- \qquad (1.2)$$
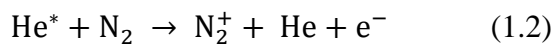
The helium metastables also react with atmospheric water vapour to produce water clusters following the reaction below:

$$He^* \ + \ nH_2O \ \rightarrow He + (H_2O)_{n-1}H^+ + OH^- \qquad (1.3)$$
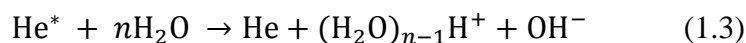
Charged water clusters can also be generated by energy transfer from excited nitrogen species. These water clusters then lead to proton transfer to molecules

if the molecule M has a higher proton affinity than the ionised water clusters [33]:

$$(H_2O)_n H^+ + M \rightarrow [M + H]^+ + n H_2O \qquad (1.4)$$
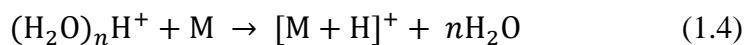
The ionisation energy of water is 12.6 eV which is below that of helium [34], as shown in Figure 1.6.
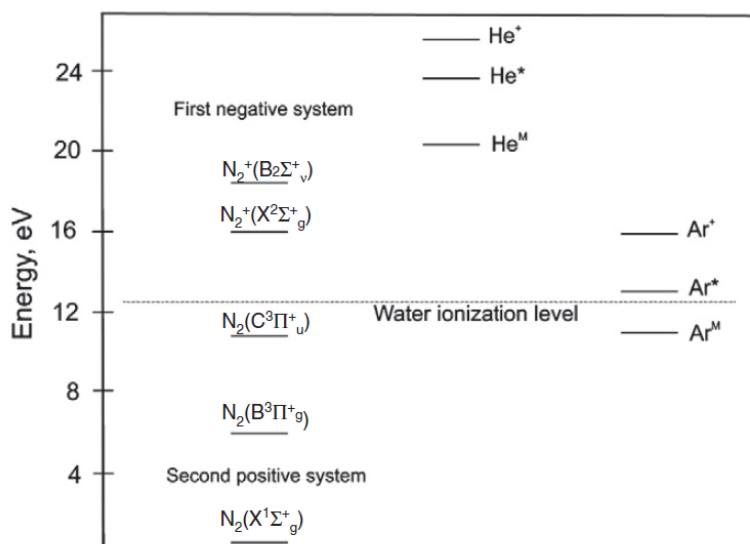
Figure 1.6. Partial term diagram for energy levels of He, Ar and N_2 as well as the water ionisation threshold. The terms refer to the different ionisation states of the nitrogen molecule with $X^1\Sigma^+_g$ being the ground state. He^+, He^* and He^M refer to the ionised, excited and metastable states of the noble gases. Figure and caption reproduced from [35, 36].

The generation of negatively charged ions has been investigated much less than the generation of positive ions. Thermal electrons generated from the collisions between electrons and gas-phase molecules, are thought to undergo electron capture by atmospheric oxygen generating O_2^-, which then ionises analytes [9, 37, 38]:

$$O_2 + e^- \rightarrow O_2^- \qquad (1.5)$$

$$O_2^- + M \rightarrow [M + O_2]^- \rightarrow M^- + O_2 \qquad (1.6)$$
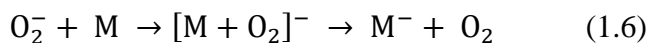
It is possible that other mechanisms of ion formation also occur: electron capture dissociation, deprotonation and anion attachment [37].

1.2.4 Characterisation studies using optical emission spectroscopy

Numerous studies have been carried out investigating the optical emission spectra from ambient plasma sources. These measure not only the constituents of the discharge but also their spatial location. Results from these studies help to inform the ionisation reaction mechanisms discussed in the previous section, most importantly the transfer of charge from helium to nitrogen and subsequently to water clusters.

Optical emission spectroscopy studies of DBD [35, 36, 39-41], FAPA [16, 42], LTP [28, 43, 44] and RF-generated atmospheric pressure glow discharge (APGD) [35] plasma sources all detect the same characteristic ions from the sources, namely, He, N_2^+ (first negative system), N_2 (second positive system) and OH, the energies of these are shown in Figure 1.6. Atomic species, H and O were also detected in a helium LTP [28, 43]. As well as identifying the plasma constituents, these studies have localised them in and/or outside of the plasma device, *i.e.* in the plasma or in the afterglow. It should be noted that all the studies mentioned here utilised a helium discharge.

Emission spectra from DBD, RF-generated APGD and DART discharges show the same ions detected for all the sources with only the relative intensities

varying; He I emission lines are much greater for the RF and DART sources compared to the DBD [35]. However, N_2^+ emission lines were dominant in all three sources. This implies that the processes of excitation and energy transfer are likely to be similar in all three sources. The emission from nitrogen species comes from the collisional transfer of energy from excited He species to N_2 impurities in the helium gas as well as the atmosphere [17, 45]. It is thought that nitrogen excited state species quickly lose their energy through collisional deactivation with water clusters as dominant background signals come from water clusters that have formed from reactions with N_2^+.

The distribution of species inside and outside an LTP probe showed that the maximum emission for OH, He, O and H occurred inside the probe whereas N_2 and N_2^+ were in the open atmosphere [43]. Further spatially resolved measurements showed that the largest amount of He is at the very edge of the torch [28], then decreased rapidly away before having a local maxima, as shown in Figure 1.7. These local maxima are at the same geometric position, 2 to 5 mm depending on the flow rate, as the maxima of the N_2^+ species showing that their processes of ionisation/excitation are likely to be linked. The maximum for N_2 occurs at a greater distance from the end of the probe compared to N_2^+. It was initially thought that Penning ionisation was the only mechanism for nitrogen excitation [43], but these later studies show that charge transfer between the helium dimer ion He_2^+ and atmospheric nitrogen creating N_2^+ also occurs, and the minimum contribution from this reaction is 30% [28].
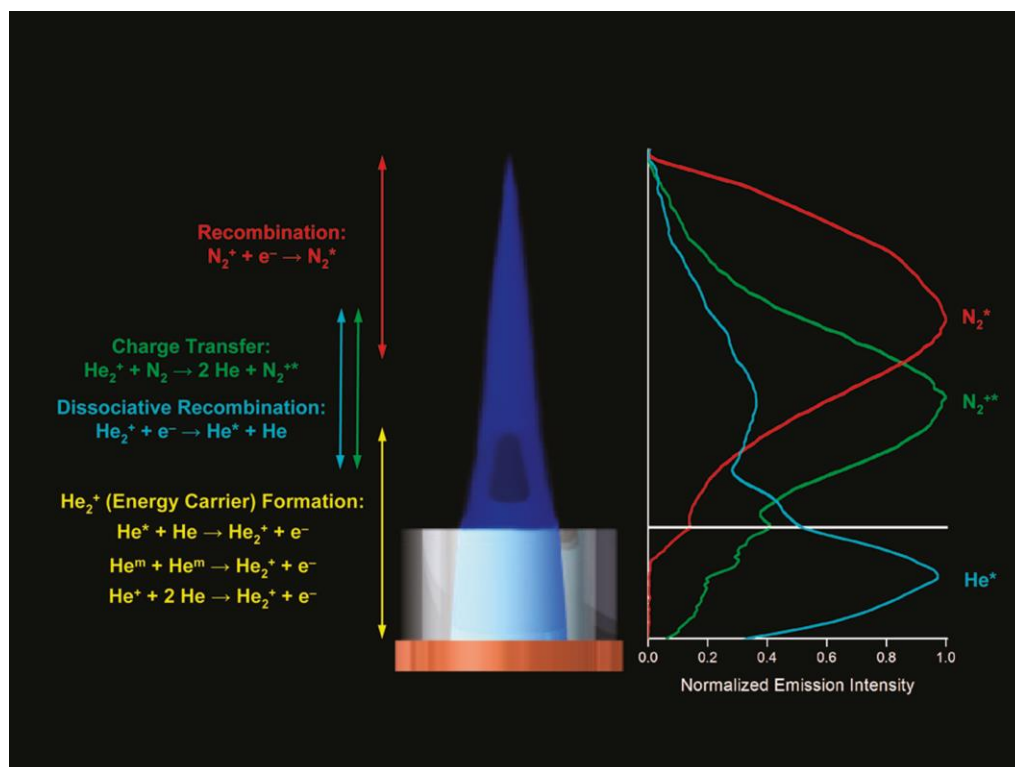
Figure 1.7. Schematic diagram showing the identified spatially dependent reactions for the afterglow and reagent-ion formation in the LTP probe ambient ionization source. Figure and caption reproduced from [28].

These spatially-resolved results are also similar for the DBD [41] and FAPA sources [42], where optical emission spectroscopy measurements showed that in the afterglow region the strongest emitting species are OH and N_2^+, and also that no emission from helium species was observed. Inside the APGD, high-energy atomic helium lines, helium excimer He_2^*, oxygen, nitrogen, NO, OH, N_2 and N_2^+ were observed.

Nitrogen impurities in the helium gas supply used for DBDs are very important. These decrease the breakdown voltage [46]. Computer modelling of a DBD with different levels of nitrogen impurity show that the level of impurity has a great effect on the charge particle densities [47]. Below 1 ppm

nitrogen, He_2^+ ions dominate the positive charge. N_2^+ ions steadily increase in density reaching a maximum at about 8 ppm and determining the positive charge in the discharge until 10 ppm. From 17 to 600 ppm the positive charge is dominated by nitrogen and in particular N_4^+. These results were calculated at low pressures and it in envisaged that at atmospheric pressure the results would change quantitatively but would still follow the same patterns.

Water vapour impurities in the gas supply are also thought to have an effect and are the dominant source of OH emission, although an addition of <100 ppm of water vapour into the gas supply greatly reduced the emission signals from all species [43].

1.2.5 Mass spectra of plasma sources

An insight into the plasma species and ionisation mechanisms can also be gained from studying the background mass spectra from the plasma sources as well as the molecular, fragment and adduct ions. Background spectra in the positive ion mode from an LTP probe, Figure 1.8, includes protonated water clusters $(H_2O)_nH^+$, as well as NO^+, O_2^+, O_3^+ [44]. These are similar to the background spectrum from FAPA, whose dominant peak is the protonated water dimer, $(H_2O)_2H^+$ [17]. Larger water clusters as well as NO^+, O_2^+ and H_2O^+ are also observed. In DART and MHCD, protonated ammonium NH_4^+ is also detected [21, 30].
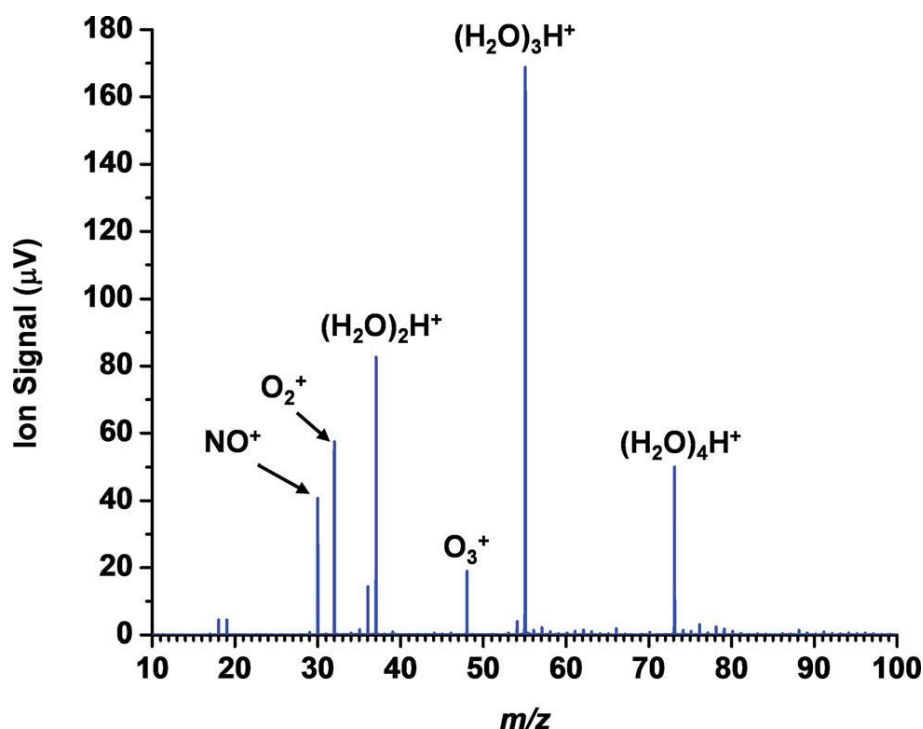
Figure 1.8. Averaged positive ion background mass spectrum of the LTP probe operated with a 6 kVp–p, 10 Hz square wave. Figure and caption reproduced from [44].

The background mass spectrum can change dramatically with operating conditions as is the case with DART; the relative abundance of the $O_2^{+\bullet}$ peak and molecular ions varies when the distance between the ion source and sampling orifice changes, or when excess moisture is eliminated and/or oxygen is bled into the DART sample gap [30]. Introducing other reagents into the ionising region can also change or enhance the mass spectra. An example of this is when analysing cholesterol; using normal conditions a weak hydride abstraction peak $[M-H]^+$ and a large dehydration peak $[M+H-H_2O]^+$ are observed; when fluorobenzene vapour is present or conditions to maximise $O_2^{+\bullet}$ are used then a molecular ion is observed.

The type of ions formed depends on the compound family. In general, protonated molecular ions are observed for polar compounds whereas for non-polar compounds, the non-protonated molecular ion is observed. This is true for FAPA [17] as well as the LTP [48]. Although sometimes both M^+ and $[M+H]^+$ are observed, particularly when the compound is in a high concentration [17]. Hydride abstraction producing $[M-H]^+$ ions is observed for aliphatic compounds; chemical ionisation with NO^+ is known to produce hydride abstraction and oxidation [49]. The addition of water molecules, either one or more, to the protonated molecular ion has also been detected [45].

In the negative ion mode, $O_2^{-\bullet}$ is the most abundant background ion in DART, with $NO_2^{-\bullet}$, $CO_3^{-\bullet}$, $HCO_3^{-\bullet}$ and $HCO_4^{-\bullet}$ also detected to a lesser extent [9, 38]. However, NO_3^- is the most abundant background negative ion detected from FAPA [23] and LTP [50]; very small amounts of NO_3^- are detected in the DART mass spectrum [38]. Explosives are the compounds most commonly analysed in the negative ion mode with ambient plasma sources. This is because they have high electron affinities that indicate that they will readily form negative ions by electron capture [51]. These produce M^-, $[M-H]^-$, $[M-NO]^-$, $[M+NO_2]^-$, $[M+NO_3]^-$, $[M+Cl]^-$ ions for the explosives PETN, RDX and TNT using DBDI [52], DART [37], FAPA [23] and LTP [50, 53]. Although not many other applications use the negative ion mode, the mass spectra are dominated by deprotonated species [54].

Fragmentation of molecules is sometimes also observed, *e.g.* in the analysis of common gaseous solvents with mass >200 Da using FAPA [45]. The ratio of

fragment to molecular ion has also been observed to change over time in the analysis of amino acids using DBDI [18]; the molecular ion decreased and the fragment ion increased with time. The "softness" of the different ambient plasma sources, DART, FAPA and LTP, has been compared based on the relative fragmentation for the analysis of methyl salicylate [55].

1.3   Characterisation of plasma sources

1.3.1 Optimisation

Before ambient plasma sources can be properly utilised as a reliable source for different mass spectrometry applications, optimisation and characterisation of the sources needs to be performed. Optimisation of plasma sources has mainly focused around the power and discharge gas flow rate settings, as well as what gas is used for the discharge gas. Generally, the samples used for optimisation are pure analytes selected for a particular application, *e.g.* forensics or homeland security.

The optimisation of parameters for LTP and DBDI have focused on the analysis of explosives [53], drugs [56] and amino acids [18]. Discharge gas type and flow rate have been investigated leading to an optimised setting of 250 ml/min for helium to achieve the maximum signal intensity for $[RDX+NO_3]^-$ [53]. For the $[M+H]^+$ ion of paracetamol 300 ml/min was optimal [56]. Air, argon and helium have all been investigated for use as the discharge gas in LTP and DBDI, with helium generally being the most

favoured due to its high ionisation energy, and also achieves the best signal-to-noise ratio [18]. However, for the microwave-induced plasma desorption ionisation source, MIPDI, argon is the preferred discharge gas as the ignition of a helium plasma requires a much higher power than helium and is also unstable [57].

Using these studies as an example, the power settings of the LTP must be carefully optimised for each application; when analysing RDX, similar mass spectra were obtained for the power range 2.5 to 30 W [53], whereas for paracetamol and amino acids signal intensities increased as the power was increased [18, 56]. In these studies it was also noted that at higher powers the sample surface was eroded. This has also been observed when analysing with the APGD [58] where thermal degradation and charring to a tablet were observed above 75 W, and also for the MIPDI source [57].

Increasing the discharge voltage, and hence the power, also increases the surface temperature of the LTP [59]. As explained in the previous section, thermal desorption is thought to be one of the principal desorption mechanisms, therefore increasing the temperature is an advantage for analysing less volatile molecules. This topic is explored in much more detail in Chapter 5. Using an array of LTP probes, up to 19 bundled together [60], the temperature of the surface could be increased from 25 to 60 °C without drastically increasing the discharge voltage. This array of probes is also able to increase the plasma footprint hence increasing the sampling area, an advantage for some applications.

1.3.2 Methods to enhance analysis

As with any developing technique, modifications and improvements to the original design are continuously being carried out. Here are detailed some of these improvements in source design that improve sensitivity and repeatability.

One of the methods that has been used to greatly improve the sensitivity is heating of the sample. This has been demonstrated for DBD [35, 61], and for many studies using LTP for the analysis of explosives, drugs and crude oil, [53, 62-65]. This lowers the limit of detection by an order of magnitude. As discussed in section 1.2.3, thermal desorption is a necessary step especially for non-volatile compounds.

However, sometimes it is advantageous to cool the sample to either reduce damage, for delicate samples such as art works [66], or to reduce the evaporation, for the analysis of volatile compounds [67]. In the first example, the temperature was controlled by adjusting the temperature of the discharge gas and cooled to -30 °C by using liquid nitrogen to cool the helium gas. A different method was employed in the second example; a Peltier cooling stage was employed to increase the persistence of the sample on the substrate.

There has been little development of the LTP source itself since its first use for ambient mass spectrometry; exceptions to this include the bundling of several, 7 or 19, LTP probes together [60]. This increased the sampling area without increasing the surface temperature or helium flow rate. Another modification to

the LTP replaced the central electrode with pencil graphite [26]. This source is able to be used in two different grounding configurations; either the ground plate is placed under the discharge or a ground electrode is placed around the discharge tube. Different levels of fragmentation were observed from the two configurations when analysing volatile organic compounds, VOCs; the first mode produced molecular ions while the second produced fragments.

It is clear that further improvements to the sources can be carried out to improve repeatability, spatial resolution, and to enable the analysis of different compounds.

1.3.3 Two-step combined laser and plasma sources

Two-step ambient desorption/ionisation sources combining laser-based desorption/ablation are also growing in popularity alongside single-step sources. The laser is used to ablate or desorb material from the surface which produces a plume that merges with the electrospray or plasma beam, and hence the desorption and ionisation processes are separated. The first of these sources developed used an electrospray source for post-ionisation; electrospray-assisted laser desorption/ionisation (ELDI) [68] which uses a 337 nm pulsed nitrogen laser, and laser ablation electrospray ionisation (LAESI) [69] which uses a mid-IR laser. Plasmas have also been used for the post-ionisation step. One of the main advantages of these techniques is the ability to ablate smaller spots than would be possible with single-step sources, therefore opening up possibilities for mass spectrometry imaging with improved spatial resolution.

Several groups have reported the coupling of DART with laser systems. These have used IR lasers for pharmaceutical tablet analysis [70], visible lasers (532 nm) for the analysis of metallic samples [71], and a multiwavelength laser operating in the IR, visible and UV (1064, 532 and 355 nm) [72, 73]. A simplified version of this latter source using only one wavelength, 532 nm, has also been used for mass spectrometry imaging [74].

Plasma-assisted multiwavelength laser desorption ionisation (PAMLDI), has also been combined with thin layer chromatography (TLC) plate analysis [72] and graphite-coated paper has been used as the substrate [73]. Like traditional DART, it was necessary to heat the metastable stream to obtain good signal intensities and sensitivity; a temperature of greater than 300 °C was needed to detect the compounds studied. The heating increased the internal energy of the metastable helium ions but did not cause thermal desorption of the analyte. Also no analyte ions were observed when the laser was switched off therefore the authors propose that photoionization dominates the desorption process. UV or visible lasers were found to be optimal for the molecules tested: dyes, drug standards and tea leaf extracts.

Other ambient plasmas that have been coupled with laser desorption include a DBD source combined with a near-IR diode laser [75]. This greatly enhanced the detection of low vapour pressure pesticides, pharmaceuticals and explosives, showing that the use of laser desorption not only improves spatial resolution but also sensitivity. Another DBD source coupled with laser desorption uses a different configuration whereby the ablated species flow

through an active capillary that serves as both an ionisation source as well as the inlet to the mass spectrometer [27, 76]. For the detection of volatile solid samples laser ablation was not necessary, however, with laser ablation detection of non-volatile samples was possible [27].

1.4   Application areas

This thesis is mainly concerned with the metrological development of ambient mass spectrometry sources; however, as with any new and emerging technique the requirement to show its usefulness and applicability is paramount. Hence a large amount of the papers published on plasma AMS have concentrated around showing its capability to analyse a wide variety of samples, in comparison to the amount of papers discussing the fundamental mechanisms of these sources. The analysis of pharmaceuticals and drugs of abuse by plasma AMS is one of the largest application areas and has been carried out using different plasma sources. Explosives analysis has also been shown to be another successful application area. However, there have been limited publications on the use of ambient plasma sources to analyse biological samples. As might be expected, due to the DART source being commercially available, it is the most frequently used ambient plasma source; however, only homemade plasma sources are discussed in this section. A brief summary on different application areas is given below and summarised in Table 1.2.

Table 1.2. A summary of application areas successfully demonstrated by ambient plasma mass spectrometry and some example publications.

Application area	Molecule/Matrix	Technique	References
Volatiles	Fragrances	LTP	[67]
	VOCs	LTP	[77]
Pharmaceuticals and drugs of abuse	Drugs of abuse	APGD	[58]
	Ibuprofen, loratidine, acetaminophen, and cocaine from banknotes	Microplasma	[21]
	Including hormone and cardiovascular drugs, and drugs of abuse	LTP	[56, 62]
	Paracetamol, ibuprofen, aspirin	PADI, micro-PADI	[19, 78]
Explosives	RDX, PETN, TNT	LTP	[50, 53]
		DBD	[52]
Polymers	PEG, PET, Nylon, plasticisers	FA-APGD	[79]
	PTFE	Micro-PADI	[78]
Agrochemicals	On fruit peel and extracts	LTP	[80, 81]
	In fruit juice and fruit peel	APGD	[82]
	Agrochemical standards	DCBI	[83]
Foodstuff	Coffee beans	LTP	[59]
	Melamine in milk	LTP	[65, 84]
	Garlic, onion	PADI	[19]
	Fatty acids in olive oil	LTP	[54]
Bioanalysis	Micronutrients	PPAMS	[85]
	Amino acids	DBDI	[18]
	Bacteria- fatty acid ethyl esters	LTP	[86]
	Fatty acid ethyl esters	LTP	[87]
Others	Chemical reaction monitoring	LTP	[88-91]
	Crude oil	LTP	[63]
	Lithium ion battery electrolytes	LTP	[92]
	Inks in artworks	LTP	[66]

There are some limitations to what can be successfully analysed by plasma sources, the most significant being the limited mass range with no analytes generally detected above 1000 Da, and also slightly coupled to this, the inability to analyse (large) biomolecules. An example of this is in the analysis of bacteria using LTP [86]; fatty acid ethyl esters were detected between *m/z* 200 to 300, but no fatty acids, phospholipids or lipopeptides were detected, in contrast to DESI which was able to detect these.

The molecular classes that can be successfully analysed have been surveyed in an investigation comparing the relative ionisation efficiencies for a large group of compound families using LTP, electrospray ionisation (ESI) and atmospheric pressure chemical ionisation (APCI) [48]. The LTP ionises nonpolar and polar compounds with low molecular weight such as amines, amides and imides very successfully. Aldehydes and polycyclic aromatic hydrocarbons (PAHs) could be ionised to a moderate extent. However, ionic species such as ammonium chloride salts were not detected. It is not certain if this is due to their non-volatility or other molecular properties.

Matrix effects

One of the advantages of ambient mass spectrometry is the ability to directly analyse samples in their native state with minimal or no sample preparation. However, as no separation technique is required, other issues are encountered. These include more complex mass spectra as well as matrix effects and ion suppression. Examples of molecules analysed in complex matrices include drugs in biofluids (saliva, urine and hair) [62], agrochemicals on fruit [80],

explosives in hand creams [50] and micronutrients in blood plasma [85]. Ion suppression was observed for drugs analysed in urine with the limit of detection increased by 1 to 2 orders of magnitude [62]. As well as detecting from complex matrices, ambient mass spectrometry can also detect analytes from different substrates, such as glass, PTFE, polyethylene, cloth, copper foil, filter paper and TLC plates [18, 45, 50].

Sensitivity and quantitation

Limits of detection (LODs) have been determined for various applications, and have a large range, from nanograms to femtograms, depending on the molecule and application. For explosives, LODs between 0.5 - 1 pg [53] and 1.5 - 400 pg [50] have been recorded. These LODs were improved when the sample was heated to 120 °C reducing to $0.45 - 90$ pg [50]. The LOD of pure agrochemical standards analysed by LTP [80] were also improved when using a heated substrate with LODs of $0.3 - 45$ pg achieved; for a desorption corona beam ionisation (DCBI) source agrochemicals with concentrations as low as $1 - 10$ ng were detected [83]. For pharmaceuticals, ibuprofen, loratidine, acetaminophen, and cocaine, LODs in the range $0.4 - 14.3$ ng/ml were acquired using a microplasma device [21]; whereas for the LTP, the detection limit was between 0.5 and 1000 ng/ml [62] dependent on the drug. For volatile and semi-volatile fragrances analysed using LTP [67], LODs in the pg range were achieved. This study also used a cooling stage, set to 10 °C, to increase the persistence of these high volatility molecules on the substrate.

Quantitative analysis using ambient plasma sources has been carried out, although there are limited studies, and these are considered to be semi-quantitative. Poor repeatability and reproducibility is one of the main limitations; analyses of drugs and agrochemicals using LTP have reported repeatabilities ranging from 4.3 to 43% [62] and $10 - 30\%$ [80] respectively. However, better repeatability using LTP has been reported for the analysis of melamine, with repeatabilities of $5 - 10$ % reported [65], and for the analysis of L-alanine using DBDI a repeatability of 5.8% was reported [18]. The repeatability for quantitative analysis using FAPA has also been improved by introducing a new sample introduction system: drop-on-demand sampling for analysing small amounts of liquid samples [93]. This has improved the repeatability from 35 to 8%. Linear dynamic ranges between 2-3 orders of magnitude have been reported for DBDI [94], LTP [62, 65, 67, 80, 84] and FAPA [45] analysis. The use of internal standards is one method to improve the reproducibility for quantitative measurements and has been used in the analysis of volatile fragrances (δ-damascone) using LTP [67]. The use of room temperature ionic liquids (RTILs) acting as a matrix-assisted DCBI analysis greatly increased the repeatability for the quantitative analysis of small molecules including pharmaceuticals and pesticides [95], improving the RSD from 14.3% to 2.8%. Previous analysis of pesticides using DCBI had poorer repeatability with relative standard deviations between 20 and 30% [83].

Rapid throughput

One of the major advantages of ion sources operating at atmospheric pressure is the ability to rapidly analyse many samples. This advantage makes it a very promising technique for on-line analysis in production lines and for quick quality control checks [96]. High throughput analysis has been exemplified in several publications, such as the rapid screening of pharmaceuticals using LTP [56]. For each tablet only 3 seconds of analysis time was required to get sufficient information about the active ingredient, with 18 samples analysed in 1.9 minutes. However, the time of analysis varies, with 8 samples of contaminated milk powder analysed in 3 minutes, taking 25 seconds per sample [65], and analysis using SRM mode able to identify four semi-volatile compounds within 38 seconds [67]. As well as analysing individual samples, real-time one and two-step organic reactions occurring in less than a minute can also be monitored [89]. To enable greater use of high throughput, an automated sample introduction system is required as sample exchange is often the limiting step. Complex sample geometries will be more difficult to analyse with added uncertainty in their measurements.

Imaging using plasma AMS

As with all surface mass spectrometry techniques, the ability to image the surface is of utmost interest. There have been very few publications concerning mass spectrometry imaging using ambient plasma sources. This is in contrast to DESI where over 100 articles have been published showing the technique's imaging capabilities, especially concerning biological tissue. However, partly due to the limitation in the desorption footprint and the effect of the plasma on

the surrounding area, and partly due to the types of sample commonly analysed by plasma sources, there has not been much focus on the development of plasma sources for imaging. Currently, there are 7 reported publications using plasmas for imaging applications. These include the LTP source for imaging of works of art [66], fragrances [67] and arrays [60], and a micro-plasma used to image polymers and cardamom seeds, Figure 1.9, with a resolution of 147 µm [97].
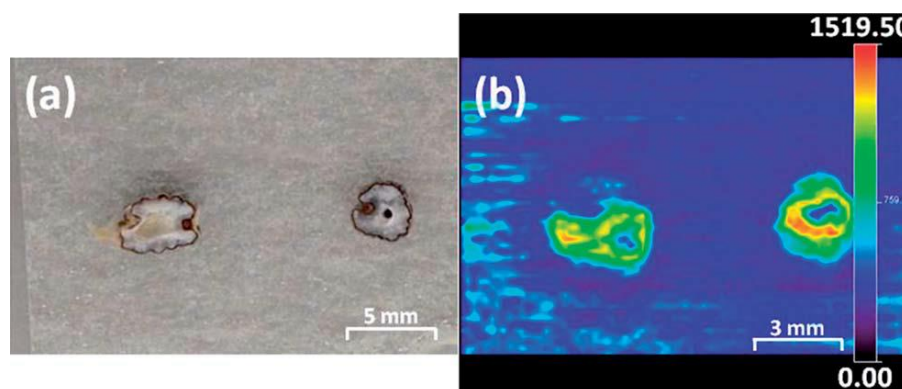
Figure 1.9. (a) An optical image of two halves of different cardamom seeds. (b) Positive ion MS image of the seeds shown in (a) using the variation in intensity (counts) of the ion at *m/z* 81, displayed by the scale bar on the right hand side. Figure and caption reproduced from [97].

One of the ways to achieve better spatial resolution from plasma sources is to couple them with laser ablation and use the plasma as a post-ionisation source. A multiwavelength laser was coupled to a DART source, and subsequently termed PALDI (plasma assisted laser desorption ionisation), for the analysis of *Radix Scutellariae* (mint root) and inks where 60 µm spatial resolution was achieved [74]. Laser ablation using a UV laser has also been used in conjunction with FAPA [98] for imaging as well as depth profiling applications. A spatial resolution of better than 20 µm was reported for the

imaging of printed lines of caffeine-doped ink. This is the best resolution reported using an ambient plasma source with or without an extra desorption/ablation step. However the best achieved vertical and horizontal spatial resolutions differ due to limitations in the scan speed and spacing of the scan lines.

An indirect method of imaging using DART has also been developed which allows for the imaging of non-planar surfaces. This uses a robotic sampling probe to obtain a small amount of analyte on an acupuncture needle which is then inserted into the ionising gas stream of the DART source [99]. By acquiring analyte from different places on the sample a chemical image can be built up, with the resolution limited by the precision of the robotic sampling arm, in this case 3 mm.

Mini mass spectrometers

One of the great advantages of not requiring a vacuum for ambient mass spectrometry sources is that they can be coupled to many types of mass spectrometer including mini mass spectrometers [100]. Ambient plasma sources have been particularly suited to these mini mass spectrometers due to their small size, robust geometry as well as low gas flow rates and power consumption. This has been recently exemplified by a handheld LTP ionisation source with a small helium cylinder integrated into it, reaching ng detection limits for some pesticides [101], and a fully portable backpack mass spectrometer with a handheld LTP system [102]. Obviously, mini mass spectrometers do not have the same capabilities as bench-top instruments,

however limitations in mass resolution and detection limits can be partly overcome by using tandem MS. This technology would be most useful for in-field analysis of explosives, drugs and foodstuffs; *in situ* analysis of melamine in milk [84], agrochemicals on fruit [81], drugs of abuse [102] and explosives [101, 102] has already been demonstrated using this system.

1.5   Summary

Many aspects of ambient plasma techniques used in mass spectrometry have been outlined in this review of the literature. These sources offer many advantages such as minimal or no sample preparation meaning any shape or size sample can be analysed, rapid analysis times enabling high throughput, and coupling to mini MS for field work. However, as shown in this review, these sources are still in the early stages of development and characterisation. In particular, the limitations to the types of molecule that can be analysed need to be investigated, as well as optimisation and developing the techniques to give more repeatable measurements. Studies on these issues are presented in this thesis.

The main aims of this thesis are:

- To develop the metrology for plasma-assisted desorption ionisation, including optimisation of the technique and methods to enhance analysis.

- To demonstrate some of the diverse application areas where ambient mass spectrometry can be used: from the analysis of polymers to personal care products.

- To compare different ambient mass spectrometry techniques, specifically DESI and PADI, with more established vacuum MS techniques such as SIMS.

Chapter 2

Methods

2.1   Introduction

The background review in Chapter 1 gave an overview of the current state of the art in ambient mass spectrometry. This chapter details some of the fundamentals behind the techniques and instruments used in this thesis; the different mass analysers used, the physics behind atmospheric pressure plasma devices, and a brief overview of desorption electrospray ionisation.

2.2   Mass spectrometers

Mass spectrometers use either dynamic or static electric and/or magnetic fields to separate ions dependent on their mass to charge ratio [103]. Several different types of mass analyser have been developed. To increase the performance and overcome the weaknesses of individual mass analysers, mass spectrometers often combine several mass analysers. These include the combination of linear ion trap and Orbitrap™, quadrupole/TOF and triple quadrupole. Below descriptions are given of the mass analysers used in the work in this thesis: ion traps including the Orbitrap™, time-of-flight (TOF) and quadrupole analysers, as well as the combination of more than one type of analyser (hybrid MS).

However not discussed here are magnetic and electromagnetic analysers and Fourier transform ion cyclotron resonance (FT-ICR).

2.2.1 Ion trap analysers

Ion traps use oscillating electric fields to trap ions in two or three dimensions; the 2D, or linear, ion trap and the 3D ion trap. The 3D ion trap was developed first, and comprises a circular electrode with two ellipsoid caps on the top and bottom that creates a 3D quadrupolar field.

2.2.1.1 The 2D (linear) ion trap

In the 2D ion trap, a four rod quadrupole ending in lenses that reflect the ions forward and backwards is used to trap ions. Ions are confined radially by a quadrupolar field and axially by an electric field applied to the end electrodes. Linear ion traps have several advantages over 3D quadrupole ion traps; firstly, a 10-fold higher ion trapping capacity and an ability to contain many more ions before space charging effects occur, and secondly, a higher trapping efficiency. Ions can be ejected along the axis of the trap, using fringe field effects by applying AC voltages between the rods and the exit lens [104]. Radial ejection of ions between the rods can also be implemented perpendicular to the axis of the trap. 2D ion trap mass analysers can be used as stand-alone mass spectrometers as well as being coupled to other mass analysers such as the Orbitrap™.

2.2.1.2   The Orbitrap™ mass analyser

The Orbitrap™ mass analyser is the most recent innovation in mass spectrometry [105], with the first commercial instrument made in 2005. The design is based on the Kingdon trap developed in the 1920s [106]; however it took many years to discover how to get ions into the trap. The Orbitrap™ also has quite a few features in common with FT-ICR MS; ions are trapped in ultrahigh vacuum to ensure very long mean free paths, and the ions are detected based on their image current and FT data processing while they are moving at significant velocities due to their high kinetic energies. The Orbitrap™ is different from other ion traps as it does not use RF or magnetic fields; instead it is an electrostatic trap. It consists of two electrodes- a central spindle shaped electrode and a barrel shaped outer electrode, as shown in Figure 2.1. The physical size of the Orbitrap™ is small; the maximum diameter of the outer electrode is 30 mm. In a newer improved version, the high-field Orbitrap™, this size is decreased to 20 mm [107, 108].
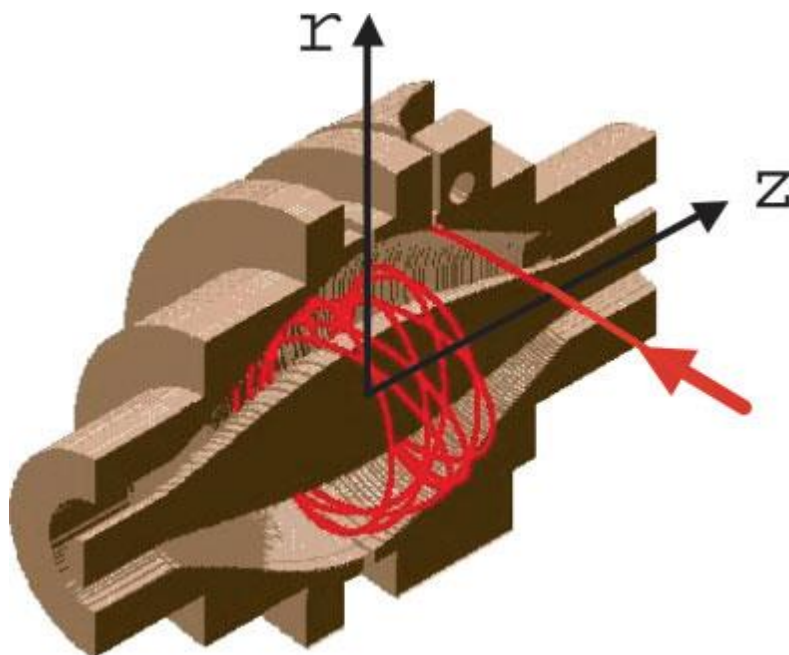
Figure 2.1. Cutaway view of the Orbitrap™ mass analyser. Ions are injected into the Orbitrap™ at the point indicated by the red arrow. The ions are injected with a velocity perpendicular to the long axis of the Orbitrap™ (the z-axis). Injection at a point displaced from $z = 0$ gives the ions potential energy in the z-direction. Ion injection at this point on the z-potential is analogous to pulling back a pendulum bob and then releasing it to oscillate. Figure and caption reproduced from [12].

Ions are injected tangentially into the Orbitrap™ through a slot displaced from the centre, as shown by the red arrow in Figure 2.1. A DC voltage is applied between the central and outer electrodes creating an electrostatic potential:

$$U(r, z) = \frac{k}{2}\left(z^2 - \frac{r^2}{2}\right) + \frac{k}{2}(R_m)^2 \ln\left[\frac{r}{R_m}\right] + C$$

(2.1)

Where r and z are cylindrical coordinates, k is the field curvature, R_m is the characteristic radius and C is a constant. The ions are injected with a kinetic energy of a few kiloelectronvolts and oscillate in the trap in spirals around the inner electrode. When the parameters are set correctly, the ions rotate in

circular paths around the central electrode, oscillating along the z axis. The axial electric field caused by the shape of the electrodes to pushes the ions towards the widest part of the trap initiating harmonic axial oscillations,

$$z(t) = z_0 \cos(\omega t) + \left(\frac{2E_z}{k}\right)^{1/2} \sin(\omega t) \qquad (2.2)$$

where z_0 is the initial axial amplitude, E_z the initial ion kinetic energy along the z-axis and

$$\omega = \left(\frac{kq}{m}\right)^{1/2} \quad (2.3)$$

is the frequency of axial oscillations, where m is the mass and q the charge of the ion. This is used to derive the m/z ratio, which can be seen from Equation 2.3 is independent of the initial properties of the ions, $i.e.$ their kinetic energy. This is one of the unique properties of the Orbitrap™ and is also the reason high mass accuracy and mass resolution can be achieved. The image current detected by the split outer electrodes is induced by this axial motion. This data is acquired as a time-domain transient, which is subsequently converted using an FFT (fast Fourier transform) to yield a frequency spectrum, in the same way as FT-ICR. These are converted using Equation 2.3 to m/z values.

The mass resolution of the Orbitrap™ [105] is given by:

$$\frac{M}{\delta M} = \left(\frac{1}{2}\right)\left(\frac{\omega}{\delta\omega}\right) \qquad (2.4)$$

Therefore the resolution is proportional to ω, $i.e.$ the inverse of $(m/z)^{1/2}$. For comparison with the other high resolution mass analyser FT-ICR whose resolution is inversely proportional to m/z, at low masses the resolution is higher using FT-ICR; however the resolution of the Orbitrap™ decreases more slowly with increasing mass. The mass accuracy of the Orbitrap™ is in the

range 2- 5 ppm. The mass resolution on the LTQ Orbitrap™ Velos, used in Chapters 4 and 5 of this thesis is 100,000 at m/z 400 [109]. But the recent improvement on the Orbitrap™ Elite gives a resolution of 240,000 at m/z 400 [107].

The limitation, and hence long time period, in developing the Kingdon trap into a suitable mass analyser came from the problem of how to get ions into the trap. To overcome this issue, short ion packets of one m/z are injected tangentially, offset from $z = 0$, into the trap, with larger m/z ions arriving later. These are then squeezed towards the central electrode by gradually increasing the voltage on this electrode, termed electrodynamic squeezing [105]. The outer electrode is kept at virtual ground whilst the central electrode is ramped down between -3 and -5 kV. The ions then begin axial oscillations without any further excitation. Prior to this injection, these ions are stored in a curved quadrupole, termed the C-trap. This is an RF-only quadrupole that uses rods with hyperbolic surfaces and is enclosed by two flat lenses with apertures for ion transport through them, Figure 2.2. The C-trap is filled with nitrogen to enable collisional cooling of the ions, although the collisions are mild enough that no fragmentation occurs. The ions form a long thin arc along the curved axis of the C-trap and are axially confined by applying a potential to the gate and trap electrodes. The RF is decreased and DC voltages are applied to direct the ions orthogonally to the axis of the C-trap where they then leave *via* a slot in the inner curved (pull) electrode. This packet of ions passes through further ion optics where they undergo acceleration to high kinetic energies and at the

same time pass through stages of differential pumping to reach the ultrahigh

vacuum of the Orbitrap™.
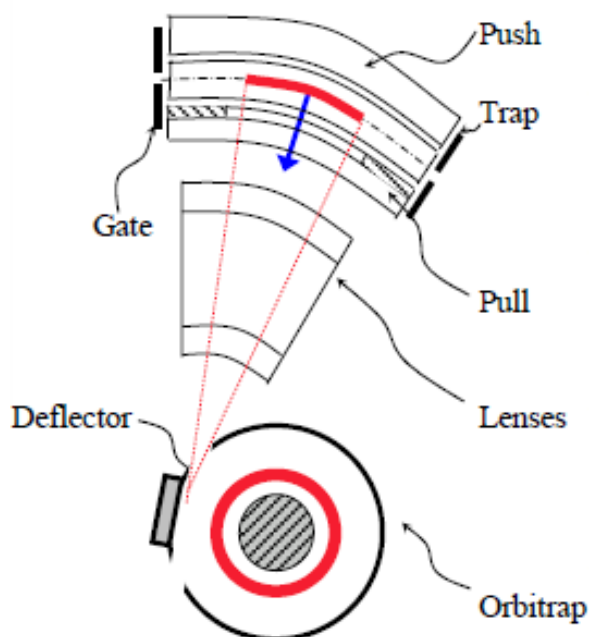
Figure 2.2. Diagram of the C-trap, used to store and cool the ions before injection into the Orbitrap™. Figure reproduced from [110].

The most successful coupling of the Orbitrap™ mass analyser is with the 2D

ion trap [111], Figure 2.3; as the Orbitrap™ operates in a pulsed mode, for

continuous ion sources such as ESI [112] and other ambient ion sources

discussed in this thesis, it is necessary to store ions before injection into the

Orbitrap™. Orbitrap™ analysers can also be used in combination with a

quadrupole mass analyser [113], named the Q-Exactive, offering a smaller

bench top version of the Orbitrap™.
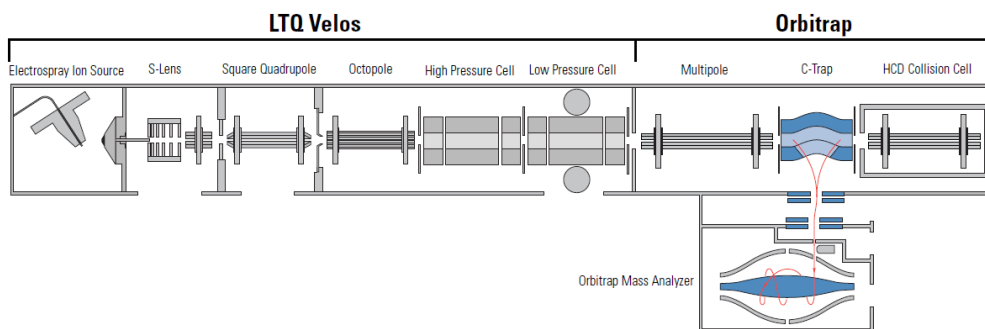
Figure 2.3. Schematic diagram of the LTQ Orbitrap™ Velos mass spectrometer, showing the dual linear ion trap design that enables efficient trapping and activation in the high-pressure cell (left), and fast scanning and detection in the low pressure cell (right). The C-trap and Orbitrap™ are shown on the right of the linear ion trap. Figure and caption reproduced from [109].

Although the Orbitrap™ offers great advantages in mass resolution and accuracy, there are some limitations and drawbacks. These include the speed of data acquisition which is limited by the detection frequency, using the highest mass resolution setting the speed is 1 second/scan, although this can be improved but at the detriment of the resolving power which is inversely proportional to the speed.

2.2.2   Quadrupole mass analysers

Quadrupole mass analysers also use electric fields to separate ions according to their *m/z* ratio. They are made up of four perfectly parallel rods that have circular or hyperbolic cross-sections. Opposite pairs of rods are held at the same polarity and an RF field is applied to them. Ions entering between the rods are attracted towards the rod of opposite charge, *i.e.* a positive ion will be

attracted to a negative rod, but the ion will change direction if the potential on the rod changes sign before the ion reaches it. Only ions of a particular *m/z* value will be able to pass through the quadrupole for any given voltage. Therefore, by scanning the RF field, ions of a wide *m/z* range can be detected.

2.2.3   Triple quadrupole mass spectrometer

Mass spectrometers consisting of several quadrupole mass analysers combined together in series have been developed; this allows tandem mass spectrometry to be performed. Three quadrupoles are used, the first and last as mass spectrometers. In the first quadrupole a single mass or range of *m/z* is selected; in the middle quadrupole, the collision cell, which is an RF only quadrupole, a collision gas, usually argon or helium, is introduced to fragment the ion or ions. These fragmented ions are then analysed by the third quadrupole.

2.2.4   Time-of-flight mass analysers

In a time-of-flight mass analyser, ions are initially accelerated by application of an electric field; this gives all the ions the same kinetic energy. The ions are separated according to their mass when they drift in a field-free flight tube; lighter ions will reach the detector first whilst heavier ions take longer as their larger mass means they have a lower velocity. This analyser is suited to coupling with ion sources that produce ions in bunches rather than continuously, *i.e.* SIMS and MALDI, and also theoretically has no upper mass limit. The mass resolution can be improved by using an electrostatic reflector, a

reflectron. This deflects the ions sending them back through the flight tube, correcting their kinetic energy dispersion. It also increases the path length of the ions without increasing the size of the instrument.

2.2.5 Quadrupole/time-of-flight (QTOF)

The combination of quadrupole and time-of-flight analysers combines the advantages of both mass analysers in terms of mass range, mass resolution and accuracy. These usually consist of two quadrupoles followed by a TOF; this can be compared to the triple quad mass spectrometer, where the second quadrupole acts as a collision cell, giving the opportunity for MS/MS analysis.

2.3   Plasma techniques

2.3.1 Definition of a plasma

Plasmas are often referred to as the fourth state of matter; a collection of freely moving charged particles, that is on average (macroscopically) electrically neutral, although it is electrically conductive. Plasmas are a very common occurrence in the natural world with all stars consisting of a plasma state, and lightning being an example of a short-term plasma. However plasmas can also be created and have many applications from TV displays, fluorescent lamps, surface cleaning as well as applications as an ionisation source in mass spectrometry, the main subject of this thesis.

To generate a plasma, energy has to be applied to a gas. This energy can be thermal or generated by applying an electric field or electromagnetic radiation, as shown in Figure 2.4.
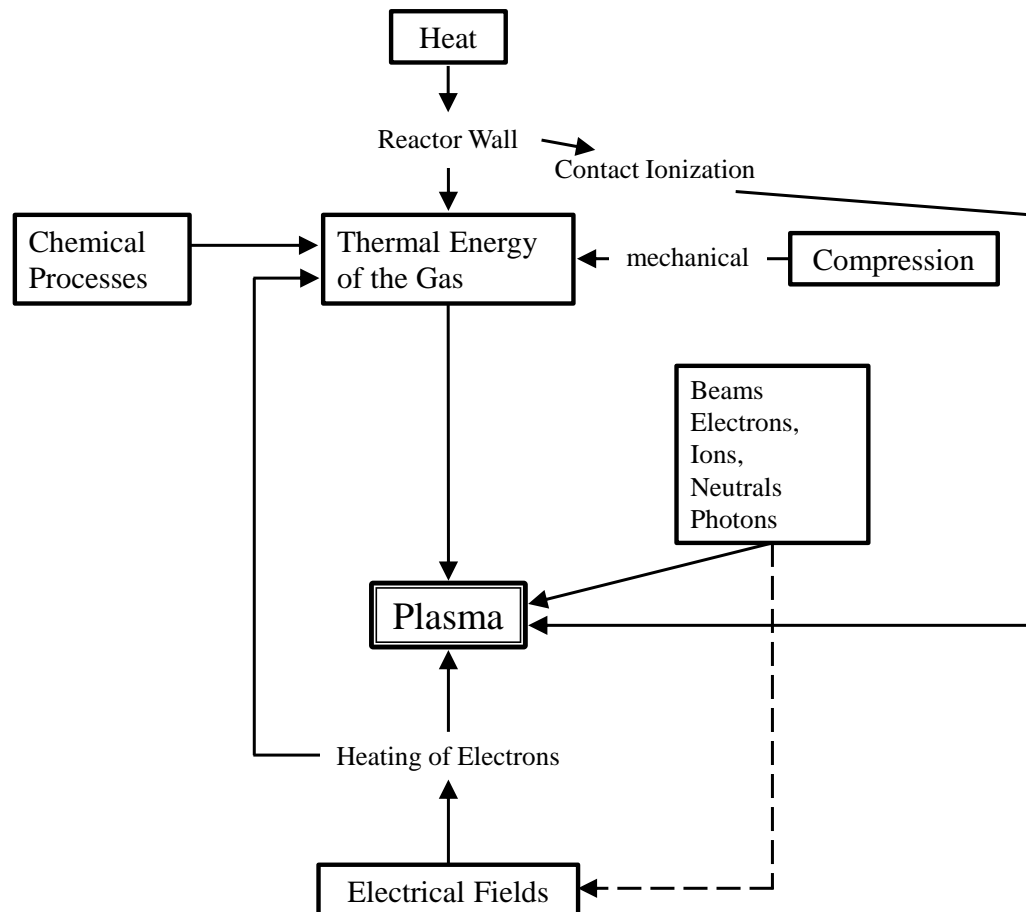
Figure 2.4. Principles of plasma generation. Figure and caption reproduced from [114].

The most common way of producing a plasma for use in technological applications is by applying an electric field to create a discharge [114]. For a plasma to be produced and sustained, electrical breakdown must occur which involves exceeding the breakdown voltage for the discharge gas. The breakdown starts with an ionisation event building up to an electron avalanche;

the electric field accelerates the charge carriers and an avalanche of charged particles is created from the collisions of these first charge carriers with atoms and molecules in the gas or on the electrode surfaces.

The breakdown voltage that must be exceeded to ignite a plasma is given by the equation below [115]:

$$V_b = \frac{Bpd}{\ln(Apd) - \ln[\ln(1 + 1/\gamma_{se})]}$$

(2.5)

where A and B are constants, p is the pressure, d the anode-cathode separation and γ_{se} is the secondary electron emission coefficient, which is the number of secondary electrons created per incident ion. The relation between V_b and pd is known as the Paschen law, and is shown for different discharge gases in Figure 2.5. This shows the minimum voltage point corresponding to the easiest breakdown conditions. This is a very important parameter that essentially shows at atmospheric pressure, large plasmas are more difficult to sustain as a higher voltage is needed; for these pressures it is advantageous to construct smaller plasmas; a d-value of below 1 mm is required to be near the minimum of the Paschen curve for almost all gases [116].
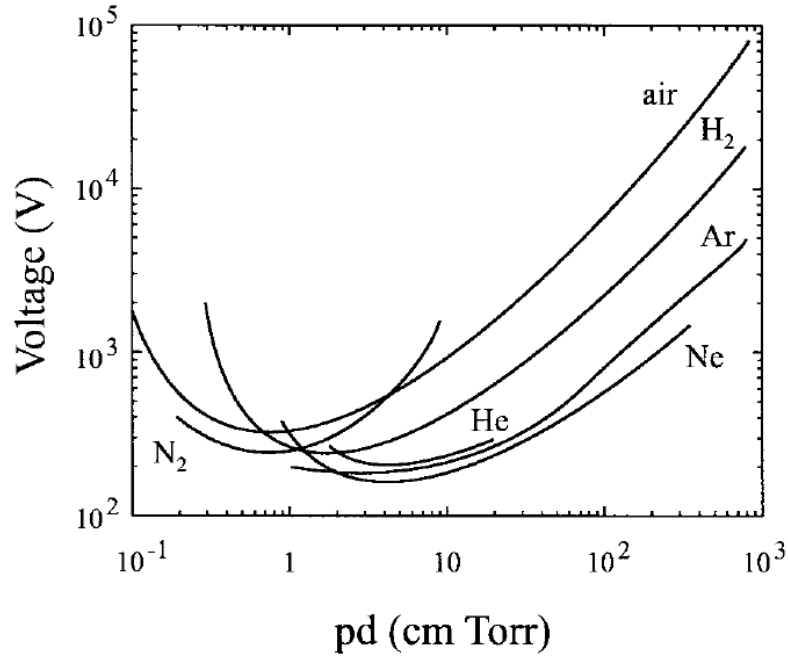
Figure 2.5. Paschen curves showing the breakdown voltage in various gases as a function of *pd*, the pressure and the gap distance, for plane-parallel electrodes. Figure and caption reproduced from [32, 117].

As shown in Figure 2.5, the curves for the different discharge gases all have slightly different shapes. The constants *A* and *B* in Equation 2.5 are experimentally determined for each gas, and their values depend on several different parameters: the collision cross-section, the ionisation potential of the gas and the secondary electron emission coefficient, γ_{se}. For noble gases, the first ionisation potential decreases with increasing atomic number, however, at the same time the collision cross-section increases. The relationship between γ_{se} and atomic number is not as well correlated. The effect of these three parameters combined is complex, and therefore the breakdown voltage cannot easily be described by any single parameter.

The current voltage characteristics for a low pressure discharge are shown in Figure 2.6. This shows the different breakdown regimes that occur at different current values.
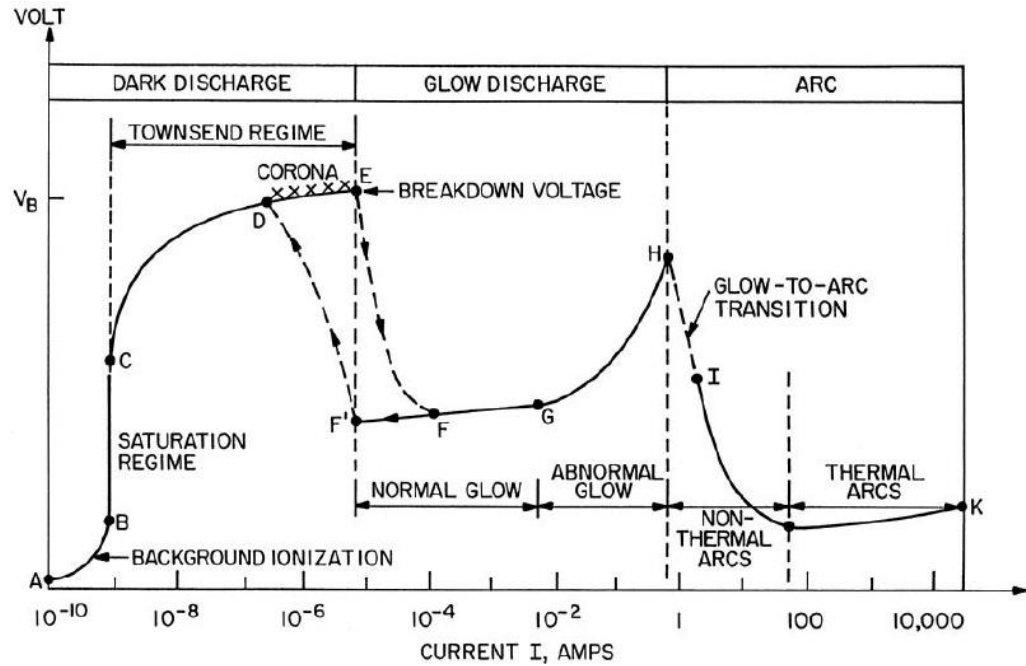
Figure 2.6. Voltage-current characteristics of a DC low pressure discharge.

2.3.2 Non-thermal plasmas

Plasmas can be classified into two broad categories, high temperature plasmas and non-thermal plasmas; this refers to their thermal equilibrium. High temperature, or thermal, plasmas are characterised by a thermodynamic equilibrium between electrons, ions and neutrals:

$$T_e \approx T_i \approx T_g \qquad (2.6)$$

where T_e, T_i and T_g are the electron, ion and gas temperature respectively. This results in a very high gas temperature, and these types of plasma are commonly used for materials processing. Non-thermal plasmas are not in thermodynamic

equilibrium, and the majority of the electrical energy goes into the production of energetic electrons rather than heating the gas stream *i.e.* the electron temperature is much greater than the cold ions and neutrals:

$$T_e \gg T_i \approx T_g \qquad\qquad (2.7)$$

However these plasmas can have ion and neutral temperatures up to approximately 1000 K. As the electrons have higher energy they collide with background atoms and molecules producing active chemical radicals and species through atomic/molecular excitation and dissociation. Two types of collisions occur, elastic and inelastic; in the first, electrons retain their energy, and in the second, they transfer it when colliding with atoms and molecules. There is also a requirement for all non-thermal plasmas: the inhibition of the glow-to-arc transition (arcing). Non-thermal plasmas are also characterised by their lower electron density, typically less than 10^{19} m^{-3}; for thermal plasmas this value is between 10^{21} and 10^{26} m^{-3}. The rest of this chapter will address non-thermal plasmas.

2.3.3 Different types of atmospheric pressure non-thermal plasmas

Atmospheric pressure plasmas can be generated by a variety of electrical discharges using either continuous direct current (DC), pulsed DC, alternating current (AC), radio frequency (RF) or microwave discharges. Figure 2.7 shows a comparison of the gas and electron temperatures for different atmospheric pressure plasmas which are discussed below. These discharges are often

generated by using short term pulsed modes. The short pulse duration prevents

the system from heating up and hence an equilibrium state from forming.
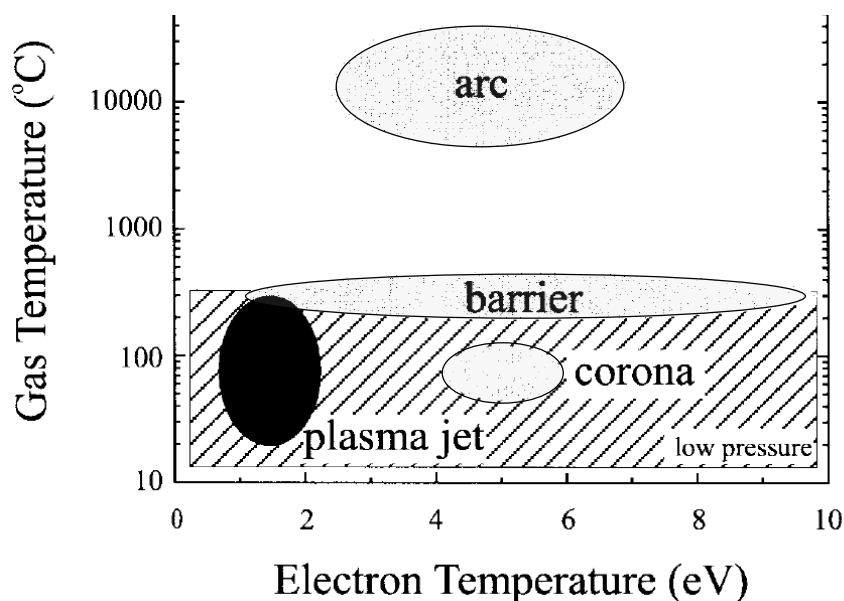
Figure 2.7. Comparison of the gas and electron temperatures for different atmospheric pressure plasmas (the plasma jet, corona and DBD) versus low pressure plasmas (the lower striped area). Figure and caption reproduced from [117].

Non-thermal RF discharges, also called plasma jets, are operated at low powers

and the impedance matching is capacitively coupled. This is in contrast to high

powered RF discharges which are inductively coupled, such as inductively

coupled plasma mass spectrometry, ICP-MS [118]. A frequency of 13.56 MHz

is most commonly used. The plasma used in this thesis is an RF discharge

based upon the plasma needle developed by Stoffels *et al.* [25] for the

treatment of biomaterials and sterilisation [119]. This source was designed to

be 'gentle', aiming for cell modification rather than destruction, for possible

applications in dentistry.

Dielectric barrier discharges (DBDs) are also used to generate non-thermal plasmas. These consist of two metal electrodes with at least one of them covered by a dielectric layer. This barrier limits the electric current and formation of sparks. The plasma is generated by short-lived, 10-100 ns, micro-discharges or streamers that develop on the dielectric layer, randomly distributed in space and time [117]. The discharge gas flows between the two electrodes which are separated by a few millimetres. DBDs are operated using AC voltages.

Corona discharges are localised, weakly luminous discharges which are generated at the tip of a sharp pointed needle where the electric field is sufficiently high. This produces a lightning crown around the tip that spreads towards the planar electrode. The plasma volume is very small. Corona discharges are operated using pulsed DC mode and high breakdown voltages are required, as shown in Table 2.1.

Table 2.1. Breakdown of atmospheric pressure plasma discharges. Table and caption reproduced from [117].

Source	V_b (kV)
Low-pressure discharge	$0.2 - 0.8$
Arc and plasma torch	$10 - 50$
Corona	$10 - 50$
Dielectric barrier discharge	$5 - 25$
Plasma jet (RF)	$0.05 - 0.2$

2.4   Desorption electrospray ionisation

Desorption electrospray ionisation, DESI, was the first ambient mass spectrometry technique that was introduced in 2004 by Graham Cooks' group at Purdue University [7]. Initial studies using the technique showed its applicability in a range of fields crossing such diverse topics as alkaloids in plant tissues [120], profiling of lipid distributions in biological tissue [121] and trace-level explosives detection [122]. Since then, many other application areas have emerged for the technique as demonstrated by the biennial reviews by Fernández *et al.* [10, 123].

The DESI source simply consists of an electrospray ionisation source which is directed towards the sample surface, as shown in Figure 2.8. This results in charged solvent droplets impacting the surface. Several studies have tried to understand the fundamental mechanisms that occur during the desorption and ionisation processes. Particle dynamics analysis has been used to measure the sizes and velocities of both the primary and secondary droplets in DESI [124]. Initial droplet diameters of 2 to 4 μm were measured; however the secondary droplets were smaller, ranging between 0.9 and 3 μm depending on their distance from the spray impact site. The velocities of the droplets changed much more dramatically with impacting droplets typically travelling at 120 m s^{-1} and secondary droplets at less than 25 m s^{-1}. The droplets scattered closer to the surface had higher velocities and it is thought that these are the most effective in analyte transfer. Computational fluid dynamic simulations of the spray contribute to the theory that a two-step analyte pickup mechanism is

involved, with initial wetting of the surface dissolving the analyte, followed by incident droplets splashing the surface creating secondary droplets that are transferred to the mass spectrometer [125, 126].
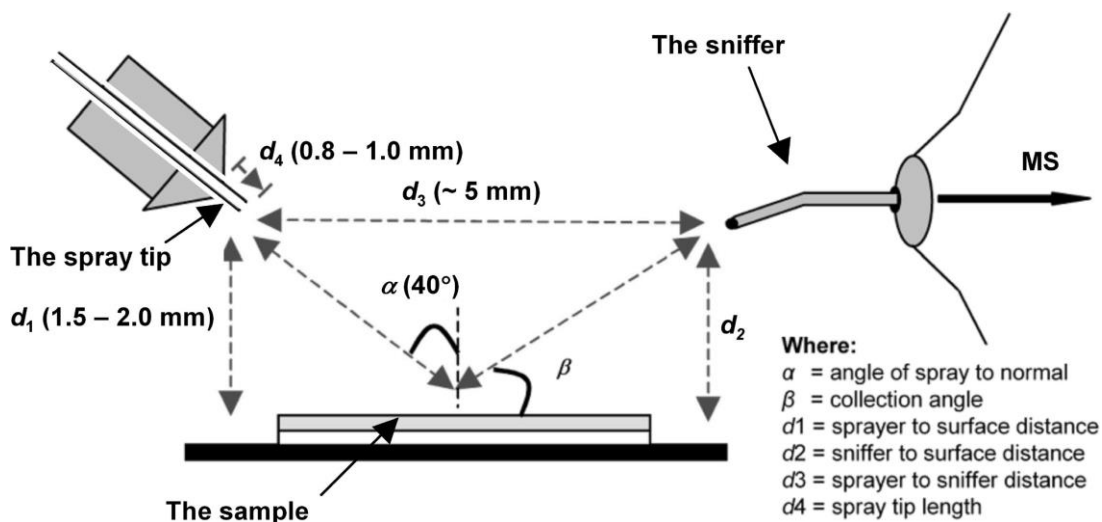
Figure 2.8. Schematic showing optimal DESI parameters. Figure and caption reproduced from [127].

Optimisation of the geometry of the DESI spray with respect to the sample and the inlet to the mass spectrometer, the "sniffer", is critical for good signal intensities and repeatability [127]. For instance, a small deviation of less than a millimetre in the spray-sample distance, d_1 in Figure 2.8, can greatly affect the signal response. The successful detection of an analyte of interest is also dependent on the geometry of the DESI spray, with lipids and explosives requiring greater distances between the spray and sample compared to peptides and proteins [128]. The solvent composition used in the electrospray also has an effect on signal intensities and spatial resolution [129]; it was found that a greater percentage of solvent compared to water, up to 100% solvent (methanol, acetonitrile, ethanol or propan-2-ol) led to a 35 fold increase in

efficiency (molecular ion counts per unit area) and a 2 fold improvement in the

erosion diameter. The successful detection of a molecule is also affected by its

solubility, greater than 1.5 g kg^{-1} is needed for effective DESI analysis [129].

Chapter 3

A comparison of SIMS and DESI and their complementarities

3.1   Introduction

In this chapter, one the most successful of the ambient surface mass spectrometries, desorption electrospray ionisation (DESI), which provides highly sensitive mass spectrometry from surfaces without the constraint of vacuum, is compared with secondary ion mass spectrometry (SIMS).

Surface chemical analytical techniques such as secondary ion mass spectrometry (SIMS) [130] are extremely powerful, providing high-sensitivity molecular information at better than 200 nm spatial resolution. However, the requirement for SIMS analysis to be *in vacuo* is, for many applications, a severe drawback. This is, of course, particularly important for biological applications. In the vanguard of these ambient methods is desorption electrospray ionisation (DESI) developed by Cooks *et al.* [7, 131]. DESI has already been shown to have great potential in a wide range of application areas from forensics and homeland security [132-135], through to counterfeit detection of pharmaceuticals [136], environmental analysis [137] and biological analysis [138, 139]. Of the wide variety of ambient desorption

methods, it is clear that DESI has one of the strongest uptakes. As with all techniques there are some disadvantages; DESI cannot generally desorb molecules that are chemically bound to surfaces, giving low signals from molecules with low ionisation efficiency, and the spatial resolution is currently limited to approximately 100 μm [140], with the best recorded value being 40 μm [141].

NPL has been involved in developing the underpinning understanding of surface analysis techniques, leading to over 100-fold improvement in repeatability in SIMS [142]. We have begun a similar approach for DESI, to improve understanding of the technique [127].

Here, we illustrate the complementarities of SIMS and DESI for the analysis of 18 industrially relevant organic molecules. DESI uses a gentler desorption mechanism to remove material from the surface than the sputtering involved in SIMS. We have investigated the DESI desorption mechanism in order to understand the materials for which DESI is effective. In particular, large fragile molecules can be detected intact, rather than heavily fragmented as in SIMS.

The objectives of this chapter are:

- To compare the characteristics and parameters used for vacuum (SIMS) and ambient (DESI) mass spectrometry.
- To show for different types of molecule, the similarities and differences in chemical information that is obtained using the two techniques.

3.2   Experimental Section

3.2.1 DESI

In this study, we use a modified nanospray source for the QTRAP 4000 mass spectrometer (Applied Biosystems, Warrington UK) for DESI experiments. This instrument offers good sensitivity, and the capability to conduct MS, MS/MS and MS^3 experiments. The other modification was the attachment of a 'sniffer' (a steel capillary) to the MS entrance to facilitate efficient collection of the desorbed material into the MS inlet.

In this work, a solvent composition consisting of 0.1% formic acid in 50:50 acetonitrile:water (18 MΩ cm^{-1}) was used throughout for the electrospray liquid. The standard operating conditions, unless otherwise stated, were an electrospray voltage of 5000 V, a solvent flow rate of 1 μl min^{-1}, a nebulising gas flow rate at around 6 L min^{-1}, an angle of incidence of either 0° or 40°, a tip-to-sample distance of 1.5 - 2 mm, a tip-to-sniffer distance of ~ 5 mm, a sniffer-to-sample distance of < 0.5 mm and a tip length of 0.8-1 mm. These conditions were found to give an optimal, stable, and repeatable signal intensity for the protonated molecule of Rhodamine B, and a good spot shape on the sample. A full explanation and discussion of the optimisation of the geometry and set-up can be found in Ref. [127].

3.2.2 SIMS

Secondary ion mass spectra were recorded using an ION-TOF time-of-flight secondary ion mass spectrometer (TOF-SIMS IV), shown schematically in Figure 3.1, with primary ions of Bi_3^+ at 25 keV energy. To measure the ion yields, four repeat spectra were taken with the same ion dose, on fresh regions, within the static SIMS limit [143]. The instrument was equipped with a bismuth-manganese liquid-metal ion source (LMIS) G-tip [144]. The ion beam could rapidly be switched between Bi^+ and Mn^+ for G-SIMS analysis [144]. G-SIMS spectra were acquired in the order Bi^+ followed by Mn^+ on the same area and then calculated as described in detail elsewhere [142, 145]. For each analysis, the ion beam was digitally rastered with a 128×128 array over an area of 100×100 µm using a combined total primary ion dose of $< 1 \times 10^{16}$ ions m^{-2}. The samples used were conducting and so no charge compensation was required.
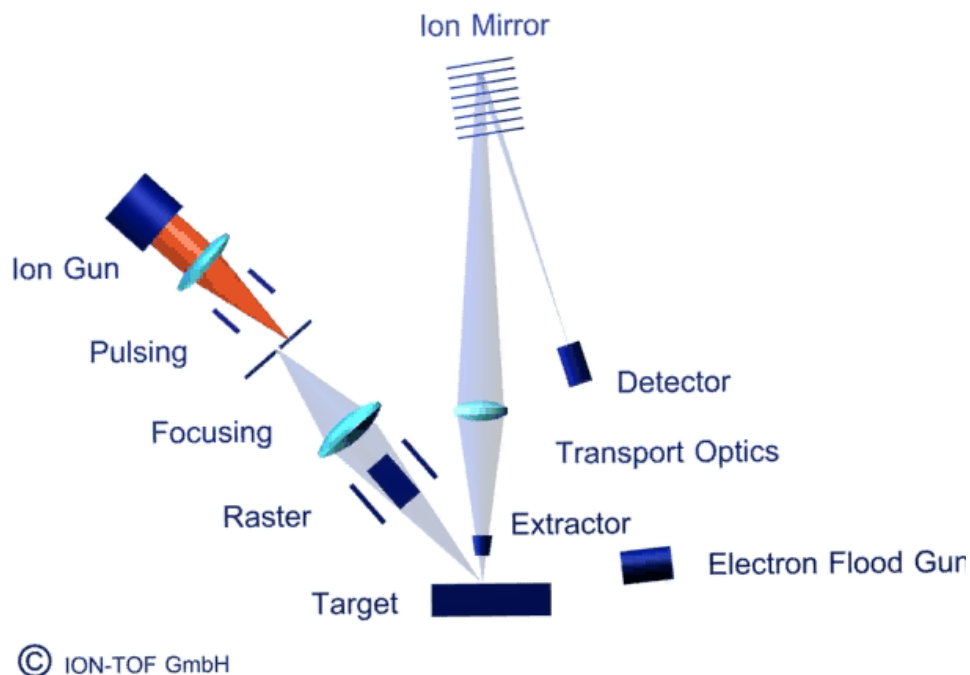
Figure 3.1. Schematic outlining the basic features of the TOF-SIMS instrument, courtesy of ION-TOF GmbH.

3.2.3 Samples

Samples of phenylalanine, rhodamine B, lysine, cholesterol (Sigma Aldrich, Poole, UK) and Irganox 1010 (CIBA, Macclesfield, UK) were thermally evaporated onto silicon wafers using an Edwards AUTO 306 vacuum coater (Crawley, UK). Samples of trehalose, chlorhexidine, hydroxyl propyl cellulose (HPC) and 1,2-dimyristoyl-rac-glycero-3-phosphocholine (DMPC) (Sigma Aldrich, Poole, UK) were spin coated onto silicon wafers using a Laurell Technologies Corporation spin coater, model WS-650Sz-6NPP-Lite (North Wales, PA, USA). Samples of erythromycin, reserpine, creatinine, atropine, carbaryl, colchicine, erythromycin ethyl succinate (Sigma Aldrich, Poole, UK), peptide His-Cys-Lys-Phe-Trp-Trp (H6387) (Cambridge Peptides, UK) and myoglobin were drop cast onto silicon wafers.

3.3   Results and discussion

SIMS and DESI both use projectiles to remove material from a surface; however, the mechanisms of removal are quite different. Table 3.1 lists some of the differences between the DESI and SIMS projectiles. DESI uses very large solvent droplets (~4 μm) to produce a very gentle desorption of material (representative energy/molecule of ~2 eV). Desorption is thought to arise through a mechanism of dissolution of material from the surface followed by secondary droplet transfer into the mass spectrometer [126]. The DESI technique is able to desorb large amounts of material very quickly, due to the high rate of water droplets impacting the surface. In contrast, SIMS is extremely energetic and, coupled with its need for vacuum, it is less good for analysing fragile samples, but the small projectile size and focus enable imaging close to the nanoscale (100 nm spatial resolution can be achieved). SIMS is also extremely surface sensitive, generally detecting only the top monolayer. SIMS has a low rate of erosion and ionisation, making MS/MS techniques, where a large number of ions are needed, difficult.

Table 3.1. A representative comparison of common projectiles and parameters used in SIMS and DESI, illustrating the rapidity and gentleness of DESI in comparison to the energetic SIMS.

	DESI	**SIMS**
Projectile	Water/alcohol mixtures	Metal clusters
Projectile size	~ 4 μm	~ 1 nm
Energy/constituent in projectile	~ 2 eV	300 eV to 25 keV
Rate of erosion	~ 7000 $\mu m^3 s^{-1}$	~ 1 $\mu m^3 s^{-1}$
Source	Chromatic	Monochromatic

SIMS and DESI mass spectra were obtained from 18 industrially relevant organic samples to ascertain the practical effectiveness of each of the techniques. In general we saw three different types of behaviour, which we describe in more detail below. First, in some cases such as chlorhexidine, DESI and SIMS were able to identify the molecule equally well, Figure 3.2. DESI and SIMS exhibited similar spectra, with a strong molecular ion peak set against a background of peaks. The SIMS background arises from a large number of fragmentation products both of the molecule, as well as of any contamination present at the surface. The DESI background arises from the electrospray solvent, populating the mass spectrum with signal from solvent clusters. This is important as it can significantly reduce the signal-to-noise ratio and occasionally swamp the molecular signals or those of trace analytes. The solvent background interference is often significantly less in negative ion mode DESI MS.
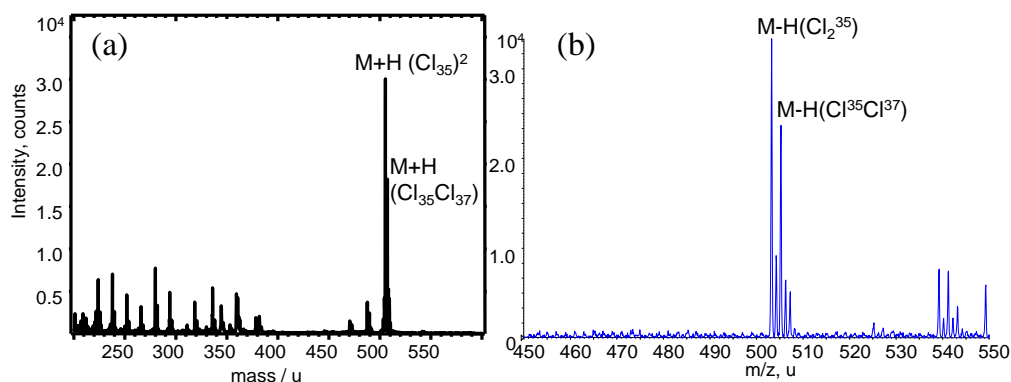
Figure 3.2. Mass spectra of chlorhexidine using (a) SIMS analysis with Bi_3^+ primary ions at 25 keV energy, and (b) DESI using solvent composition of 50:50 ACN:H2O with 0.1% formic acid.

Analysis of the protein myoglobin, with mass of ~ 16,000 Da, highlights a stark contrast in the ability of the techniques. The structure of myoglobin is shown in Figure 3.3 (a), with the iron-containing haem fragment highlighted. The SIMS spectrum of the protein, shown in Figure 3.3 (b), has the peak characteristic of the protonated haem molecule ($C_{34}H_{32}O_4N_4Fe^+$ at mass 616.12 Da) and amino acid residues, within a very large background of fragmentation peaks. This spectrum can be simplified dramatically with the use of G-SIMS [142, 145], as shown in Figure 3.3 (c), with the background reduced and the characteristic heme peak the most intense peak in the spectrum. In comparison, the DESI spectrum, shown in Figure 3.3 (d), contains the protonated heme peak at 616.12 Da, as well as a strong signal from the intact protein. The intact myoglobin molecular ion is observed, with a charge envelope around the M^{17+} ion at *m/z* 943.0, highlighted in Figure 3.3 (d). This illustrates the gentle nature of DESI, leading to the ability to observe intact proteins, giving it a definite advantage in the analysis of large or fragile molecules. In addition, DESI-MS often has the capability to routinely conduct MS/MS of a given peak (something still difficult in SIMS). Breaking down the molecule into fragments with MS/MS enables an improved signal-to-noise ratio, supports identification and aids structural characterisation. This can be a critical advantage for the identification of complex biological molecules. However, SIMS gives the opportunity for three-dimensional nanoscale resolution of chemistry and, in addition, has the potential to determine the orientation of ordered molecules at surfaces [146]. The gentle nature of DESI may lead to difficulty in breaking covalent bonds, making it unsuitable for the analysis of molecules covalently bound to a surface.
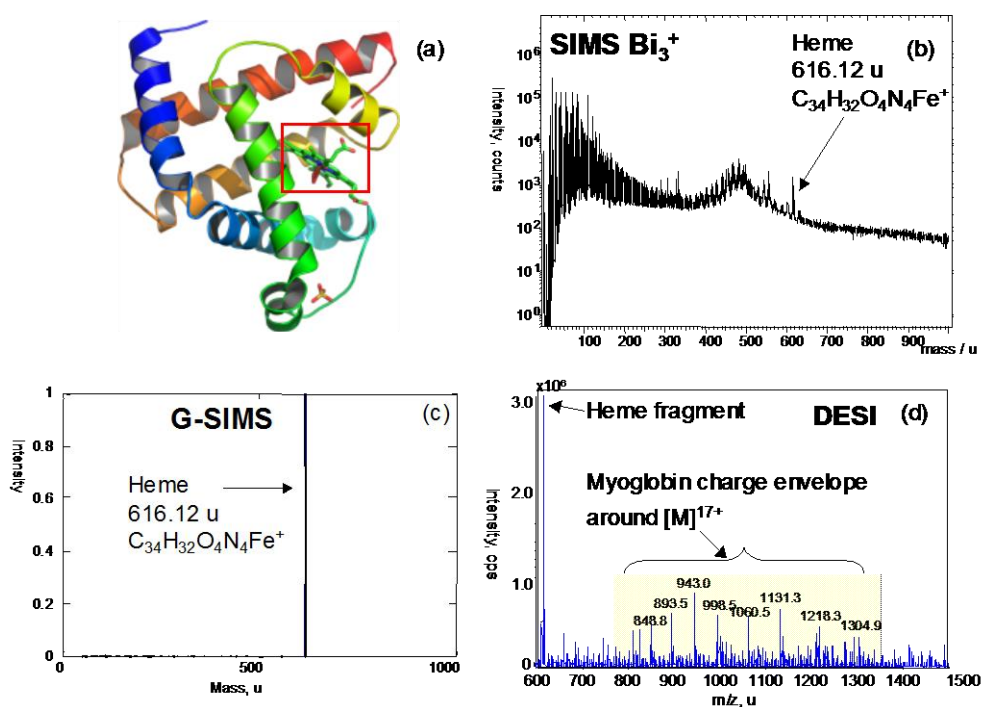
Figure 3.3. (a) Myoglobin structure with the heme fragment circled. Positive ion mass spectra using (b) SIMS, (c) G-SIMS and (d) DESI-MS of myoglobin. The heme fragment ion is labelled and in (d) the protein charge envelope highlighted.

There are ranges of molecules that do not seem to be easy to detect with DESI. Some examples seen in this study include Irganox 1010, carbaryl, lysine, cholesterol and hydroxy propyl cellulose. A number of studies have investigated the inclusion of different additives to the electrospray solvent in DESI to enhance or change the charge states [147], improve sensitivity and selectivity [132, 148] and improve the detection of less polar compounds [149]. This has often been termed reactive DESI and may aid the detection of the molecules, but is not studied here. Presently, more development is required to understand reactive DESI and its areas of use. To start to identify regions within which DESI or SIMS is most useful, we illustrate in Figure 3.4 a matrix

within which molecules can be classified, depending on the successfulness of DESI and SIMS analysis. The important attributes of the aqueous solubilities of the molecules and their functional groups is given by the associated symbols. This shows that the effectiveness of DESI is not primarily dependent on solubility. It may be that functionality or polarity has a stronger effect. This is studied in more detail elsewhere [129].
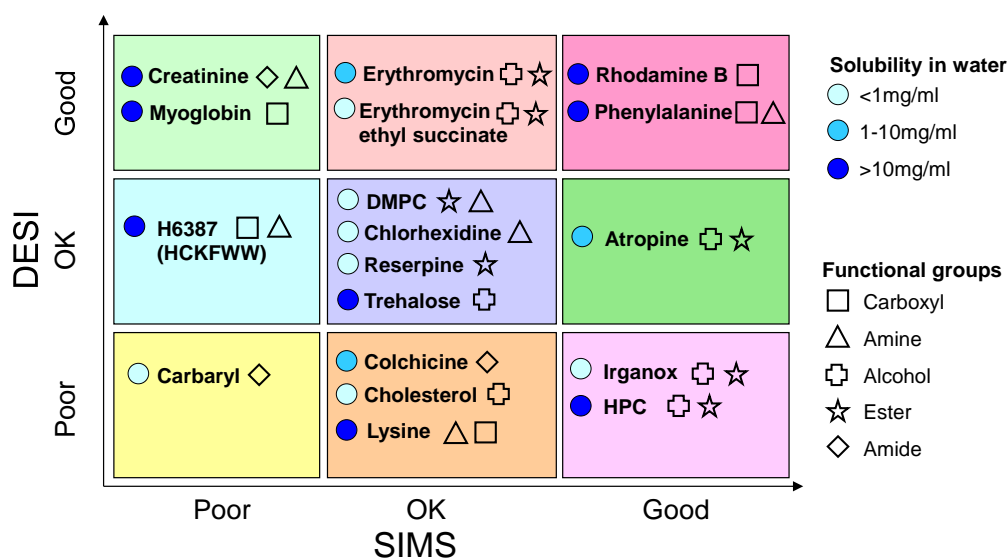
Figure 3.4. The effectiveness of SIMS and DESI analysis for 18 organic molecules. A key to their solubility in water and functional groups is included. Shortened names for some of the molecules: HPC- hydroxypropylcellulose, DMPC- 1,2-dimyristoyl-rac-glycero-3-phosphocholine, H6387- peptide His-Cys-Lys-Phe-Trp-Trp

Figure 3.4 allows us to begin a classification and ordering of molecules to aid our understanding of the causes of their detection efficiencies. The complementarity of Figure 3.4 may be seen by allocating the value 1 for "Good" and 0.5 for "OK". These values are approximate and preliminary, and the exact position of a given molecule within the matrix is open to debate, and may be moved by the use of reactive DESI or different SIMS primary ions.

SIMS then has a total score of 9.5 out of a possible 18 or 53%. DESI receives a similar 50% - not significantly different with only 18 samples. More importantly, if both techniques are used together, this rises to 72% - a result expected if the essential signal generating processes had different origins in SIMS and DESI as discussed.

3.4   Conclusions

Table 3.2 summarises the different qualities of SIMS and DESI analysis and the complementarities of the two techniques. From the range of samples we have studied here, we can start to classify different molecules according to the effectiveness of SIMS and DESI, as shown in Figure 3.4, and this provides a framework to understand the limitations and ranges of the techniques further. Some broad generalisations can already be made about the types of spectra seen.

1. For large molecules and biologicals, DESI is advantageous.

2. For some molecules, SIMS and DESI exhibit similar spectra.

3. Some molecules are unobservable with DESI, dependent on ionisation, surface binding, solubility and functionality.

The ambient nature of DESI makes it extremely useful for quick sample analysis and *in vitro* analysis. However, for nanoscale analysis, or the detection of surface bound molecules, SIMS must be used. The ranges of use and areas of complementarities of SIMS and DESI are shown in Table 3.2. At present, DESI shows great potential for a wide range of analysis; however, further work

is needed to assess the fundamental limitations of DESI and understand the rules that lead to poor or no detection of particular molecules.

It is clear that there is a gap for ambient mass spectrometry of important industrial and biological molecules such as Irganox and cholesterol, as shown in Figure 3.4. Therefore, in the following chapters, we explore the capability and metrology of an ambient plasma desorption ionisation source, a complementary technique that will address some of these measurement gaps.

Table 3.2. Comparison of the different qualities of DESI and SIMS

	DESI	SIMS
Molecules detected	• Small molecules • Peptides and proteins • Inks and dyes • Molecules weakly bound to the substrate	• Small molecules • Inks and dyes • Molecules strongly and weakly bound to the substrate
Molecules not detected	• Molecules strongly bound to the substrate • Low solubility molecules	• Proteins and large peptides • Volatiles
Spectral information	Full MS/MS	MS with some structural information
Background signal	Significant background from source liquid	Background of fragmentation species and contamination
Sensitivity	Good (ng)	Excellent (fg or ag)
Repeatability	~15% over a day	Better than 2 %
Spatial Resolution	~150 μm	< 100 nm
Quantitation	Quantitative with internal standard	Semi-quantitative (quantitative for known reference samples)

Chapter 4

Effects and optimisation of analytical parameters for signal intensities of molecules and polymers using PADI

4.1   Introduction

In this chapter, the optimisation and characterisation of a plasma-assisted desorption ionisation (PADI) source is presented. This includes optimisation of the source geometry to maximise signal intensities, and variation of the plasma power which results in different levels of fragmentation. Thermal imaging of the plasma is also carried out for the first time. Polymer analysis is possible using PADI with characteristic ions identified; this is discussed in detail later in the chapter.

As discussed in Chapter 1, ambient mass spectrometry is a relatively new area, with the innovation of desorption electrospray ionisation (DESI) [7] in 2004 heralded the important area of ambient mass spectrometry (AMS) [10]. Within this growing domain, plasma-based desorption and ionisation techniques have

developed as one of the leading variants, with several different types of operation and configuration.

Polymers are an important class of material used in many advanced technologies, for example drug delivery coatings on medical devices. Secondary ion mass spectrometry (SIMS) is one of the principal techniques for studying such materials giving high-resolution imaging in 2D and 3D [150]. However, samples need to be prepared for analysis in the vacuum system, usually to reduce the sample size and the sample needs to be mounted to reduce topographical effects. Consequently, whilst SIMS is excellent at studying materials in detail it is not well suited to on-line analysis in a production environment. An ambient mass spectrometry technique with the capability for polymer analysis is therefore desirable. There have been a limited number of studies using ambient mass spectrometry to analyse polymers. DESI has been used to successfully analyse poly (ethylene glycol) (PEG) [151]. Poly (tetramethylene glycol) (PTMG) and polyacrylamide (PAM) were also analysed with limited success. Bulk polymer surface analysis of biopolymers, synthetic homo- and co- polymers has been carried out using FA-APGD-MS [79]. In that study, ions were detected from all the polymers analysed in the positive ion mode but were limited to a mass range below m/z 500. Phthalic acid esters in PVC toys were analysed using DART [152], but ions coming from the PVC are not discussed. Analysis with an atmospheric plasma system, almost identical to PADI, showed that the mass spectra from a series of substituted polyethylenes (PEs) [153] was complex with ions due to fragmentation of the polymer and from reactions in the plasma also detected.

Pulsed radio frequency glow discharge time-of-flight mass spectrometry (GD-TOFMS) has been used for the analysis and depth profiling of single and multi-layer polymers [154]. This has the limitation that only ions under m/z 100 are detected [155]. PADI and a smaller variant, micro-PADI, have been used to analyse PTFE [78]. The mass spectra from these two sources show mainly the same ions but with different intensity distributions; for the micro-PADI, an ion series corresponding to $[C_3F_2 + [CF_2]_n + (OH)]^-$ is the most dominant with ions detected up to 700 Da, whereas for the traditional PADI many more ion series are detected up to a mass of 900 Da.

Here, we study the effects of the key operating parameters for PADI on the spectral intensities to provide guidance for analysts. We use the optimised conditions to show the effectiveness of PADI for the analysis of four polymers; PTFE, PMMA, PLA and PET.

The objectives of this chapter are:

- The development of the metrology for PADI, including optimisation of the geometrical and operational parameters.

- Measurement of the surface temperature, its variation with plasma power and the effect on signal intensities.

- Analysis of polymers using PADI, showing unique fingerprint spectra from each polymer.

4.2   Experimental Section

4.2.1 Samples

Uniform thin films of valine ($\geq$ 99.5% purity, Sigma Aldrich, Poole, UK) were thermally evaporated onto glass slides (Superfrost, Thermo Fisher, UK), with thicknesses between 380 nm and 520 nm, using an Edwards AUTO 306 vacuum coater (Crawley, UK). Thickness measurements were made using a M2000 spectroscopic ellipsometer (Woollam, USA). Four different polymers were analysed. Poly (methyl methacrylate) (PMMA) and poly (ethylene terephthalate) (PET) were analysed in bulk form from 1 mm thick amorphous sheets (Goodfellow, Cambridge, UK). Polytetrafluoroethylene (PTFE) was also analysed in bulk form as thread-seal tape (RS, Corby, UK). Poly (lactic acid) (PLA), M_W ~ 124000 (Sigma Aldrich, Poole, UK) was dropcast onto a glass slide. Initial PADI experiments analysing PMMA spun cast on to silicon wafer were unsuccessful at detecting any ions from PMMA. This was found to be due to conducting properties of the sample; therefore further experiments were carried out with polymers on insulating substrates.

4.2.2 PADI

The PADI set up consists of an RFG050 radio frequency generator, operating at 13.56 MHz, and an AMN150R automatic matching network (Coaxial Power Systems Ltd, Eastbourne, UK), attached with a coaxial cable to the plasma pen. It was found that the automatic matching network (which sets the impedance to reduce reflections) did not work sufficiently well in this arrangement and had to be optimised manually. Figure 4.1 shows a schematic of the set up as well as

a photograph of the plasma. The plasma pen is made up of a tungsten wire, diameter 0.75 mm, encased in ceramic tubing, ID 1 mm OD 2 mm, to insulate it, with the sharpened tip of the needle exposed for 7 mm. An outer glass tube, ID 2.5 mm OD 4 mm, encases the ceramic tube and needle, and the end of the glass tube is flush with the needle. A grounded copper electrode of 10 mm width is attached to the outside of the glass tube 3 mm from the end. Helium gas, 99.996% pure (BOC, Guildford, UK), enters through a nylon Swagelok T-fitting, where it subsequently flows between the ceramic and glass tubes to the exposed sharpened end of the tungsten wire. The helium flow rate is controlled *via* a flowmeter (Cole-Parmer, London, UK), and a flow rate of 820 mlmin[-1] was used [156]. High RF voltages are used in the PADI system; therefore caution must be taken when the plasma is on.
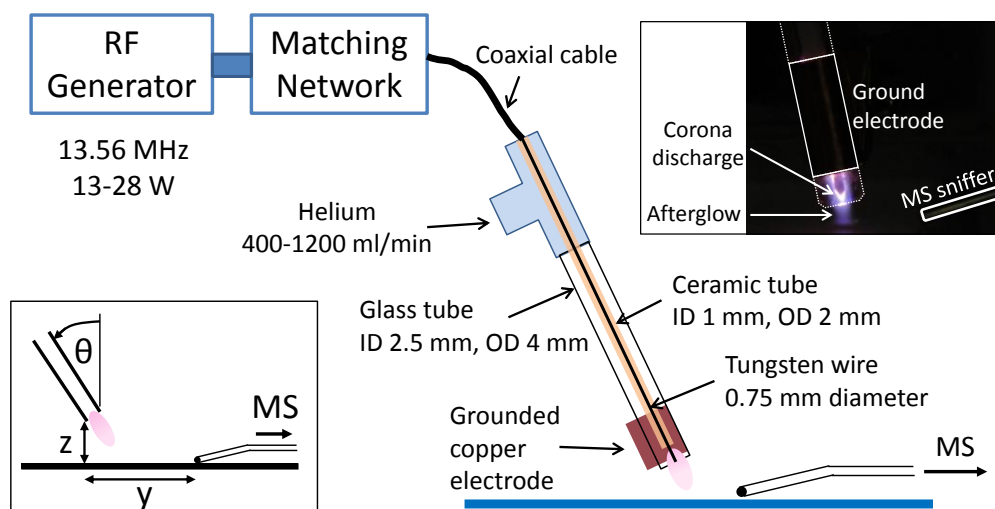
Figure 4.1. Schematic of the PADI setup, with details of the dimensions and materials of the components that make up the source. Inserts of the geometrical parameters studied and a photo of the plasma.

4.2.3 Mass spectrometer

A Thermo Scientific LTQ-Orbitrap™ Velos mass spectrometer was used in both positive and negative ion modes. MS^2 and MS^3 were used to confirm the identity of ions, where necessary. Mass spectra were acquired for 2 minutes. The mass spectrometer was programmed to collect up to a maximum Orbitrap™ injection time of 500 ms, using an AGC (automatic gain control) setting of 5×10^5. The AGC is designed to fill the trap with the optimal amount of ions to ensure that the signal intensities are high and that the spectra are not distorted by space-charging effects. All data were acquired using the Orbitrap™ mode with the highest resolution setting of 100,000 (at m/z 400), unless otherwise stated. All data were recorded after the plasma was switched on. The capillary temperature was set to 150 °C. The standard ion transfer tube was replaced with an extended version, subsequently referred to as the 'sniffer' as shown schematically in Figure 4.1. Samples were placed on a 2-axis stage (Prosolia, Indianapolis, IN, USA) below the sniffer.

A QSTAR Elite quadrupole time-of-flight (Q-TOF) mass spectrometer (Applied Biosystems, USA) was used for the helium flow rate and the RF input power optimisation experiments using triethanolamine and hydroxycitronellal in section 4.3.1. The QSTAR was operated in the positive ion mode with an m/z range of 50 - 1000. An extended ion transfer tube was also fitted to the inlet of the mass spectrometer. For these experiments the inlet capillary was not heated.

4.2.4 Temperature measurements

Thermal imaging of the plasma system was performed using a FLIR systems InfraCAM thermal imager and a FLIR systems SC5000 thermal imager (West Malling, Kent, UK). The measurements discussed in the results section are the temperature at the centre of the analysis spot on the surface, which is also where the temperature was highest. Data acquired from the cameras were analysed using FLIR systems ThermaCAM^{TM} Researcher Pro 2.9 and Altair software. The emissivity of the glass sample (0.92) was taken into consideration when calculating the temperature. A heated sample stage was constructed to perform thermal desorption measurements. This was made using a glass slide covered in a thin film of indium tin oxide (ITO) with electrodes attached through which a current, 0.08 to 0.2 A, was passed to heat up the stage.

4.3   Results and discussion

4.3.1   Optimisation and analysis of small molecules with PADI MS

When moving from one analysis spot to another, PADI needs a settling period before the signal intensities stabilise. Figure 4.2 shows a typical example for the $[M-HCOOH+H]^+$ ion from valine, using an RF input power of 22 W, showing the intensity becoming more stable after 20 seconds. We believe this is due to the surface heating up when the plasma is first moved to a new

position, and that the temperature reaches a plateau after 20 seconds. Therefore, in this study we sum the intensities over a 100 second period following the first 20 seconds to account for the stabilisation period. Temperature effects are discussed in greater detail later in the chapter. Fluctuations in the signal intensity have a relative standard deviation of approximately 10%. Analysis of ion chromatograms show that some background ions such as phthalates at m/z 149.023 (phthalic anhydride $[C_8H_4O_3 + H]^+$), 205.086 $[C_{12}H_{12}O_3 + H]^+$ and 279.159 (dibutylphthalate $[C_{16}H_{22}O_4 + H]^+$), have a strongly fluctuating signal, with relative standard deviations of over 70% over 120 seconds; these ions are likely to come from the laboratory air. Whereas other background ions, at m/z 73.065 $[C_4H_8O + H]^+$ and 136.021 $[C_7H_5NS + H]^+$, which come from the substrate, are much more stable with relative standard deviations of around 6% over the same period.
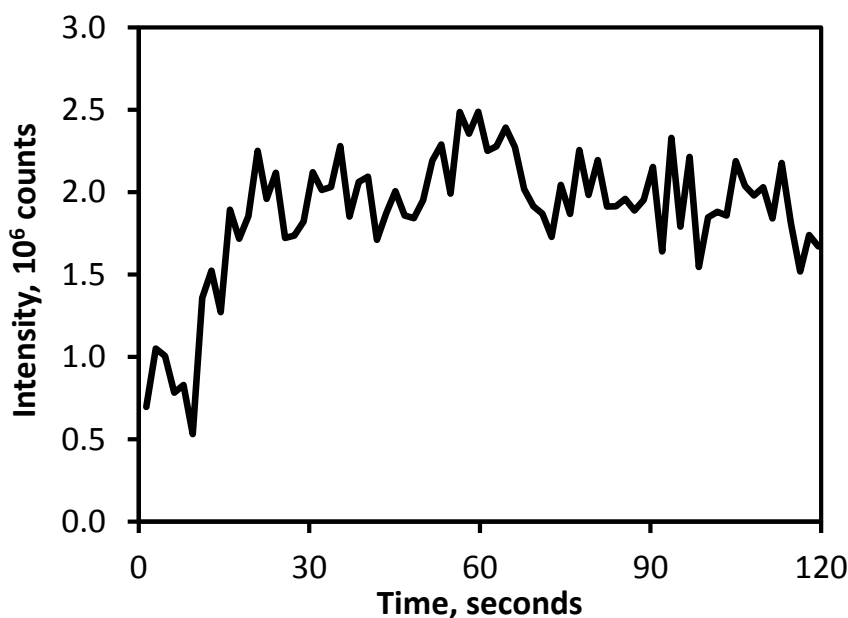
Figure 4.2. Ion chromatogram of the $[M-HCOOH+H]^+$ ion from valine, showing the signal becoming more stable after 20 seconds.

Generally, for measurements acquired using PADI, we have found that the standard deviation is approximately proportional to the average signal intensity. This shows that the noise is dominated by systematic effects such as instability in the plasma rather than random noise. This has important consequences for the future use of multivariate statistical analysis where an understanding of the noise distribution is essential for effective use [157]. It is also important for analytical purposes since the signal-to–noise ratio does not improve with increased acquisition time. Clearly, the source stability needs to be improved and new designs are being studied [78]. To improve the statistics in this study, 5 repeat measurements were acquired and an average taken, with the associated sample standard deviation used for the error bars in the figures.

We now use a thin film of valine on a glass slide as a model system to study the effects of geometrical parameters (z, y, θ) shown in Figure 4.1, the RF input power, P, and the sample temperature T. To investigate the effects of varying the helium flow rate, F, hydroxycitronellal and triethanolamine samples were used. Figure 4.3 (a) shows the positive ion mass spectrum from valine using the optimised parameters ($z = 2$ mm, $y = 7$ mm, $\theta = 0°$ and $P = 22$ W) identified later in the text. For comparison a mass spectrum of a blank glass slide, Figure 4.3 (b), is shown. As well as the protonated molecular ion, peaks corresponding to $[M-HCOOH+H]^+$, $[M-CH_2O+H]^+$ and $[M-H_2+H]^+$ are also detected from valine. The $[M-HCOOH+H]^+$ ion at m/z 72.0810 is a fragment that is commonly observed for valine. However, the other two fragments have not previously been recorded. These show that the plasma is not as soft an ionisation technique as DESI [129] and desorption atmospheric pressure

chemical ionization (DAPCI) [158] where only the protonated molecular ion is observed.   The protonated molecular ion as well as the fragment $[M-HCOOH+H]^+$ were detected from valine when analysed by DBDI [18]. Using the optimal geometric and power settings, and a data set of 10 repeat measurements, a repeatability of 2.3%, for $[M-CH_2O+H]^+$, and 7.2% for $[M+H]^+$ is obtainable.
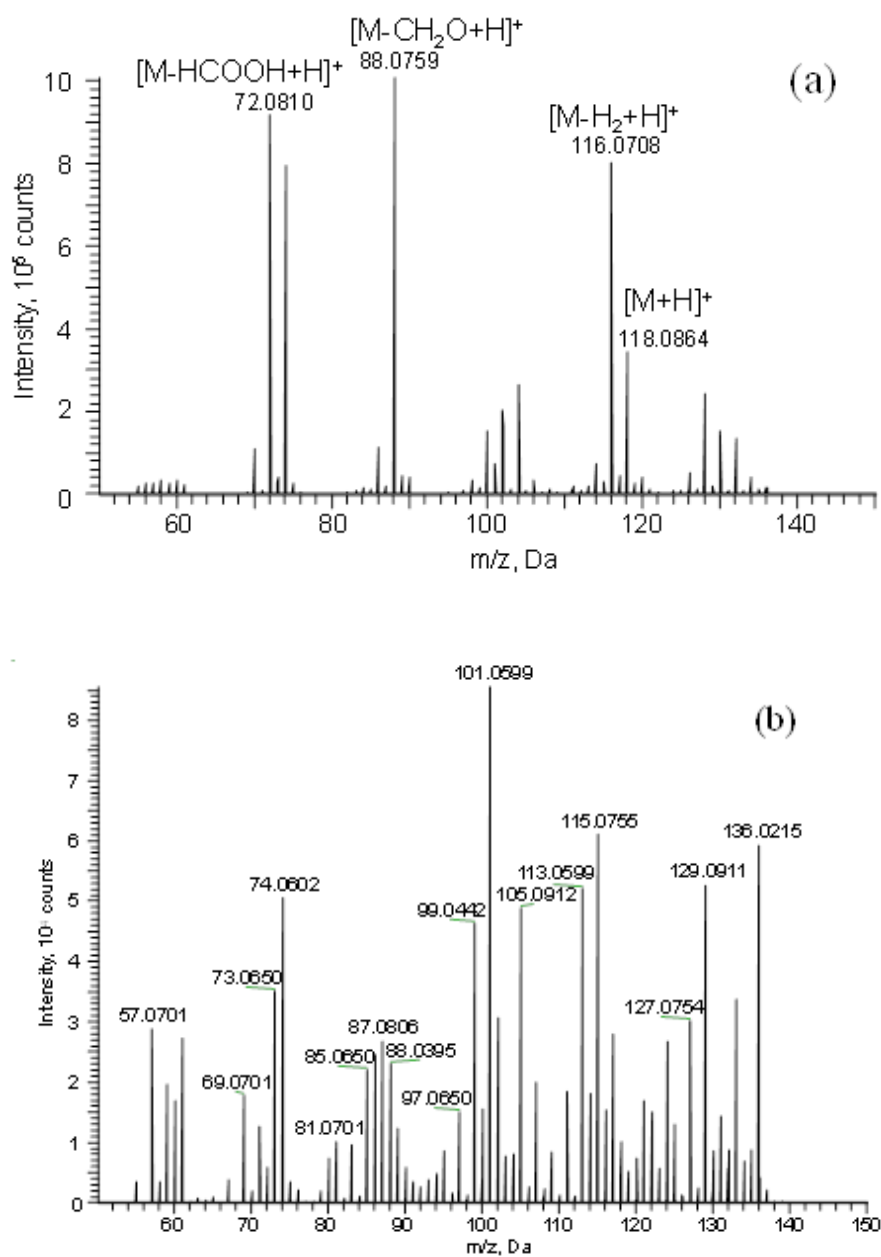
Figure 4.3. Positive ion mass spectra of (a) valine and (b) a blank glass slide using PADI-MS with $z =2$ mm, $y =7$ mm, $\theta = 0°$.

To investigate the effects of varying the helium flow rate on signal intensities, we monitored two molecules, hydroxycitronellal and triethanolamine. Figure 4.4 shows there is an increase in molecular ion intensity for the two molecules with increasing helium flow rate from 400 to 820 ml min^{-1} after which there is a decrease. The intensities are summed from the extracted ion chromatograms from 20 to 35 seconds after changing the power or flow rate conditions. Above 850 ml min^{-1}, the mass spectrometer had problems acquiring data for longer than 30 seconds due to the high gas flow saturating the mass analyser. The optimal helium flow rate is 820 ml min^{-1}, independent of the power used and the fragment analysed.
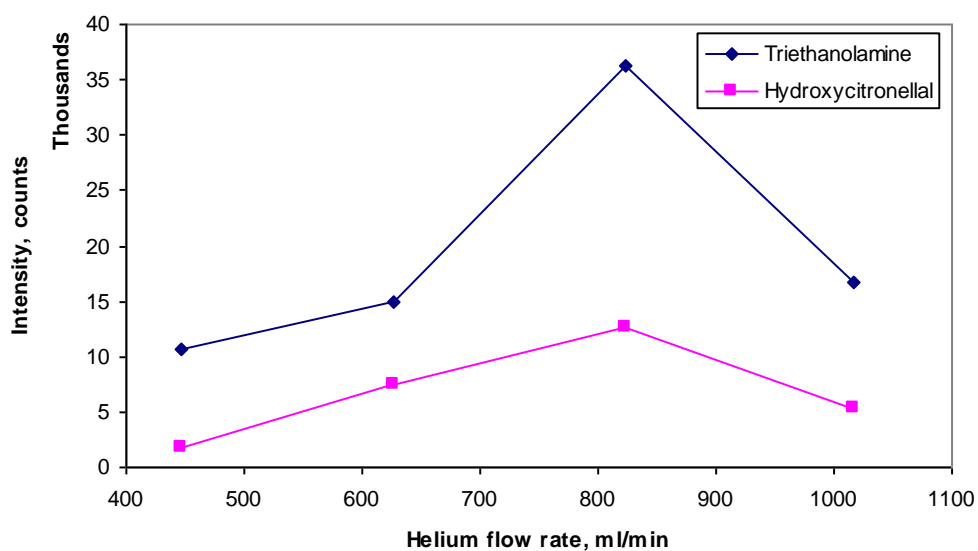
Figure 4.4. Intensity of the molecular ion peaks of triethanolamine and hydroxycitronellal using PADI-MS with power 22 W and varying helium flow rate.

Figure 4.5 (a) shows the effect of the vertical height, z, on the intensities of four ions from valine with the angle of incidence θ set at 0° (normal), and using $y = 7$ mm. For each ion the intensity increases as the plasma moves closer to the surface. When the plasma is closer to the surface it desorbs a larger amount

of material as can be seen from the images inset in Figure 4.5 (a); when $z = 0.5$ mm, the area desorbed in 2 minutes is 24.5 mm^2, whereas when $z = 2$ mm this area reduces to 0.6 mm^2 and when $z = 4$ mm this reduces again to 0.4 mm^2. We can work out the efficiency of analyte material transferred into useful signal by dividing the signal intensity by the amount of material desorbed from the corresponding experiment. From this we deduce that the optimal plasma height is $z = 2$ mm.

With $z = 2$ mm and $\theta = 0^o$ fixed we show in Figure 4.5 (b) the effect of the plasma to sniffer distance, y, on the spectral intensities. When the plasma is very close to the sniffer, the signal intensities are low. At such close range the plasma plume and afterglow are sucked into the sniffer. In addition, the sniffer is held at 0 V and this may affect the plasma characteristics. Later, we discuss how conducting substrates can greatly affect the mass spectrum. As the plasma moves away from the sniffer, intensities increase to a maximum at 7 mm after which they decrease again due to the ions not being efficiently collected into the spectrometer through the sniffer. A value of $y = 7$ mm is recommended.

The third geometric parameter to consider is the angle of the plasma to the surface normal, θ. Figure 4.5 (c) shows the effect of angle of incidence on the spectral intensities with the other parameters fixed at $z = 2$ mm and $y = 7$ mm. The effect of incidence angle does not appear to be strong but intensities are generally highest at $\theta = 0^o$ and so this value is recommended.
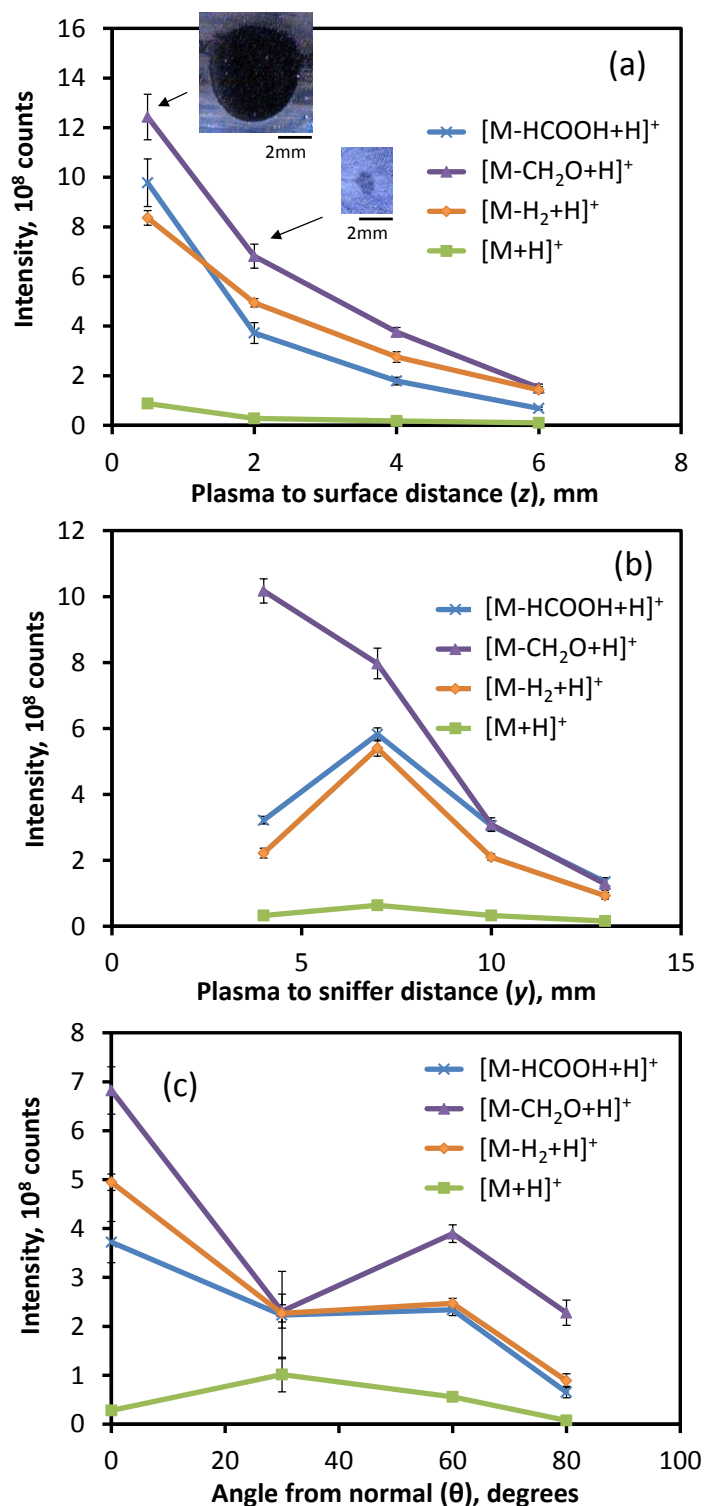
Figure 4.5. Variation of intensity of the $[M-HCOOH+H]^+$, $[M-CH_2O+H]^+$, $[M-H_2+H]^+$ and $[M+H]^+$ valine peaks with (a) z, the distance between the plasma and surface (inset are images of the erosion craters at $z = 0.5$ mm and 2 mm), (b) y, the distance between the plasma and sniffer, and (c) θ, the angle of the plasma from the normal. All the other parameters are kept constant, as defined in the text.

In Figure 4.6 (a), we show the effect of plasma power on the valine spectral intensities with the other parameters fixed at $z = 2$ mm, $y = 7$ mm and $\theta = 0^o$. This is the power from the RF generator and not the power on the end of the needle, which will be lower due to losses in the cable between the generator and needle. As can be seen from this figure, the intensity of all the ions starts low at 13 W and then increases as the power is increased. What is interesting is that the intensity of different ions peak at different powers, with $[M-CH_2O+H]^+$ reaching a maximum at 22 W. $[M-HCOOH+H]^+$ and $[M-H_2+H]^+$ both reach a peak at 25 W. The $[M+H]^+$ intensity is still rising at the maximum RF input power used, 28 W. Figures 4.6 (b) and (c) show the variation of triethanolamine and hydroxycitronellal with P. Similar behaviours to valine are observed for these molecules: generally, the intensities increase with RF power. However, some, the $[M+O-H_3]^+$ ion from hydroxycitronellal and the $[M-H_3O]^+$ ion from triethanolamine, decrease in intensity as the RF power is increased. This may be dependent on other parameters such as humidity. It should be noted that these samples were analysed using the QSTAR mass spectrometer.
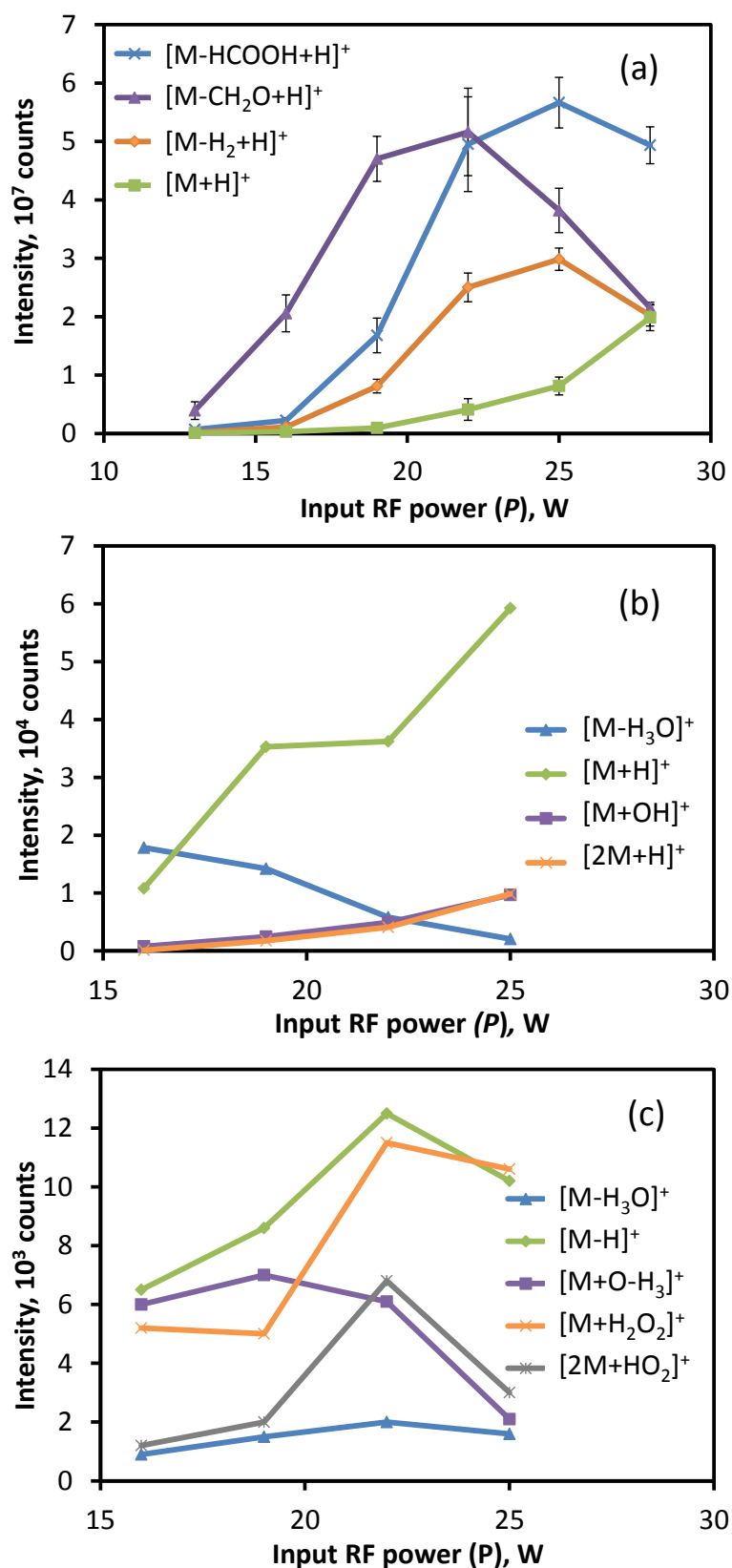
Figure 4.6. Effect of the variation of P, the input RF plasma power, on (a) intensity of the $[M-HCOOH+H]^+$, $[M-CH_2O+H]^+$, $[M-H_2+H]^+$ and $[M+H]^+$ valine peaks acquired using the Orbitrap™ MS, (b) intensities of $[M-H_3O]^+$,

$[M+H]^+$, $[M+OH]^+$ and $[2M+H]^+$ triethanolamine ions, and (c) $[M-H_3O]^+$, $[M-H]^+$, $[M+O-H_3]^+$, $[M+H_2O_2]^+$ and $[2M+HO_2]^+$ hydroxycitronellal ions acquired using the QSTAR MS. All the other parameters are kept constant, as defined in the text.

It is generally thought that desorption by plasma sources [28] occurs through thermal processes. We therefore measure the effect of plasma input power, P, on the valine sample and glass slide temperature using IR thermometry (as described earlier). All other parameters are set at the optimised settings as previously discussed. The ambient temperature of the glass substrate when the plasma is switched off is measured to be 24 ± 5 °C (the laboratory temperature is 22 °C). Figure 4.7 shows that there is an approximately linear increase in temperature with P similar to results reported for LTP [159]. A discontinuity is observed at around 17 W. At the lowest power setting used, 13 W where the plasma can only just be visibly seen, the temperature of the surface is 35 °C. For this study we went up to a maximum of 28 W which resulted in a surface temperature of 130 °C. All temperature measurements have errors of $\pm$ 5 °C due to the accuracy of the thermal imaging camera. Figure 4.8 (a) shows an example thermal image for $P = 18$ W with parts of the experimental arrangement labelled to assist orientation. The temperature distribution at the surface is approximately Gaussian with some asymmetry as the plasma is drawn in the direction of the sniffer. Line scans across the profile are shown in Figure 4.8 (b) for 13 W $\leq$ $P \leq$ 28 W. The FWHM is approximately constant at 3 mm diameter.
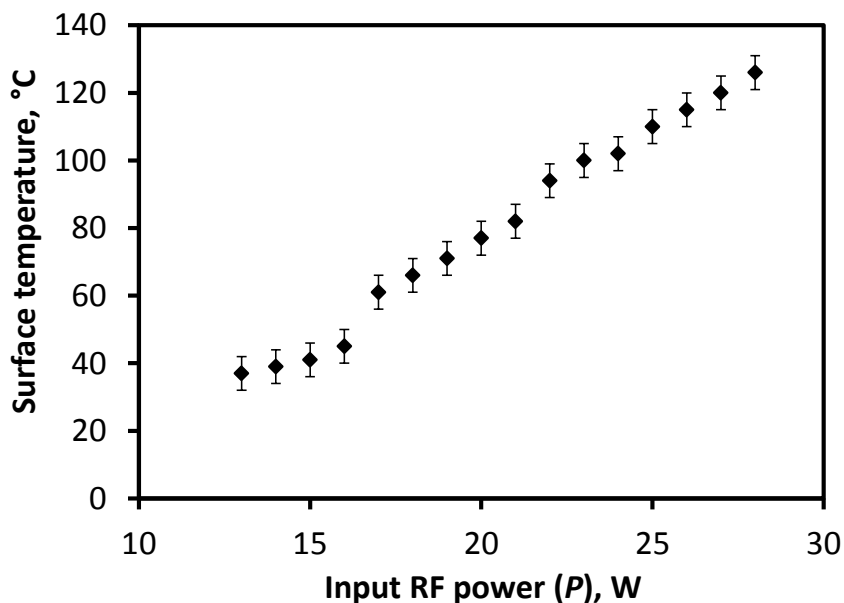
Figure 4.7. Variation of the temperature at the sample surface when changing the input RF plasma power, using optimal geometry settings.
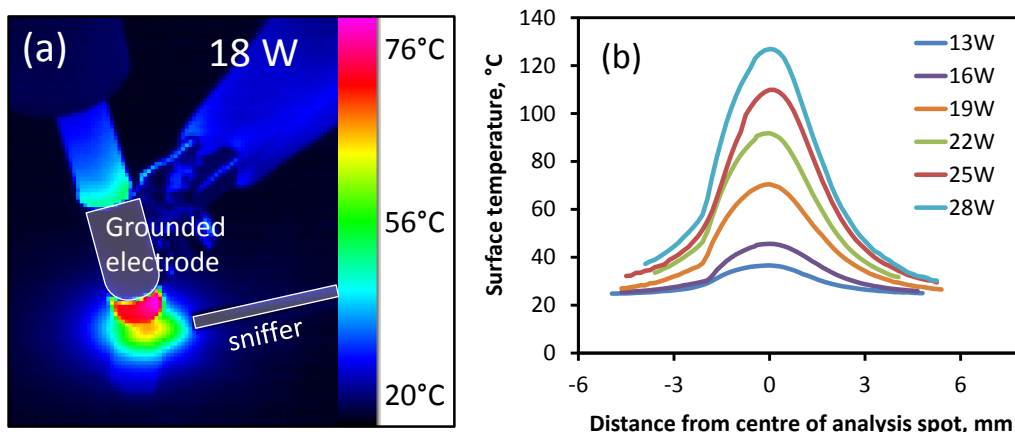
Figure 4.8. (a) Thermal image of plasma at a power setting of 18 W. (b) temperature linescans through the centre of the interaction area at the surface for different plasma powers.

In Figure 4.9 (a), we re-plot the data from Figure 4.6 (a) with a temperature scale calibrated from Figure 4.7. For delicate samples, such as biological material or thin polymer films it is important to keep the sample temperature low and therefore P should be limited to low powers although this results in a

much lower sensitivity, especially of the protonated molecular ion. Alternative methods, such as a pulsed plasma source may reduce the temperature without such a strong effect on sensitivity. An alternative approach is to use a plasma with a wider surface area such as the bundled arrays developed by Dalgleish *et al.* [159]. However, as we see later in Chapter 5, substances with low vapour pressure require heating of the sample for sufficient sensitivity and therefore minimal *P* could be beneficial.

To understand whether the changes in signal intensities with increasing power as shown in Figure 4.6 (a), are due directly to thermal desorption, experiments were performed using a heated sample stage. The temperature of the stage was varied from 35 to 100 °C. A power setting of 13 W was used which results in a surface temperature of 35 °C. Results from this experiment are shown in Figure 4.9 (b). At 13 W, the intensity of the $[M-CH_2O+H]^+$ valine ion remains more or less constant when the temperature of the stage is increased. The other valine ions all increase with intensity as the temperature of the sample stage increases. The $[M+H]^+$ ion shows the largest relative increase in intensity and it dominates the spectrum above 74 °C. It was observed with thermal imaging that when the sample stage is at a higher temperature than the plasma, the plasma effectively cools the sample so that the sampling spot is at a slightly lower temperature than the surrounding sample, but not as low as when the sample is not heated.
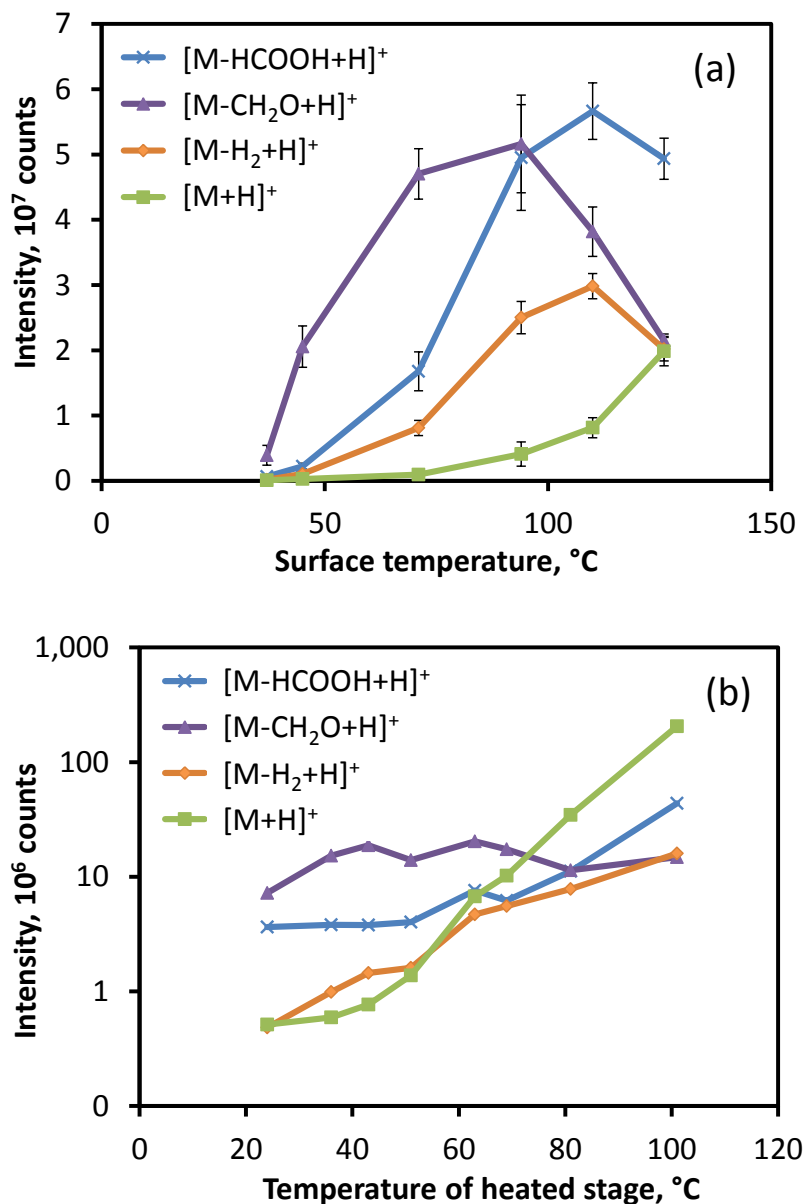
Figure 4.9. Variation of the signal intensity of different valine ions (a) when varying the input RF power, and (b) when using a heated sample stage with an input plasma power of 13 W.

Figures 4.9 (a) and (b) do not show the same degree of increasing intensities. Thermal desorption increases the signal intensity from all the valine ions except the $[M-CH_2O+H]^+$ ion. However, increasing the power, which also increases the temperature, has a more complicated effect on the ion intensities; this increases the intensity of all the valine ions up to a point, with different

ions reaching their maximum intensity at different powers. From this we tentatively summarise that desorption is principally by a thermal process and that the plasma power affects relative intensities through fragmentation and ionisation mechanisms. We later prove that sensitivity is directly proportional to vapour pressure.

4.3.2   Analysis of polymer substrates using PADI MS

As discussed earlier, the ability to analyse polymers in ambient conditions is of great benefit in industrial applications. Four polymers, PTFE, PMMA, PLA, PET, were analysed by PADI-MS using the optimal geometry settings from Section 4.3.1. Of the four polymers, ions were detected from PMMA and PLA in both positive and negative ion mode and from PET and PTFE only in the negative ion mode, as shown in Figures 4.10 to 4.13. The major ion series from each polymer in the positive and negative ion modes are displayed in Tables 4.1 and 4.2.

Initial experiments were made with thin films of polymer spun cast onto silicon wafer substrates, which is common for SIMS analysis. However, it was found that the conducting substrate affected the plasma and no ions were detected from the polymer even though erosion clearly occurred. When a glass substrate was used in place of the silicon then good mass spectra were acquired. This is an important effect that needs to be considered in the context of industrial samples, for example coatings on metal.

Non-thermal desorption can occur *via* electronic excitation. However, in metals and semiconductors, excitons (bound states of electron-hole pairs) have extremely short lifetimes of less than 100 attoseconds. This means they recombine too quickly to allow for effective desorption, leading to the inability to detect any ions from these substrates.

Below we give a brief explanation of the ion series observed for each polymer:

4.3.2.1   PTFE

The negative ion spectrum, shown in Figure 4.10, has four distinct ion series; $[CF + (CF_2)_n + O]^-$, $[C_2F + (CF_2)_n + O_3]^-$, $[CF + (CF_2)_n]^-$ and $[(CF_2)_n + C_2O_4H]^-$ with the latter dominating above *m/z* 500. We were able to detect polymer fragments up to *m/z* 1200; this is higher than those reported previously which only reached *m/z* 900 [78]. The mass spectrum is similar to that obtained previously with PADI [78], with the same ion series detected, although the ion intensity distribution is slightly different; this could be due to the different settings that were used for the two experiments. Thermal processes alone cannot be responsible for the desorption of such large fragments of polymer. It seems likely that bond cleavage followed by adduct ionisation is responsible. We were not able to detect any ions from PTFE in the positive ion mode, however positive ions have been observed when using glow discharge mass spectrometry [160].
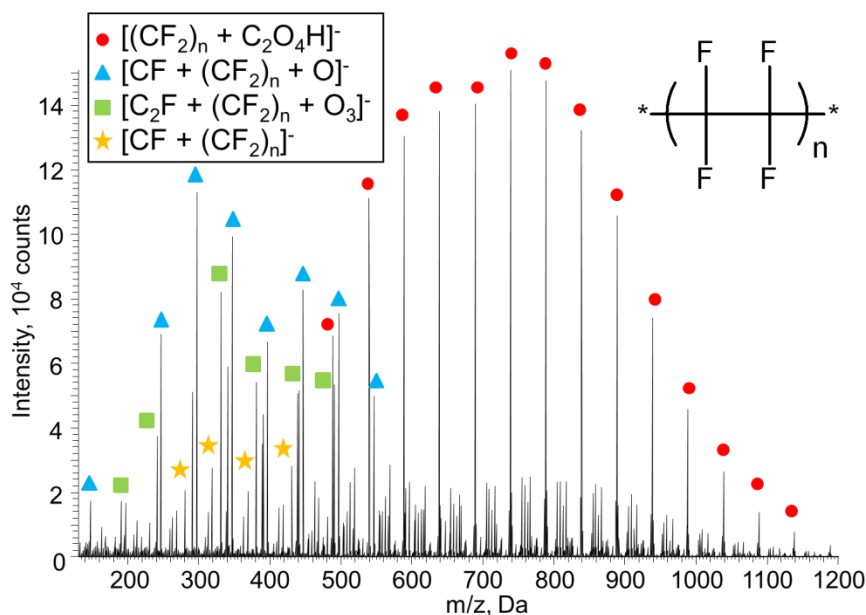
Figure 4.10. Negative ion mass spectrum of poly tetraflurorethylene (PTFE) using PADI-MS. Inset is the structure of PTFE. The PADI settings used are the optimal ones described in Section 4.3.1.

4.3.2.2 PMMA

Positive ions were detected in the range m/z $300 - 500$ as shown in Figure 4.11 (a) with fragments series with between 3 and 5 monomer units identified. It appears that bond scission occurs with the loss of C_xH_y from possibly both ends of the fragment with subsequent ionisation by an oxygen adduct. The negative ion spectrum is populated with fragment ions up to approximately m/z 600, as shown in Figure 4.11 (b). The ions detected in the negative ion mode also show that the polymer has undergone bond scission and large amounts of oxygen adducts are also observed. Positively charged polymer fragments with oxygen adducts have previously been reported [153] for atmospheric plasma mass spectrometry. In the negative ion mode there are many peaks detected. These are in repeating series consisting of 2-3 peaks, separated by CH_2 or O. These

peaks are commonly polymer fragments that have lost odd numbers of hydrogen atoms (H, H_3, H_5 or H_7) and gained oxygen (O_2, O_3 up to O_7). For convenience of display without clutter, only selected ions have been labelled in Figure 4.11 and included in Table 4.2.
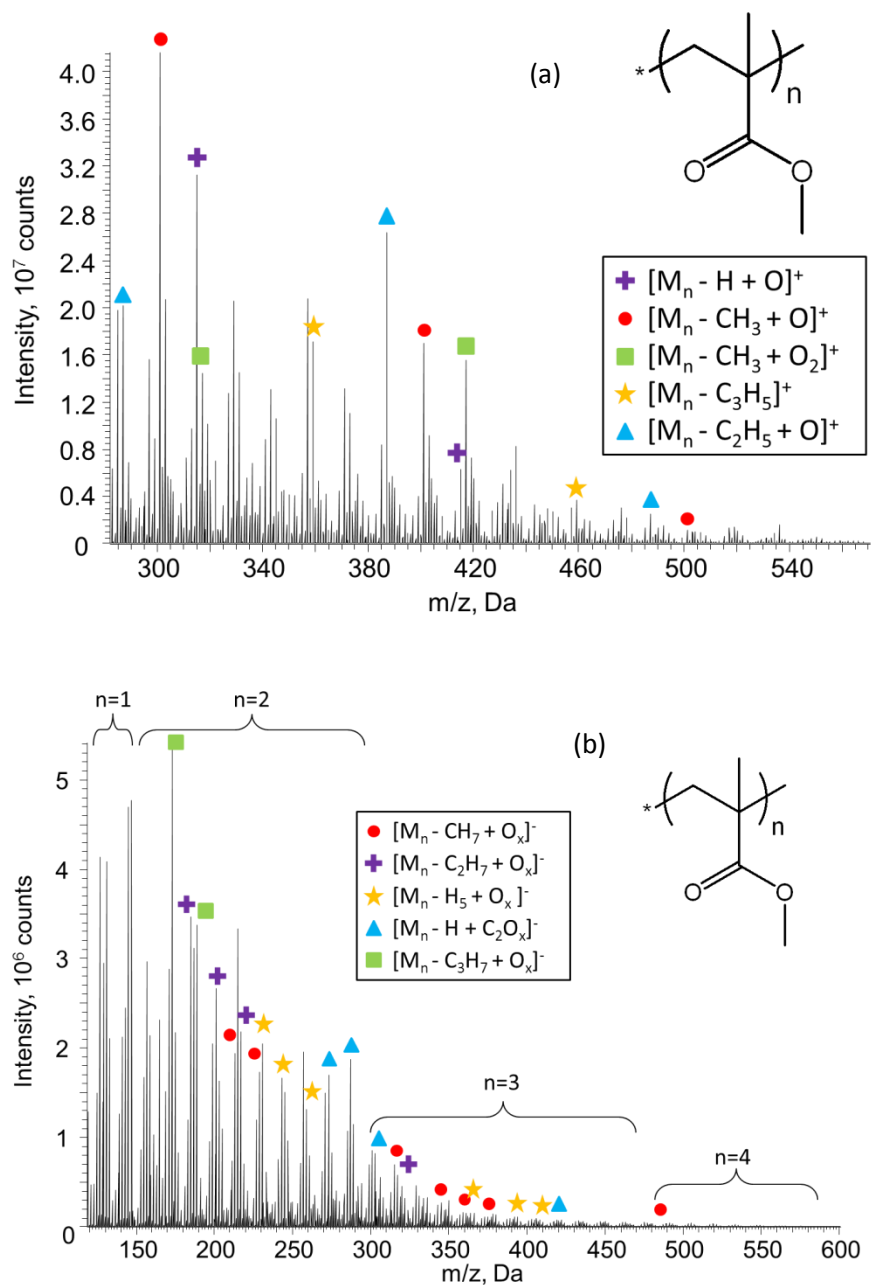
Figure 4.11. (a) Positive ion mass spectrum and (b) negative ion mass spectrum of poly methyl methacrylate (PMMA) using PADI-MS. Inset is the structure of PMMA. The PADI settings used are the optimal ones described in Section 4.3.1.

4.3.2.3   PLA

Characteristic mass spectra are observed in both positive and negative ion polarities as shown in Figure 4.12 with ions consisting of up to 6 repeat units detected. We again observe the addition of oxygen and the loss of hydrogen in the negative ion mode. In the positive ion mode the ions typically contain nitrogen adducts.
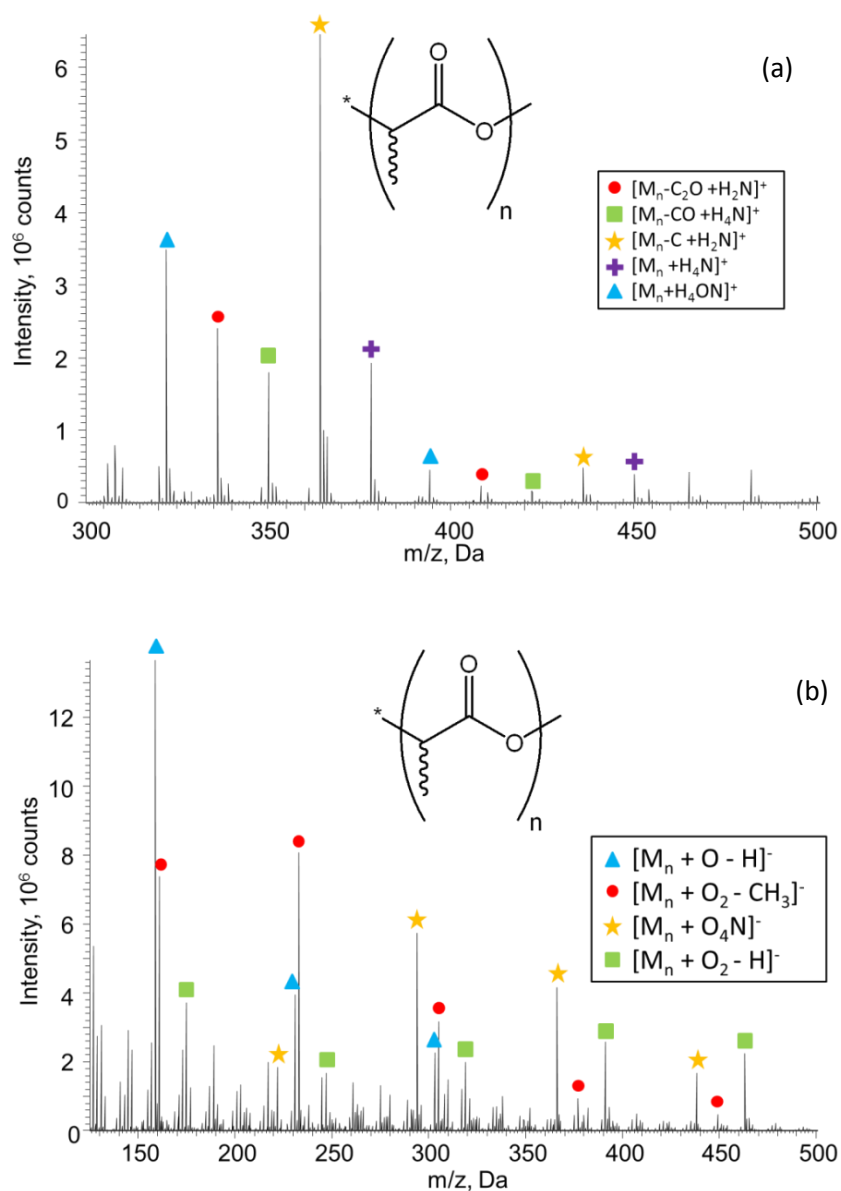
Figure 4.12. Mass spectra of poly(lactic acid) (PLA) using PADI-MS (a) positive ion mode and (b) negative ion mode. Inset is the structure of PLA. The PADI settings used are the optimal ones described in Section 4.3.1.

4.3.2.4 PET

Again, like PMMA and PLA, the same trend is observed in the negative ion mode: excess of oxygen and the loss of H or CH_3. Ions were only detected in the negative ion mode; this is in contrast to Jecklin *et al.* [79] who detected ions from PET in the positive ion mode using the FA-APGD.
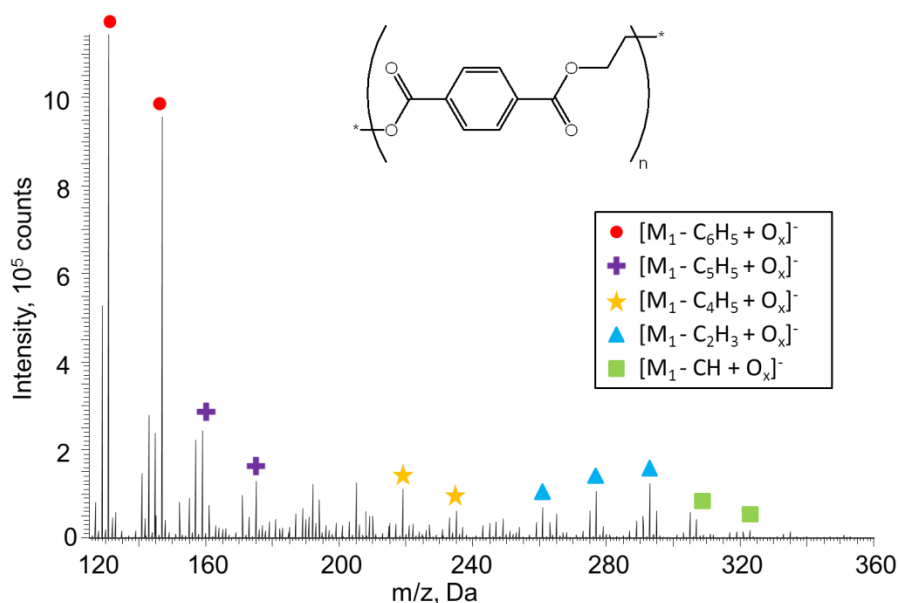
Figure 4.13. Negative ion mass spectrum of poly(ethylene terephthalate) (PET) using PADI-MS. Inset is the structure of PET. The PADI settings used are the optimal ones described in Section 4.3.1.

Table 4.1. Ions detected in the positive ion mode from PMMA and PLA

PMMA			PLA		
Ion	n	Mass	Ion	n	Mass
$M_n - H + O$	3	315.1451	$M_n-C_2O +H_2N$	4	264.1088
	4	415.1980		5	336.1295
$M_n - CH_3 + O$	3	301.1295	$M_n-C +H_2N$	3	220.0817
	4	401.1823		4	292.1027
	5	501.2350		5	364.1244
$M_n - CH_3 + O_2$	3	317.1245	M_n+H_4N	4	306.1196
	4	417.1772		5	378.1401
	5	517.2300		6	450.1614
$M_n - C_3H_5$	4	359.1715	$M_n-CO +H_4N$	3	206.1031
	5	459.2243		5	350.1452
$M_n - C_2H_5 + O$	3	287.1137	M_n+H_4ON	2	178.0715
	4	387.1665		3	250.0923
	5	487.2193		4	322.1139
				5	394.1351

Table 4.2. Ions detected in the negative ion mode from PTFE, PMMA, PLA and PET

PTFE			PMMA			
Ion	n	Mass	Ion	n	x	Mass
$(CF_2)_n+C_2O_4H$	8	488.9625	$M_n-C_3H_9+O_x$	2	2	187.025
	9	538.9593			3	203.0199
	...	....	$M_n-C_3H_7+O_x$	2	1	173.0456
	20	1088.9232			2	189.0406
	21	1138.9198				
$CF+(CF_2)_n+O$	4	246.9811	$M_n-CH_7+O_x$	2	2	213.0407
	...	...			3	229.0357
	9	496.9651		3	3	329.0878
	10	546.9619			4	345.0827
					5	361.0782
					6	377.0731
				4	6	477.1256
$C_2F+(CF_2)_n+O_3$	2	190.9771	$M_n-C_2H_7+O_x$	2	1	185.0457
	3	240.9741			2	201.0406
	...	...			3	217.0356
	9	540.9550		3	3	317.0822
$CF+(CF_2)_n$	5	280.9830	$M_n-H_5+O_x$	2	2	227.0564
	6	330.9798			3	243.0514
	...	...			4	259.0464
	9	480.9701		3	4	359.0989
					6	391.0887
					7	407.0835
$F+(CF_2)_n$	5	268.9830	$M_n-H+C_2O_x$	2	3	271.0828
	6	318.9798			4	287.0778
	...	...			5	303.0726
	13	668.9573		3	6	419.1201
$CF+(CF_2)_n+O_2$	3	212.9791	$M_n-H_3+C_2O_x$	2	4	285.0621
	4	262.9760			5	301.0566
	...	...		3	7	433.0993
	12	662.9504			8	449.0942
$F+(CF_2)_n+O_3$	9	516.9531	$M_n-H_5+CO_x$	3	7	419.0837
	...	...			8	435.0786
	18	966.9201		4	7	519.1359
			$M_n-H_3+C_3O_x$	4	8	561.1465

PLA			PET	
Ion	n	Mass	Ion	Mass
M_n+O-H	1	87.0081	$M_1-C_6H_5 +O_x$	130.9981
	2	159.0294	(x=1,2)	146.9932
	3	231.0510		
	4	303.0722	$M_1-C_5H_5 +O_x$	158.993
	5	375.0932	(x=2,3)	174.988
M_n+O_2-H	2	175.0246	$M_1-C_4H_5 +O_x$	218.9778
	3	247.0459	(x=5,6)	234.9727
	4	319.0670		
	5	391.0882		
	6	463.1093		
$M_n+O_2-CH_3$	2	161.0087	$M_1-C_2H_3 +O_x$	260.9885
	3	233.0302	(x=6,7,8)	276.9833
	4	305.0515		292.9783
	5	377.0725		
	6	449.0936		
M_n+O_4N	2	222.0251	$M_1-CH +O_x$	306.9944
	3	294.0467	(x=8,9)	322.9887
	4	366.0677	M_1-H+O_x (x=9,10)	334.9887
	5	438.0888		350.9835

The polymers were analysed using a range of RF powers, from 13 to 28 W, to see the effects on fragmentation and sensitivity. For this, the polymers were only analysed in the negative ion mode and a fresh spot on the polymer sample was analysed each time. An example for PMMA is shown in Figure 4.14. Here, the ion intensity is very low at 13 W and then it increases as the power increases. The initial rise occurs between 16 and 22 W dependent on the size of the fragment with smaller fragments increasing at lower powers, 16 W, and larger fragments beginning to increase in intensity at 22 W. Similar behaviours were observed for the other materials with signal intensities rising with RF power and larger ions requiring higher powers for detection. We summarise this behaviour for each material in Figure 4.15 by plotting the power required to achieve 50% of the maximum intensity against the mass of each ion. The data are compressed around 25 W as our maximum power used was 28 W but

the trends are clear. It is clear that RF powers > 23 W are required to detect higher mass ions. This is equivalent to a surface temperature of approximately 100 ^{o}C.
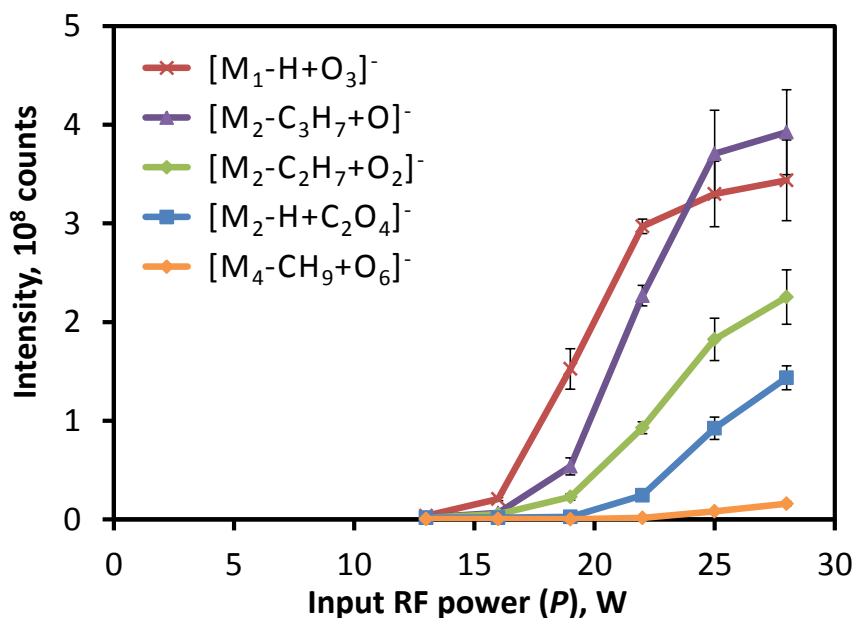
Figure 4.14. Variation of signal intensities for five PMMA ions analysed in the negative ion mode, with changing plasma power. The PADI geometry settings used are the optimal ones described in Section 4.3.1.

The glass transition temperatures of the four polymers are 117 °C, 105 °C, 60 °C and 72 °C for PTFE, PMMA, PLA and PET respectively. However, the melting temperatures of all four polymers are above 150 °C and therefore the power needs to be kept below 28 W.
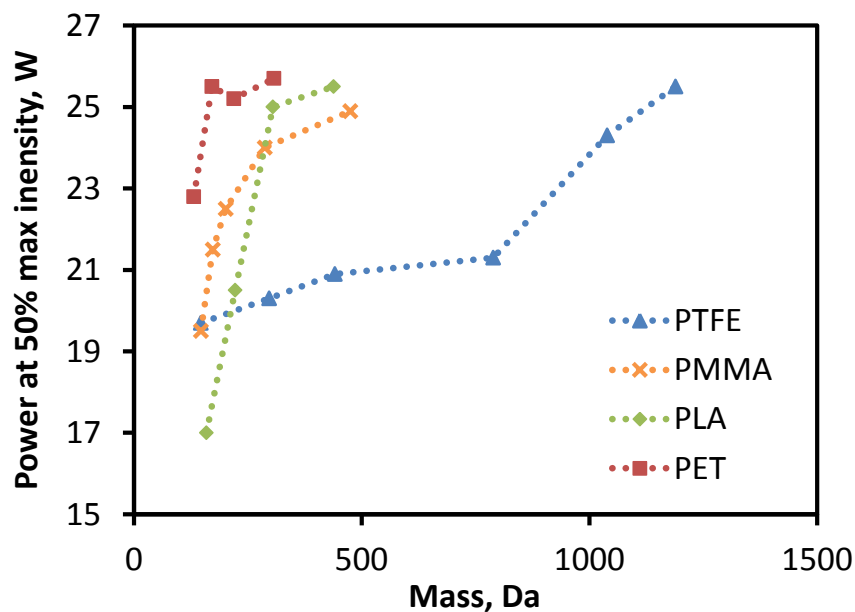
Figure 4.15. Plasma power at which ions of different mass reach 50% of their maximum intensity for the four polymers analysed, in negative ion mode.

4.4   Conclusions

In this study we use a model system of a valine overlayer on glass to investigate the effects of the principal parameters on the spectral intensity; namely the plasma to surface distance, z, plasma to "sniffer" distance, y, the angle of the plasma from the surface normal, θ and the RF power, P. We recommend values of $z = 2$ mm, $y = 7$ mm and $\theta = 0^{o}$ for this particular experimental system. The power, P, significantly affects the absolute and relative ion intensities with the protonated molecular ion maximising at higher plasma powers than other fragment ions. Control of P could be used to select the amount of fragmentation in the spectrum with, counter-intuitively, less fragmentation at higher P. The temperature of the surface in contact with the plasma is measured using thermal imaging. This shows an approximately

Gaussian distribution at the surface with a full-width at half-maximum of approximately 3 mm, which is independent of plasma power. The surface temperature is shown to increase approximately linearly with P, and at 25 W is equal to 110 ^{o}C. We show, using a temperature controlled stage and a low value of P equivalent to a surface temperature of 35 ^{o}C, that the behaviour of signal intensities with P does not result simply from surface heating alone but must be caused by other plasma mechanisms.

The relative standard deviation of the signal intensities is found to be approximately 7% which results from the PADI source and not the mass spectrometer. Improvements to the design are being developed to achieve better stability, which is necessary for analytical use.

We demonstrate the effectiveness of PADI for the analysis of four industrially relevant polymers: PTFE, PMMA, PLA and PET. Characteristic "fingerprint" mass spectra are detected, generated through bond-cleavage and oxidation mechanisms. We postulate that the mechanism is firstly a bond scission process followed by thermal desorption. The spectra are interpreted using the high mass accuracy (< 3 ppm) and mass resolution (~100,000) of the Orbitrap™ mass spectrometer and the key peaks tabulated for reference. We show that the size of the emitted ions depends on P with larger fragments at higher values. This behaviour is similar for each of the four polymers and generally $P > 23$ W is required for the analysis of larger fragment ions though care needs to be taken not to exceed the melting point of the polymer.

Chapter 5

The importance of sample form and surface temperature for analysis by PADI

5.1   Introduction

In the previous chapter, results were presented on the optimisation of PADI. It was found that sample temperature is an important parameter and we now study this in depth as well as the effect of sample form. Many different types of samples have been analysed in the literature using plasma based ambient mass spectrometry sources, however, comprehensive studies of the important parameters for analysis are only just beginning. Here we investigate the effect of the sample form and surface temperature on the signal intensities in plasma assisted desorption ionisation (PADI).

It has been observed that molecules of lower volatility are more difficult to analyse using plasma-based techniques. There are generally two different routes to enhance the desorption and/or ionisation of these analytes, although most of these methods involve increasing the temperature of the sample. The first of these routes is integral to the source design; in DART, the carrier gas can be heated up to 500 °C and is typically operated at 200 °C, which facilitates the desorption of many types of analyte. Desorption corona beam

ionisation, DCBI, also uses a heater to increase the helium gas temperature up to 450 °C; generally a temperature of at least 150 °C is required for successful analysis indicating that thermal desorption plays a major role [83]. It has been shown that the separation of compounds due to their volatility can be achieved by steadily increasing the temperature of the gas [83], and this has also been shown using DART [161]. Other plasma sources, such as the microwave-induced plasma desorption/ionisation source, MIPDI [57], increase the sample temperature by increasing the power of the plasma. However, sources such as the LTP are generally limited to much lower temperatures, typically 30 °C [20], therefore additional means are required to enhance the desorption. Several groups have reported combining LTP with sample substrate heating to enhance desorption for *e.g.* drugs of abuse [62] where the limit of detection was improved by at least an order of magnitude when the sample was heated to *ca.* 100 °C. The detection of explosives has proved difficult using the conventional LTP source; increasing the sample temperature using a heat gun [50] or localised heating of the sample using a non-contact halogen lamp [64] have enhanced the sensitivity for the detection of explosives, PETN, TNT, RDX, HMX and tetryl. Sample heating has also improved the analysis of petroleum crude oil samples [63]. In the DART source, although there is integral heating through the carrier gas, a method has been developed to rapidly vaporise samples using a heated metal sample grid [162], which provides a temperature rise to 350 °C in less than 15 seconds. Two additional desorption methods, a continuous-wave diode laser and a heating block, used in conjunction with the DBDI plasma jet, were compared for the analysis of non-volatile compounds [75]. When analysing a range of pharmaceuticals and pesticides, the analyte

response was almost always greater when using the diode laser rather than the heated substrate. Other thermally assisted methods exist, such as Leidenfrost phenomenon-assisted thermal desorption (LPTD) coupled to DBDI [163]. This has been used to analyse non-volatile molecules morphine, cocaine, therapeutic drugs, melamine and a peptide. Flash desorption has also been used in conjunction with DBDI [61]. Here, a filament delivers a high temperature for a very short time to the sample to desorb it. The addition of 0.9% hydrogen to the helium gas used in a DBDI plasma was also shown to increase signal intensities by a factor of 10 for caffeine [164], although this improvement in desorption is presumed to be from non-thermal mechanisms.

The physical state of the analyte for ambient plasma analysis has not been as thoroughly investigated. Gases, liquids and solids have all been analysed but authors have been less specific about how the form of the sample affects analysis. However, recent studies by Chan and Nah [165, 166] have shown that when analysing submicron organic aerosols, the particle size, and most importantly surface area, have an effect on the relative signal intensities, with smaller particles having a higher relative signal intensity.

From the literature, we can see that volatility and thermal desorption can play an important role in ambient mass spectrometry. Conversely, mass spectrometry has also been used to measure the vapour pressure and heat of sublimation values of several dicarboxylic acids using the atmospheric solids analysis probe (ASAP) [167]. This utilises the mass spectral intensities to

measure the evaporation rate of the molecule when increasing the analysis temperature.

Here we investigate two different aspects that are important for PADI analysis, namely the sample form and the effect of additional sample heating.

The objectives of this chapter are:

- To understand how signal intensities vary with vapour pressure, for samples in both powder and thin film form.
- To enhance signal intensities using thermal desorption, especially for the analysis of molecules with lower vapour pressures.

5.2   Experimental Section

5.2.1 Samples

Samples in the solid form of methyl paraben, stearic acid, phenylalanine, cholesterol, leucine, (Sigma Aldrich, Poole, UK), Irganox 1098 and Irganox 3114 (CIBA, Macclesfield, UK), were prepared as thin films or as powder on glass slides. The thin film samples were prepared from a solution consisting of between 2 and 15 mg ml^{-1} and several 2 μl aliquots were deposited onto cleaned glass slides (Superfrost, Thermo Fisher, UK) and left to dry at room temperature. This resulted in a thin film of the molecule on the glass slide. The time dependence of selected mass fragments shows no dramatic decrease within the analysis time, indicating that we are not consuming the entire dried aliquot. We can therefore be sure that the differences observed in the intensities

that are discussed in the results section are not a result of varying amount of substance. Powder samples were prepared by placing the as received powder on to double-sided sellotape, itself placed on a glass slide. This is to stop the powder being blown around the surface by the PADI gas flow. The powder samples had a uniform coverage of greater than 90% on the surface measured by optical microscopy. The powders had a wide distribution of particle sizes, between 2 and 200 μm, dependent on the analyte; for Irganox 1098 and Irganox 3114 the sizes were between approximately 2 and 20 μm and for the other analytes the sizes were between approximately 20 and 200 μm. The size distribution is non-uniform and includes crystals and agglomerates. These ranges of particle sizes were determined using optical microscope images of fresh samples. Liquid samples of geraniol (Sigma Aldrich, Poole, UK), benzyl salicylate, triethanolamine and linoleic acid (Alfa Aesar, Heysham, UK) were also prepared into solutions and deposited onto glass slides.

5.2.2 PADI

The PADI set up is explained in detail in the previous chapter [168]. The power setting used for all the experiments in this chapter is 13 W. Helium gas, 99.996% pure (BOC, Guildford, UK), is used as the discharge gas. The helium flow rate is controlled *via* a flowmeter (Cole-Parmer, London, UK), and a flow rate of 820 ml min^{-1} was used [156]. This generates a plasma region that extends up to 2 mm from the tip.

5.2.3 Mass spectrometer

A Thermo Scientific LTQ-Orbitrap™ Velos mass spectrometer was used in both positive and negative ion modes. MS^2 and MS^3 were used to confirm the identity of ions where necessary. The mass spectrometer was programmed to collect up to a maximum Orbitrap™ injection time of 500 ms, using an AGC (automatic gain control) setting of 5×10^5. All data were acquired using the Orbitrap™ mode with the highest resolution setting of 100,000 (at *m/z* 400). The capillary temperature was set to 200 °C. The standard ion transfer tube was replaced with an extended version. Samples were placed on a 2-axis stage (Prosolia, Indianapolis, IN, USA). All data were recorded after the plasma was switched on for 1 minute. Mass spectra were acquired for 1 minute and all data plotted are for the integrated signal over this time interval. Three repeat measurements were taken for each data point.

5.2.4 Temperature measurements

Thermal imaging of the plasma system was performed using a FLIR systems InfraCAM thermal imager (West Malling, Kent, UK). The measurements discussed in the results section are the temperature at the centre of the analysis spot on the surface, which is also where the temperature was highest. Data acquired from the camera were analysed using FLIR systems ThermaCAM^{TM} Researcher Pro 2.9 software. The emissivity of the glass sample (0.92) was taken into consideration when calculating the temperature. The same heated sample stage discussed in Chapter 4 was used.

5.3   Results and discussion

5.3.1 The importance of sample form

As mentioned in the introduction, many different molecules have been analysed in the past by ambient plasma mass spectrometry, some of these were very successful; however there are certain classes of molecules that have not been analysed with success. It is vital to understand what types of molecules can be analysed effectively by PADI and the important parameters for this analysis. One of these is the form of the sample. We have observed that it is possible to get signal from a variety of analytes when they are in powder form, even at low plasma power. However when the same molecules are deposited in a thin film on a glass slide, either by thermal evaporation or deposited aliquots, then it is sometimes difficult to detect any characteristic ions. Since this is clearly a major issue for an analytical technique we conducted a systematic study.

PADI mass spectra were acquired from the solids in Table 5.1 as both thin film and powder samples. A low plasma power, 13 W, was used which corresponds to a surface temperature of approximately 37 °C. Figure 5.1 (a) shows the signal intensity for a characteristic ion, given in Table 5.1, for the thin film and powders as a function of the vapour pressure of the molecule, at 25 °C, on a log-log scale. The signal intensity plotted is the integrated signal for 60 s. Firstly, it is clear that there is an approximately power law relationship between the intensity, I, and the room temperature vapour pressure, V_{25}, given

in Equation 5.1. This strongly indicates that thermal desorption will be necessary to achieve reasonable signal intensities from low vapour pressure substances.

$$I = AV_{25}{}^{b} \qquad (5.1)$$

For powders A= 2.35 × 10^8 counts Pa^{-1}, b = 0.28, for thin films A= 5.32 × 10^7 counts Pa^{-1}, b = 0.52. It should be noted that the power law relation for thin films excludes cholesterol, point H in Figure 5.1 (a). An explanation of the relatively low intensity of cholesterol is given later. Secondly, it is clear that the signal intensity is significantly higher for powders than for thin films. The enhancement increases with reducing vapour pressure and is 5000 for Irganox 3114 (K). For typical analytical conditions, approximately 10^5 counts integrated over 1 minute acquisition are required to give a sufficiently good quality spectrum. With this condition, it means that only substances with a vapour pressure greater than 10^{-4} Pa can be analysed as thin films. However, all the substances in Table 5.1 could be successfully analysed in the powder form. In these samples, the range of powder sizes is large, between 2 µm and 200 µm as noted in the experimental section, with the Irganox powders being the smallest (2 to 20 µm). Even though their sizes and range are much smaller, data for the Irganox powders are still included as they have a much lower vapour pressure than the other molecules analysed. It is possible that the surface area of the powder may affect the signal intensity, but we are not able to deduce a correlation from this data between particle size and the signal intensities observed in Figure 5.1 (a). A more detailed study of how the particle size affects the signal intensity will be part of a further investigation.

Table 5.1. Molecules analysed in this study and their physical properties

Molecule	Label in figures	Monoisotopic mass, Da	Vapour pressure, Pa at 25 °C (V_{25})	Sample form at room temperature, 25 °C	Characteristic ion used in this study
Geraniol	A	154.1358	4.00 [a]	Liquid	$[M-H]^+$
Methylparaben	B	152.0473	0.11 [b]	Solid	$[M+H]^+$
Benzyl salicylate	C	228.0786	2.40×10^{-3} [b]	Liquid	$[M+H]^+$
Triethanolamine	D	149.1052	4.79×10^{-4} [a]	Liquid	$[M+H]^+$
Linoleic acid	E	280.2402	1.16×10^{-4} [a]	Liquid	$[M-H]^+$
Stearic acid	F	284.2715	9.63×10^{-5} [a]	Solid	$[M-H]^-$
Phenylalanine	G	165.0790	3.49×10^{-5} [b]	Solid	$[M+H]^+$
Cholesterol	H	386.3549	2.39×10^{-5} [b]	Solid	$[M-OH]^+$
Leucine	I	131.0946	7.36×10^{-7} [b]	Solid	$[M+H]^+$
Irganox 1098	J	636.4866	1.20×10^{-12} [c]	Solid	$[M+H]^+$
Irganox 3114	K	783.5186	7.00×10^{-13} [c]	Solid	$[M+H]^+$

Notes: [a] experimental database value, [b] calculated using the modified Grain method, [c] from technical datasheet

Figure 5.1 (b) shows the ratio of intensity in powder to thin film form as a function of the vapour pressure at 25 °C on a log scale. The molecules that have higher vapour pressure, such as methyl paraben (B) (vapour pressure 0.11 Pa) have very similar signal intensities in the two forms. However, as the vapour pressure of the molecule decreases the ratio of the signal intensity of the powder and the thin film starts to increase dramatically. Generally an enhancement of greater than 10^2 is observed. This ratio is always greater than 1 as the signal intensity for the powders is always higher than that of the thin films. Interestingly, cholesterol has a much greater signal enhancement; the signal intensity is over 10^5 times greater than thin film form. From Figure 5.1 (a) it is clear that the signal intensity for cholesterol in thin film form is around 10^3 times lower than would generally be expected for molecules with this vapour pressure. It would appear that the change in substance form has recovered this signal.
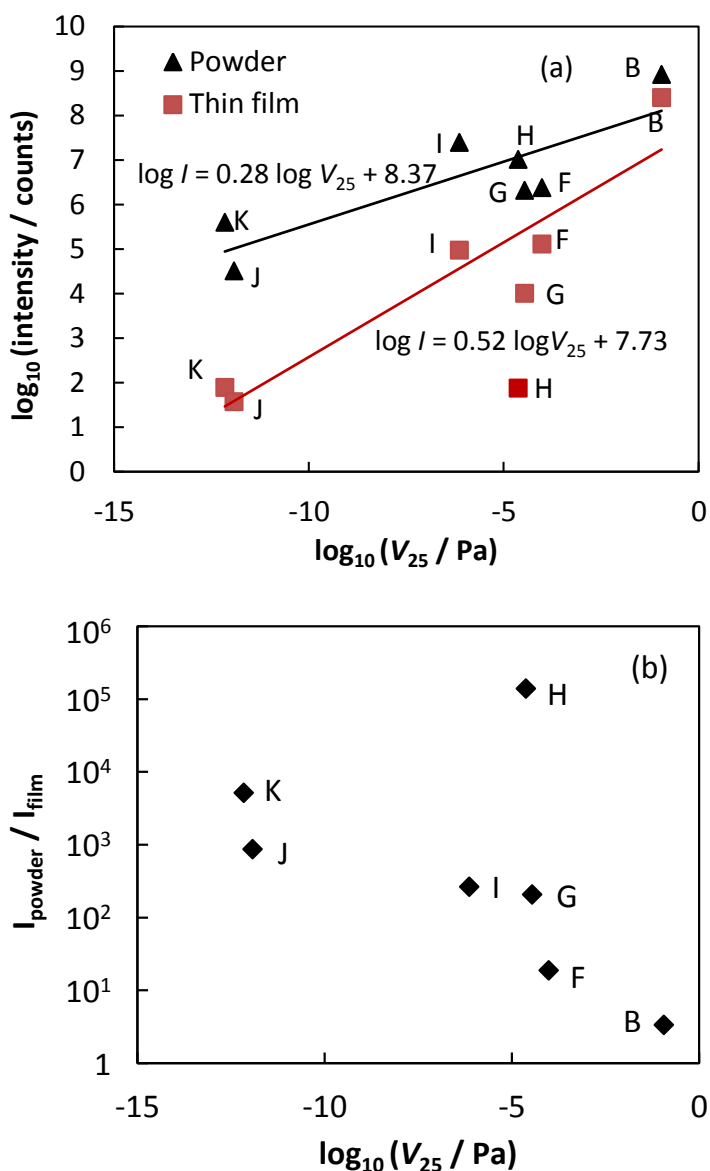
Figure 5.1. (a) Variation of the signal intensity, integrated over 60 s, for a series of molecules with differing vapour pressures analysed at room temperature as thin films (squares) and powder (triangle). The molecules are labelled as indicated in Table 5.1. Vapour pressures quoted are at 25 °C and are listed in Table 5.1. Fits to the points are made using a power law given by Equation 5.1. *N.B.* the fit for the thin film excludes cholesterol (H). (b) Ratio of the intensity for substances in powder and thin film form at room temperature.

The strong effect of vapour pressure on the signal intensity indicates that the principal desorption mechanism is likely to be thermal and we investigate this

effect in more detail later. It is therefore expected that powders, as they have a much higher surface area, heat up more rapidly and there is also a larger amount of surface molecules that can be desorbed. A similar result was observed by Chan *et al.*[165]; firstly, that the signal intensity from aerosols increases with decreasing size when analysing with the same DART gas temperature; and secondly, that the intensity increases when the vapour pressure of the aerosol is also increased when analysing at a given gas temperature.

The vapour pressure, or pressure difference Δp, can be correlated to the radius of a particle *via* the Young-Laplace equation:

$$\Delta p = \frac{2\gamma}{r} \qquad (5.2)$$

Where r is the radius of a particle and γ is the surface tension. Equation 5.1 describes how the signal intensity is proportional to vapour pressure and by substituting this into Equation 5.2 we now have a relationship between intensity and radius:

$$I \propto V_T \propto r^{-1} \quad (5.3)$$

As discussed above, the effect of vapour pressure on the signal intensity indicates that thermal effects dominate the desorption process. It is also possible that exciton-induced desorption can occur and this is a non-thermal effect. For this case, the signal intensity is proportional to the square of the radius:

$$I \propto r^2 \quad (5.4)$$

By examining how the signal intensity varies with particle radius, we can begin to understand if thermal or non-thermal processes dominate desorption.

However, due to the limited range of particle sizes analysed in this study, we are not able to provide a clear correlation between the radii and their corresponding intensities. A future study analysing a wider range of particle sizes would enable us to further understand desorption/ionisation processes.

The vapour pressure is increased by heating the sample and this provides a means to analyse a wider range of molecules with PADI. To study the effect of temperature on signal intensity, we used a heated sample stage with the PADI source set a low power of 13 W, to reduce additional heat of the substrate to approximately 37 °C. Three molecules spanning a wide range of vapour pressures were analysed in both sample forms to study the effect of sample temperature. These molecules are methyl paraben, phenylalanine and Irganox 3114 with vapour pressures of 0.11 Pa, 3.5×10^{-5} Pa and 7×10^{-13} Pa respectively.

Figure 5.2 (a) shows the effect of increasing the temperature from 37 °C to 190 °C for phenylalanine, resulting in around 5 orders of magnitude increase in signal intensity for the thin film form and 3 orders of magnitude for the powder form. For the thin film form the intensity reaches a maximum at 150 °C, whereas the powder form has a plateau at the same intensity from approximately 125 °C. The melting point of phenylalanine is 283 °C. In Figure 5.2 (a), we also show how the vapour pressure of phenylalanine varies with temperature. This is calculated using the integrated form of the Clausius-Clapeyron equation [169] given in Equation 5.5:

$$V_T = V_{T^*}e^{-\chi} \ \text{ where } \chi = \left(\frac{\Delta_{sub}H}{R}\left(\frac{1}{T} - \frac{1}{T^*}\right)\right) \quad (5.5)$$

where V_{T*} is the vapour pressure at temperature, $T*$, V_T is the vapour pressure at temperature, T, R is the gas constant and $\Delta_{sub}H$ is the enthalpy of sublimation of phenylalanine, 154 kJ mol^{-1} [170]. This gives an approximate value for the vapour pressure as function of temperature, assuming that the enthalpy of sublimation is independent of temperature over the temperature range analysed. We observe in Figure 5.2 (a) that the calculated vapour pressure is strongly correlated with the [M+H]$^{+}$ intensity from the thin film sample. Therefore we can express the signal intensity variation with temperature as a function of the vapour pressure at that given temperature, given by Equation 5.6:

$$I(T) = 2 \times 10^6 \, V_T^{0.926} \qquad (5.6)$$

Here the vapour pressure, V_T, is also a function of temperature and is given in Equation 5.5. This equation can be applied from room temperature up to 150 °C. Above 150 °C the signal intensity plateaus rather than increasing in line with the modelled vapour pressure. We suggest that this is caused by a limitation in the concentration of chemical ionisation precursor in the gas phase.
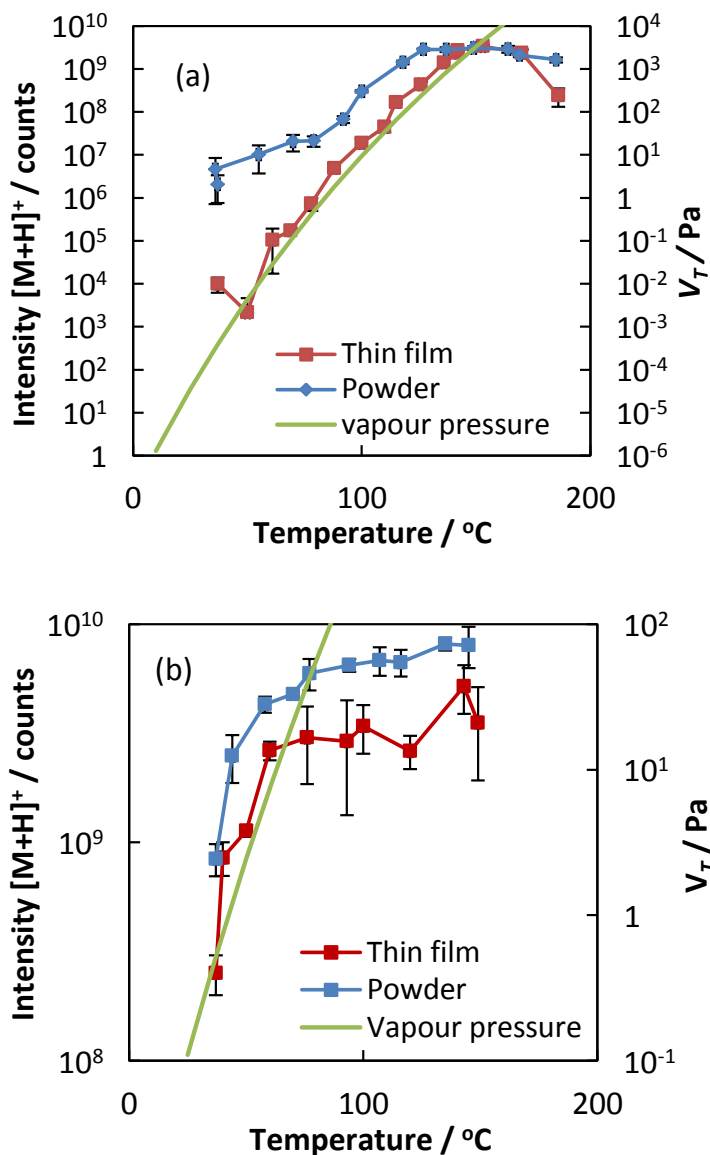
Figure 5.2. Intensity of [M+H]+ from (a) phenylalanine (plotted as "G" elsewhere) and (b) methyl paraben (plotted as "B" elsewhere), as a function of sample temperature for both thin film and powder forms. Also plotted is the variation of vapour pressure with temperature calculated using Equation 5.5.

The signal intensities also increased when the sample temperatures of methyl paraben and Irganox 3114 were increased. For both substance forms of methyl paraben, additional heating resulted in only one order of magnitude increase in intensity, as shown in Figure 5.2 (b). The temperature at which the maximum intensity is reached, 140 °C, and also the intensity at this temperature, is almost

the same for both sample forms. The melting point of methyl paraben is 127 °C; melting of the powder and thin film is observed when the temperature of the sample is raised above 120 °C. The variation of vapour pressure with temperature was also calculated for methyl paraben using Equation 5.5. The signal intensities for methyl paraben plateau above 75 °C. We can rewrite Equation 5.6 for methyl paraben:

$$I(T) = 6 \times 10^8 \, V_T^{0.737} \qquad (5.7)$$

However, this relation can only be applied between 40-60 °C as the signal intensities do not correlate with the vapour pressure values above 60 °C. Figure 5.2 (b) shows that we cannot always express the signal intensity as a function of temperature-dependent vapour pressure. Due to the limited range of molecules studied here, we are not able to deduce if this is an effect of the molecular properties or ionisation effects.

Irganox 3114 shows an even greater magnitude of increase in intensity when the sample is heated from 37 to 200 °C, with the signal intensity of the powder sample increasing by 3 orders of magnitude and thin films by almost 7 orders of magnitude. A temperature of 120 °C is needed to obtain the same signal intensity for the thin film as the powder sample at room temperature. A value for the enthalpy of sublimation is not available in the literature for Irganox 3114, we are therefore unable to calculate how the vapour pressure varies with temperature.

The signal enhancement, *E*, is defined as the ratio of the maximum and minimum intensities and values of this for the three molecules are given in

Table 5.2. The general trend shows a strong increase in E as the vapour pressure reduces and the effect is suppressed for the powders. It is very evident that both sample form and vapour pressure have a substantial effect on the sensitivity and this can be mitigated by increasing the sample temperature. Additional heating increases the signal intensity for both powders and thin films, due to the increase in desorption of the analyte into the gas phase enabling ionisation of a larger amount of material by the plasma source. It should be noted that when the plasma is turned off but the heated stage remains on, no ions are detected; therefore we can be sure that it is the plasma that ionises the analyte.

Table 5.2. The signal enhancement E, defined as the ratio of the maximum and minimum intensities, gained by heating of the sample for methyl paraben, phenylalanine and Irganox 3114.

	Methyl paraben	**Phenylalanine**	**Irganox 3114**
Vapour pressure (V_{25})	0.11 Pa	3.49×10^{-5} Pa	7.00×10^{-13} Pa
E **(Powder)**	10	1500	1200
E **(Thin film)**	20	3×10^5	8×10^6

5.3.2 Analysis using a heated sample stage

We have now established that the vapour pressure and form of a substance are critical parameters for PADI sensitivity. We now study in more detail the effect of sample temperature using the same experimental arrangement for analytes in thin film form only.

From Figure 5.1, we can see that there will be a great range of molecules that cannot be effectively analysed under low temperature conditions. For their analysis extra methods must be undertaken to aid desorption/ionisation. Therefore, a heated sample stage was used with a low plasma power, 13 W, so that the heating from the plasma was minimal. As shown in the previous chapter [168], the sample temperature increases linearly with plasma power.

Figure 5.3 shows the data of Figure 5.1 for thin films with no sample heating together with their intensities at 80 °C, 114 °C and 144 °C. Fits of Equation 5.1 to the data are also plotted to show the general trend, although the distribution is quite scattered especially at lower temperatures. The vapour pressure values plotted are those given in Table 5.1 and are at 25 °C and not the vapour pressure at the analyses' temperature. In addition to the data of Figure 5.1 we also include the four molecules which are liquid at room temperature, listed in Table 5.1. Characteristic ions, given in Table 5.1, were observed from geraniol, triethanolamine and benzyl salicylate when there was no additional heating provided. The signal intensity for these analytes was greater than 10^7 counts for one minute of integrated signal. These molecules have relatively high vapour pressure, greater than 4×10^{-4} Pa at 25 °C. Conversely, the intensity of the characteristic ion from the fourth liquid analysed, linoleic acid, which has a vapour pressure of 1.2×10^{-4} Pa, were two orders of magnitude lower at 10^5 counts. This implies that both vapour pressure and class of molecule have an impact on the success of analysis. For most of the analytes analysed, the most intense ion detected was the molecular ion, $[M+H]^+$. However for some ions, the $[M-H]^+$ was the most intense. The ion used for analysis is noted in Table

5.1. In this study the dominant ion observed for cholesterol is $[(M+H)-H_2O]^+$, the $[M+H]^+$ is not detected when cholesterol is analysed as a powder. This may be attributed to its low proton affinity which has also made it difficult to analyse using other mass spectrometry techniques such as DESI [171] and MALDI. Other ions were also detected from the analytes; these included $[M-H_3O]^+$ which was detected from geraniol and triethanolamine, the immonium ion $[M-HCOOH+H]^+$ from the amino acids phenylalanine and leucine, and oxygen adducts were detected from methyl paraben, linoleic acid and Irganox 1098. The hydride abstraction peak $[M-H]^+$ was detected for geraniol, linoleic acid and cholesterol. This has also been observed with DART [30].
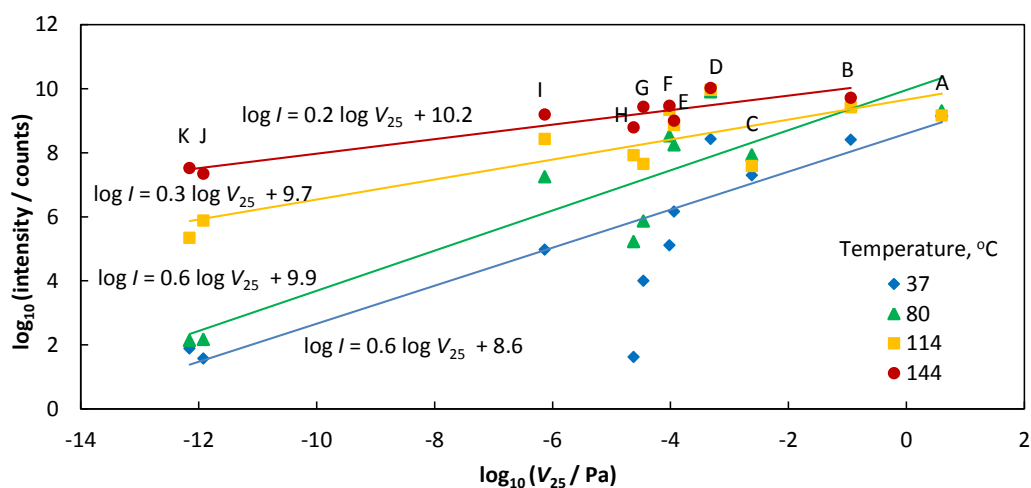
Figure 5.3. Variation of the signal intensity for a series of molecules with differing vapour pressures analysed at four different sample temperatures, 37, 80, 114 and 144 °C. The molecules are labelled as given in Table 5.1. All vapour pressure values are for 25 °C. Fits of Equation 5.1 are given to guide the eye.

These results are in agreement with previous work published on the PADI analysis of personal care products and their components [156]. The molecules

detected in that study, siloxanes and phthalates, have vapour pressures greater than 10^{-4} Pa.

The general relationship between vapour pressure and signal intensity, Equation 5.1, appears to be valid for both solid and liquid states. It is clear from Figure 5.3 that as the temperature of the sample is increased the signal intensity of the analyte also increases. The index, *b*, of Equation 5.1 depends on temperature and it is shown that the relative change in intensity is dependent on the vapour pressure of the analyte. The additional heated sample stage aids the desorption of the analytes, increasing the signal intensity for all the molecules analysed in this study.

In Figure 5.3 we observe that at the two lower temperatures, 37 and 80 °C, the group of analytes D-H do not follow the same general trend as given by the fits to Equation 5.1. These analytes are more strongly affected by vapour pressure at lower temperatures. Figure 5.4 shows the stronger dependence on vapour pressure of the analytes D-H at 37 and 80 °C. It is not known why the dependence is stronger but a clear power law dependence is observed.
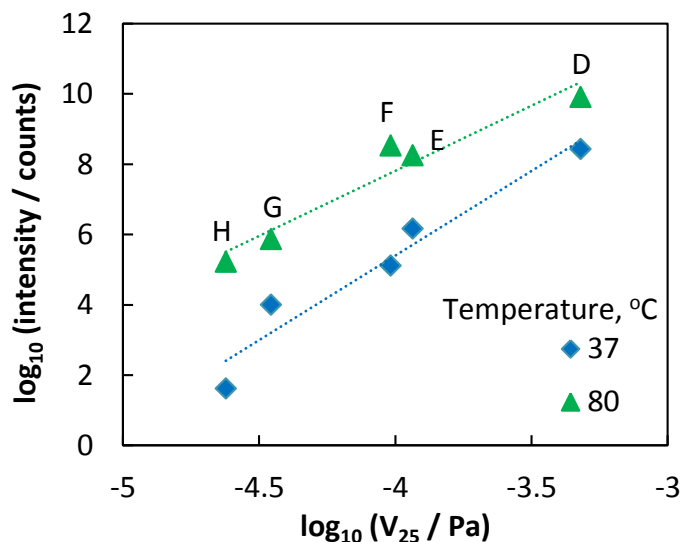
Figure 5.4. A subset of the data from Figure 5.3 showing the variation of the signal intensity for a series of molecules, D-H as given in Table 5.1, analysed at two different sample temperatures, 37 and 80 °C. All vapour pressure values are for 25 °C.

In the previous chapter we showed the effect of sample temperature on four characteristic positive ions from valine [168]. There, the intensity of $[M+H]^+$ increased approximately exponentially, whilst, for example, the $[M-CH_2O+H]^+$ ion was approximately constant. In Figure 5.5, we show similar plots from this study of benzyl salicylate and Irganox 3114 with an increased temperature range up to 200 °C. Similar effects are observed with the low vapour pressure substance, Irganox 3114, where a maximum is observed above 165 °C. For benzyl salicylate, with a room temperature vapour pressure of 2.40×10^{-3} Pa, a maximum is reached at 75 °C. We postulate that the limiting factor at higher surface temperatures is the concentration of chemical ionisation precursor in the gas phase, and this limits the amount of sample that can be ionised hence reaching a maximum in the signal intensities. For almost all of the molecules analysed, the characteristic ions follow similar trends to the molecular ion for

that molecule, as is the case for Irganox 3114 in Figure 5.5 (b). Benzyl salicylate, Figure 5.5 (a), is an exception to this trend.
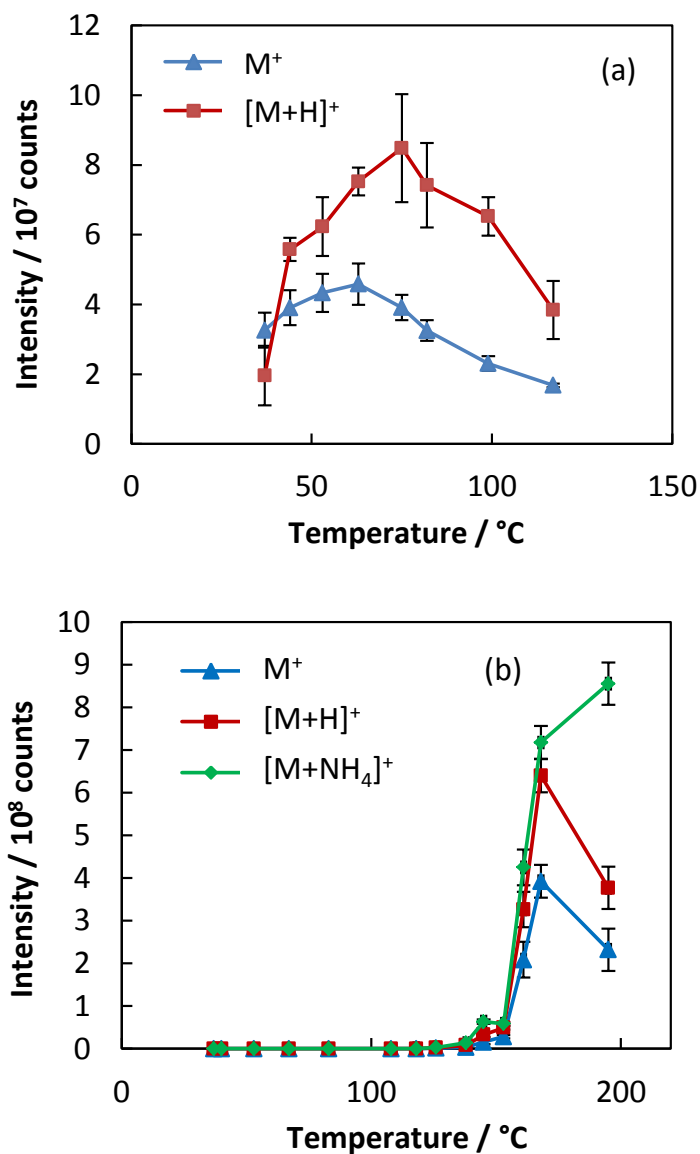
Figure 5.5. Variation of signal intensity with increasing sample temperature for (a) the M^+ and $[M+H]^+$ ions of benzyl salicylate and (b) the M^+, $[M+H]^+$ and $[M+NH_4]^+$ ions of Irganox 3114.

In this study, we find that signal intensities above approximately 10^{10} counts are not observed. For example, the maximum intensities for both forms of phenylalanine coincide in Figure 5.2 (a), and in Figure 5.3, methylparaben (B)

and triethanolamine (D) which are substances with high vapour pressure, and high signal intensities, exhibit no increase in intensity with temperature after reaching a plateau as shown in Figure 5.2 (b). All injection times in this study were below 500 ms (maximum injection time) and were generally less than 100 ms. The AGC compensates the signal intensities dependent on the injection time determined by a pre-scan carried out before each scan is acquired. The minimum injection time did not go below 0.5 ms for the data acquired; therefore saturation effects seen in the intensities later in Figures 5.2 and 5.5 are not due to reaching a limit in the capacity of the Orbitrap™, as the minimum injection time that can be used to fill the Orbitrap™ is below 0.01 ms. In a further test, the signal into the mass spectrometer was reduced by increasing the distance from the plasma source to the sniffer [168]. This reduces the signal without affecting the plasma-surface interaction. Figure 5.6 shows the plateau is still observed for triethanolamine with a threefold reduction in signal intensity. We conclude that this is not an instrumental effect of the mass analyser or transfer inlet but that the intensity is limited by the concentration of chemical ionisation precursor in the gas phase.
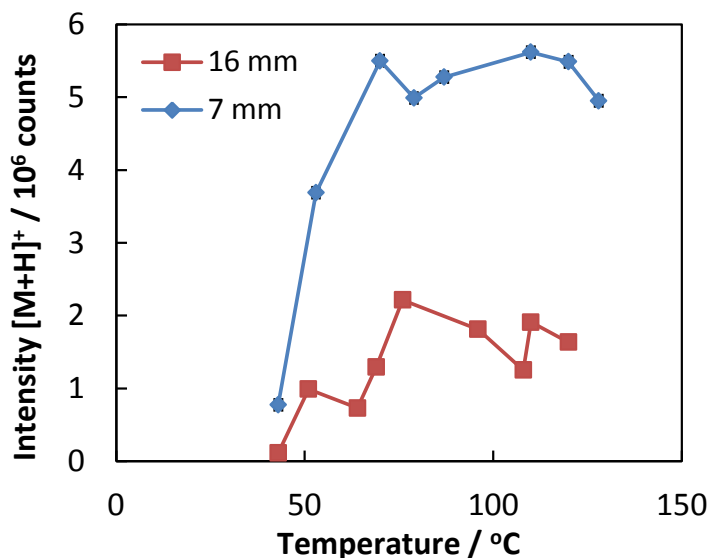
Figure 5.6. Intensity of $[M+H]^+$ from triethanolamine (plotted as "D" elsewhere) as a function of sample temperature. The data were acquired at two different plasma-sniffer distances, 7 and 16 mm. These data were taken with the AGC (automatic gain control) setting off and a fixed ion injection time of 0.8 ms. The data were acquired for 1 minute and the intensity plotted is the integrated signal over that analysis time.

5.4 Conclusions

In this chapter we have shown that the vapour pressure strongly affects the sensitivity of plasma-assisted desorption ionisation, PADI. The relationship between vapour pressure and temperature is given by the Clausius-Clapeyron equation and has a good correlation with measured signal intensities. It is also found that the form of the sample is of great importance with powders having up to 4 orders of magnitude higher signal intensity compared with a thin film. This effect depends strongly on the vapour pressure and the relationship is defined. This is attributed to the larger surface area of powders. It is vital to know the analytes for which the technique is effective and how to improve the

detection for those analytes which are not successfully analysed under normal operating conditions. When the plasma is operated in a low sample temperature mode, *i.e.* 37 °C, the vapour pressure of the analyte strongly influences the signal intensity. Thin film samples require a vapour pressure of greater than 10^{-4} Pa for analysis at room temperature. However if the sample is in a form that can be easily converted into the gas phase, such as a liquid or a powder (where the plasma can heat the sample in localised spots) then a greater range of samples can be analysed.   Thermal desorption is clearly a dominant processes in PADI. We have shown that using a heated sample stage we are able to increase the signal intensity by up to 6 orders of magnitude for thin films and 3 orders of magnitude for powder samples. It is also shown that there is saturation in signal intensity that may be caused by a limitation in the concentration of chemical ionisation precursor in the gas phase.

Chapter 6

Analysis of personal care products on fixed fibroblast cell surfaces using DESI and PADI ambient mass spectrometry

6.1   Introduction

Two ambient ionisation techniques, desorption electrospray ionisation (DESI) and plasma-assisted desorption ionisation (PADI), have been used to analyse personal care products (PCPs) on fixed fibroblast cell surfaces. The similarities and differences between the two techniques for this type of analysis have been explored in various ways. Here, we show the results of DESI and PADI analysis of individual PCP ingredients as well as the analysis of these as complex creams on fixed fibroblast cell surfaces, with minimal sample preparation.

Direct detection of small molecules from skin is an important requirement of product development for novel health and personal care products (PCPs). For example, aiding in the understanding of adsorption and efficiency of skin care products or reduction of natural malodours using deodorants. Traditionally, mass spectrometry analysis of personal care products has been largely dominated by LC and GC-MS [172-174]. These techniques involve complex

and laborious extraction and separation procedures, which target a specific molecule of interest. Ambient surface mass spectrometry offers a faster alternative to this with minimal sample preparation and imaging capability.

DESI and PADI, *inter alia*, have both been shown to have the possibility for *in vivo* analysis, with a number of preliminary experiments mainly focussed on homeland security and forensic analysis. A classic experiment was initially performed by Cooks *et al.* analysing the finger of a person who had taken 10 mg of the over-the-counter antihistamine drug Loratadine, showing the rise and fall with time of the molecule at the skin surface [7]. DESI sampling of human skin spiked with explosives was able to detect ng amounts, even from within complex mixtures doped directly onto the skin [133]. A similar experiment, with an illicit mixture of prescribed drugs (d-methamphetamine, cocaine, diacetylmorphine) doped onto human skin, clearly detected each drug within the mixture even when sampled with non-proximate (1 m from the MS) DESI directly from the skin [175]. One of the best examples of direct skin analysis with PADI showed the detection of ibuprofen from skin after application of ibuprofen gel [19]. In addition, desorption atmospheric pressure chemical ionisation (DAPCI), which uses plasma ionisation, was able to detect nicotine and urea direct from the skin of a smoker [158], and LTP was used to detect cocaine from a human finger [20]. Other ambient mass spectrometric techniques that have been used to look at skin are secondary electrospray ionisation (SESI), where skin volatiles such as fatty acids were detected [176], and extractive electrospray ionisation (EESI) [177, 178]. These promising

results suggest possible success for similar applications of PCP creams, gels and deodorants.

Personal care products are in regular use by consumers and require thorough toxicology and safety testing. Traditionally, PCPs are assumed to stay on the surface of the skin, however it is increasingly thought that penetration may occur requiring a method to test penetration effectively, preferably without the use of animal testing. Presently, *in vitro* tests are carried out which involve the use of either dead skin that is devoid of metabolic activity, which may be important for substance penetration, or skin stripping [179-181]. Skin stripping relies on the efficacy to quantitatively remove the stratum corneum and assumes that no PCP residues remain within the living skin. However, studies show that this technique is unable to remove all residues on the skin, distinguish between residues on and within the skin, and tends to overestimate systematic exposure [182]. A non-invasive direct analysis approach would allow *in vivo* analysis, enabling a modern analytical approach, rather than the crude skin stripping methodologies. One of the most widely used ingredients of PCPs are organosiloxanes and it is therefore important to develop methods for detection and imaging their distribution on skin. In addition, the determination of organosiloxanes in PCPs is important in evaluating and characterising human exposure [172]. At present, methods to measure skin penetration of siloxanes may be inefficient, therefore a simple method to scan *in vivo* penetration is important. Here, we begin a preliminary study towards a future direct non-invasive *in vivo* analysis by studying the outermost surface of the PCPs on fixed fibroblast cells, to investigate the use of ambient mass spectrometry methods such as plasma-assisted desorption ionisation (PADI) or

desorption electrospray ionisation (DESI) mass spectrometry, as a first step to fulfil this analytical requirement.

The objectives of this chapter are to use DESI and PADI for:

- The analysis of individual personal care product ingredients.

- To analyse complex skin creams in their native state and compare the different chemical information obtained.

- The analysis of fibroblast cell surfaces, examining the damage that the sources cause to the cells.

6.2   Experimental Section

6.2.1 Cells

Human dermal fibroblasts (HDFa) isolated from adult skin were bought from Invitrogen (UK). These cells were grown in growth medium 106 supplemented with low serum growth supplement (LSGS), 10 μg ml^{-1} gentamicin and 0.25 μg ml^{-1} amphotericin B (Invitrogen (UK)). Cells frozen and stored in liquid nitrogen were thawed and warmed to 37 °C. The complete growth medium, listed above, is added drop wise and the cell suspension mixed thoroughly. This cell suspension was then transferred into a 25 cm^3 culture flask and fresh medium added to the flask. Cells were incubated at 37 °C, 5% CO_2 and 95% air humidity. Once the cells were confluent, they were detached from the culture flask by using 0.025% trypsin / 0.01 % EDTA solution (Invitrogen, UK). HDFa cells harvested according to the above procedure were seeded at 20,000 cells per well in Nunc LabTek II 2-well chamber slides (5000 cells cm$^-$

[2]) for the analysis. At confluence (typically 7 days post-seeding) the cell culture medium was removed and the cells were washed with PBS. The cells were then fixed with ice-cold methanol for 10 minutes and then allowed to air dry. Stocks of the fixed HDFa cells on microscope slides were stored at 4 °C until further analysis was required by AMS. This provided a uniform monolayer of fixed fibroblast cells.

6.2.2 Samples

Three off-the-shelf anti-ageing creams from three different brands were deposited, without any dilution, onto the cell surface using a swab. Pure components of personal care products, listed in Table 6.1, (Sigma, Poole, UK, and Alfa Aesar, Heysham, UK) concentration 10 mM, were deposited onto glass microscope slides (Superfrost-Fisher Scientific, Loughborough, UK) to explore the effectiveness of the two ambient MS techniques for detection of active ingredients. Optical microscope analysis was carried out using a Leica DM IL Microscope.

6.2.3 DESI and PADI mass spectrometry

DESI analysis was conducted using a modified QSTAR Elite quadrupole time-of-flight (Q-TOF) mass spectrometer (Applied Biosystems, USA), optimised as outlined in reference [127]. The solvent composition used for DESI analysis was 90:10 methanol:water including 0.1% formic acid. This gave a spot size with diameter 0.3 mm [129]. The PADI source was coupled to the same QSTAR Elite mass spectrometer. PADI was operated with optimised settings of an input power of 22 W and a helium gas flow of 820 ml min^{-1}. The plasma

source was positioned at 30° to the normal, the distance from the plasma tip to the sniffer (the inlet to the mass spectrometer) was 10 mm and the distance from the plasma tip to the sample surface was 2 mm. The PADI spot size was 1.5 mm diameter for a 60 second analysis time. Spectra were acquired for 30 seconds for the analysis of the individual PCP ingredients and 2 minutes for the PCP creams.

6.3   Results

6.3.1 Analysis of components of PCPs

Mass spectrometric analyses of 13 molecules commonly used in personal care products were carried out with both PADI and DESI to characterise the different sensitivities of the techniques. The 13 molecules analysed are displayed in Table 6.1, which also shows the effectiveness of DESI and PADI for the analysis of each molecule. The molecules fell into four distinct classes, as indicated in Table 6.1. Firstly, both techniques gave clear detection of the molecular ion, labelled A in Table 6.1. Secondly, DESI and PADI detected the molecular ion but PADI also detected other characteristic peaks, either fragments or rearrangements of the molecule, labelled B in Table 6.1. Thirdly, DESI detected no characteristic peaks but PADI detected molecular peaks as well as fragment and rearrangement ions, labelled C in Table 6.1. Finally, DESI detected no ion from the component and PADI detected some unidentified peaks from the molecule, labelled D in Table 6.1. In total, DESI was able to detect the molecular ion, in either positive or negative MS, as

$[M+H]^+$, $[M+NH_4]^+$, $[M-H]^-$ or $[M-OH]^-$ for 9 of the molecules, but was unable to detect anything, in either positive or negative ion polarity, for 4 molecules. It may be possible to detect these 4 molecules by changing the electrospray solvent or using different chemistries to promote ionisation [129, 132]. This has not been explored here. PADI detected ions from all of the 13 PCP components in the positive ion mode, however in one case the peaks could not be assigned, even after conducting MS/MS analysis. In nearly all cases of PADI analysis, in addition to detecting the molecular ion there were also fragments present such as $[M-C_2H_3O]^+$, although the relative intensity of these fragments varied between ingredients. DESI mass spectra tend to be simpler and easier to interpret, but cannot detect all components trialled, whereas PADI is able to detect a wider range of components but the spectra can sometimes be difficult to interpret. This highlights the importance of coupling ambient mass spectrometry with high performance mass spectrometers to enable the identification of unknowns.

Table 6.1. Properties of 13 different PCP ingredients analysed by DESI and PADI MS. The table also shows the effectiveness of DESI and PADI analysis for each molecule, a ✓ denotes a clear molecular peak, a ✓* denotes molecular peaks, fragments and adducts detected from the molecule, and an X denotes no peaks or that we were not able to identify the peaks from the molecule.

	Substance	Molecular formula	Mono-isotopic mass, Da	Vapour pressure, Pa at 25 °C	Function	Structure	DESI	PADI
A	Linalool	$C_{10}H_{18}O$	154.1358	21.33	Fragrance		✓	✓
	Triethanolamine	$C_6H_{15}O_3N$	149.1052	4.79×10^{-4}	pH balancer and emulsifier		✓	✓
	Propylene carbonate	$C_4H_6O_3$	102.0317	6.00	Solvent		✓	✓
	Coumarin	$C_9H_6O_2$	146.0368	0.13	Fragrance		✓	✓
	Poly (propylene glycol) monobutyl ether	$C_4H_{10}O$ $[C_3H_6O]_n$	$74.0732 + 58.0419n$	Not available	Solvent		✓	✓
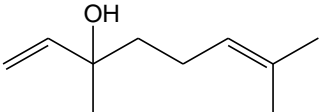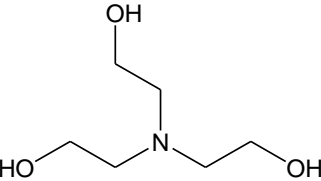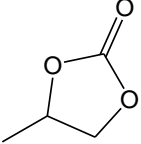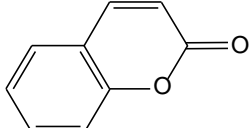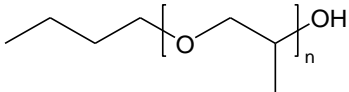
	Citronellol	$C_{10}H_{20}O$	156.1514	5.88	Fragrance		✓	✓
B	Hydroxy-citronellal	$C_{10}H_{20}O_2$	172.1463	0.77	Fragrance		✓	✓*
	Methyl paraben	$C_8H_8O_3$	152.0473	0.11	Preservative		✓	✓*
	Geraniol	$C_{10}H_{18}O$	154.1358	4.00	Fragrance		✓	✓*
C	Stearyl alcohol	$C_{18}H_{38}O$	270.2923	3.60×10^{-4}	Emulsifier		X	✓*
	Eugenol	$C_{10}H_{12}O_2$	164.0837	3.01	Fragrance		X	✓*
	Citric acid	$C_6H_8O_7$	192.0270	7.52×10^{-7}	pH controller		X	✓*
D	Benzyl salicylate	$C_{14}H_{12}O_3$	228.0786	2.40×10^{-3}	Fragrance		X	X
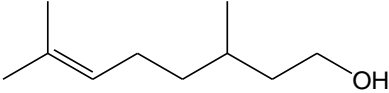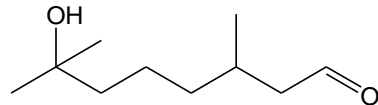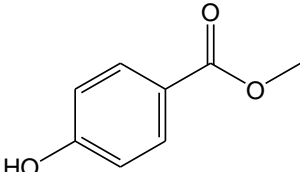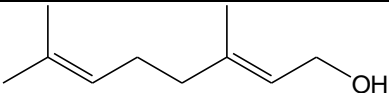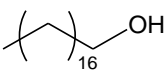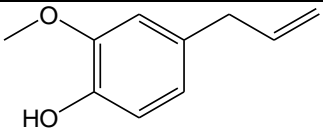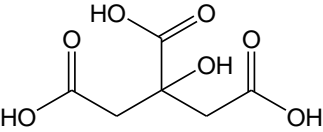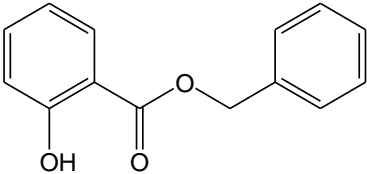
6.3.2 Analysis of PCPs

DESI and PADI were used for the analysis of PCPs direct from fixed fibroblast cells. A comparison of the similarities and differences between the mass spectra shows the useful information obtained from each technique and also their suitability for this type of analysis. PADI and DESI mass spectra from each of the three creams, with preliminary assignments made to some of the peaks, are shown in Figures 6.1 to 6.3. The linear and cyclic polysiloxanes are labelled in the mass spectra according to the convention, D_n for cyclic polysiloxanes of the form $(Si(CH_3)_2O)_n$ and L_n for linear polysiloxanes of the form $CH_3[Si(CH_3)_2O]_nSi(CH_3)_3$ where $n = 2$ to 10. PADI and DESI both detected siloxanes in all the creams. Siloxanes are a common ingredient in PCPs, acting as a carrier and giving the products a silky smooth texture [172]. DESI mass spectra mostly show the cyclic siloxane D_6, although linear siloxanes $n = 5$ to 7 are also present in Creams 2 and 3. In comparison, PADI mass spectra detects linear siloxanes with $n = 2$ to 10 for all creams although the cyclic siloxane D_6 is also present in Cream 1 and 3. In both mass spectra the siloxane peaks at masses with m/z greater than 400 are commonly ammonium adducts, whereas those with m/z less than 400 are due to the loss of methane. This is in agreement with earlier work by Schlosser [183]. The most commonly detected siloxane here is at m/z 462.15, the ammonium adduct of D_6; this is not unexpected since it is noted to be present in 50% of PCP and household products [184].
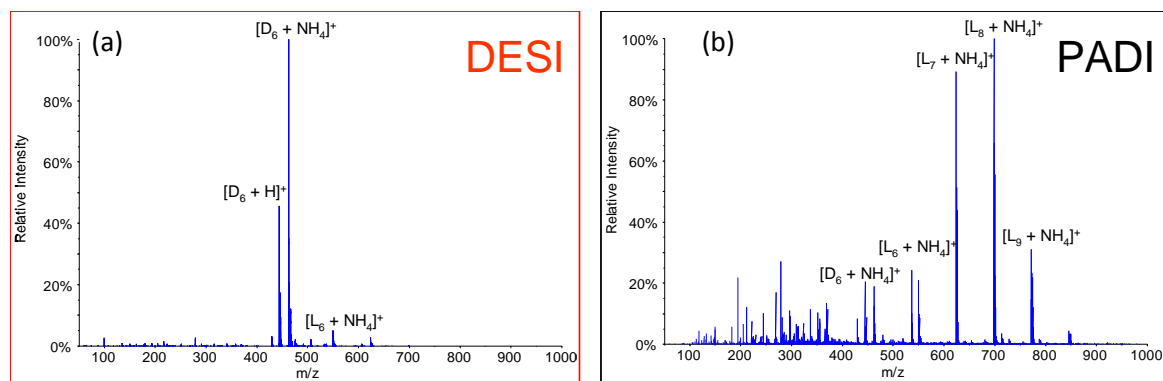
Figure 6.1. Positive ion mass spectra from Cream 1, (a) DESI and (b) PADI.
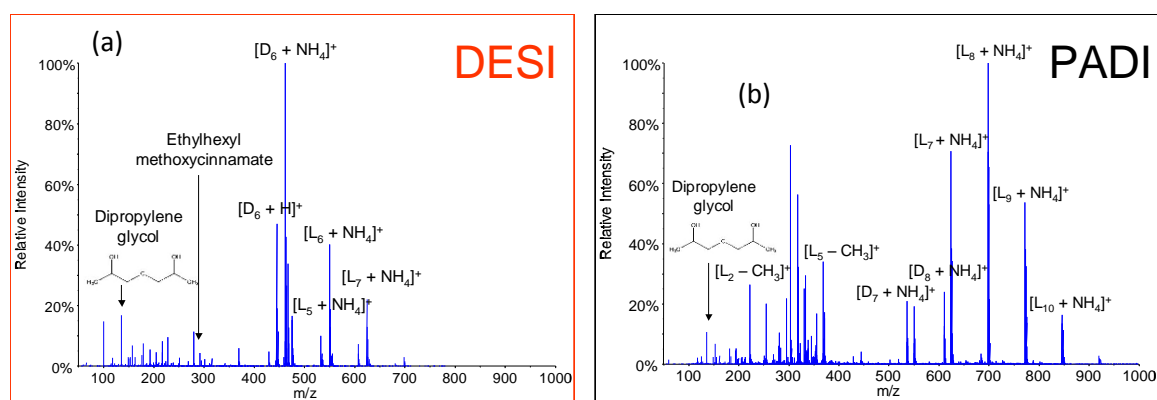
Figure 6.2. Positive ion mass spectra from Cream 2, (a) DESI and (b) PADI.
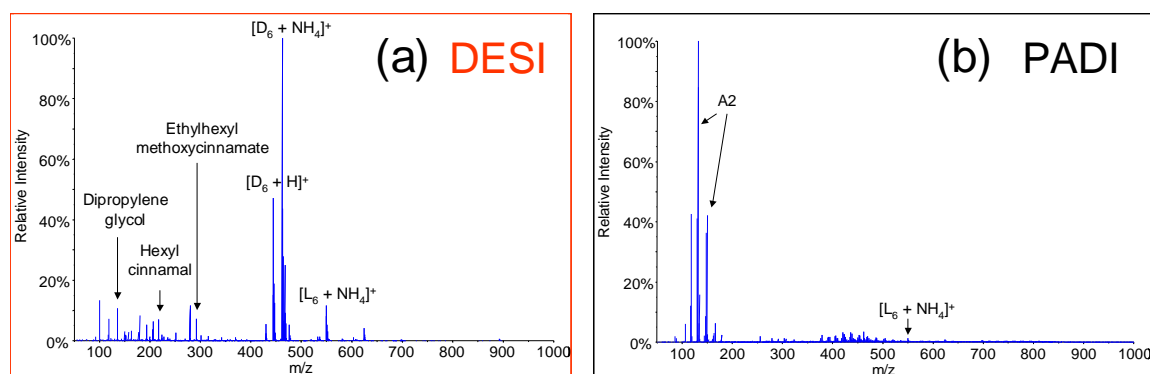
Figure 6.3. Positive ion mass spectra from Cream 3, (a) DESI and (b) PADI. A2 refers to the molecule in the second row in Section A of Table 6.1.

Cream 1 is shown in Figure 6.1 and is dominated by the siloxanes. However, the DESI and PADI mass spectra of Cream 2, Figure 6.2 (a) and (b) respectively, show dipropylene glycol. This is a common solvent used in PCPs. In addition, in Cream 2 DESI also detects ions tentatively assigned to

ethylhexyl methoxycinnamate, a sunscreen agent. The PADI mass spectrum for Cream 2 also has a large number of unidentified peaks. Figure 6.3 shows Cream 3 with a large number of small molecules with m/z between $100 - 300$ in both the DESI and PADI mass spectra. In the DESI spectrum some of these can be identified as molecular ions of dipropylene glycol, hexyl cinnamal (an aroma) and ethylhexyl methoxycinnamate. The PADI spectrum of Cream 3 is dominated by peaks from triethanolamine.

The PADI mass spectra from each of the creams changes with time. As shown in Figure 6.4, in Cream 2, dipropylene glycol has a large intensity to begin with but after 30 seconds this decreases by more than half. Concurrently, a series of peaks in the mass range m/z $300 - 350$ increase in intensity with m/z 303 dominating the spectrum after 60 s. It should also be noted that although most of the siloxanes retain their intensities, similar to L_8, the peaks relating to D_7 and L_6 decrease, similar to dipropylene glycol. It is known that cyclic siloxanes (D_n) are generally more volatile than linear siloxanes (L_n) and so will have higher mobility and be more likely to migrate to the surface. This may be due to molecules migrating to the surface of the layer. Interestingly, this may indicate the possibility to depth profile organic material with PADI [185]. Damage effects may also change signal intensities and these are being studied in detail in our development of the metrology of PADI.
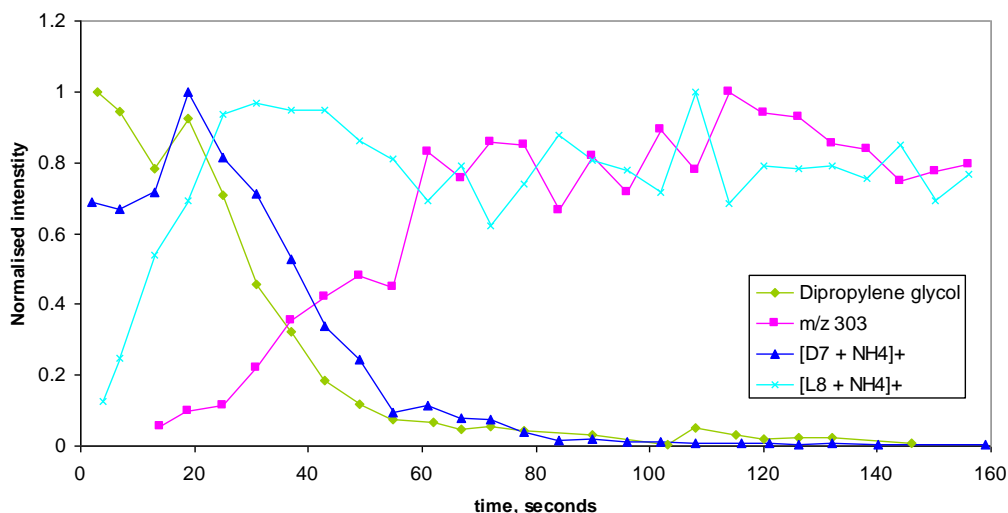
Figure 6.4. Variation of signal intensity with time for key ions detected by PADI from Cream 2. Counts are normalised to the total ion count to account for fluctuations that result from analysis with PADI.

Figures 6.1 to 6.3 illustrate that DESI and PADI are capable of obtaining useful information regarding the siloxane content and small active ingredients directly from creams applied to a fibroblast surface. These analyses were possible within an acquisition time of only two minutes direct from a fixed fibroblast cell surface and with minimal sample preparation.

For *in vivo* analysis, a first important step is to investigate whether detection direct from the fixed fibroblast cells caused any morphological damage to the cell surface. To do this DESI and PADI MS analysis were carried out for increasing times on fresh areas of the fibroblast cell sample with the cells imaged with optical microscopy after each analysis. We quantify the morphological damage to the fixed fibroblast cells by simply counting the number of intact cells present over an area of 0.5 mm^2 for each analysis time, as shown in Figure 6.5. Inset are images of the cell surface for 300 s DESI

analysis and 300 s PADI analysis. This allowed us to visualise the changes in the fixed fibroblast cells throughout the analyses. Figure 6.5 shows that there is no change in the number of fixed cells after DESI analysis, but there is a significant reduction in intact cells present after PADI analysis. To ensure that there is a less than 10% reduction in the number of cells during PADI MS, the analysis time must be kept under 5 seconds. To compare this with DESI it is important to also consider the signal, since clearly if the signal is 2 times higher one can reduce the acquisition time by half. The average total ion intensity for all PCPs over 2 minutes was 20,000 counts s[-1] and 10,000 counts s[-1] for PADI and DESI respectively. Therefore, for a PADI analysis time of 5 seconds, for the equivalent amount of signal a DESI acquisition time of 10 seconds is required. The resulting morphological damage from DESI is much less than 10%, which was the level observed for PADI for the equivalent amount of signal.
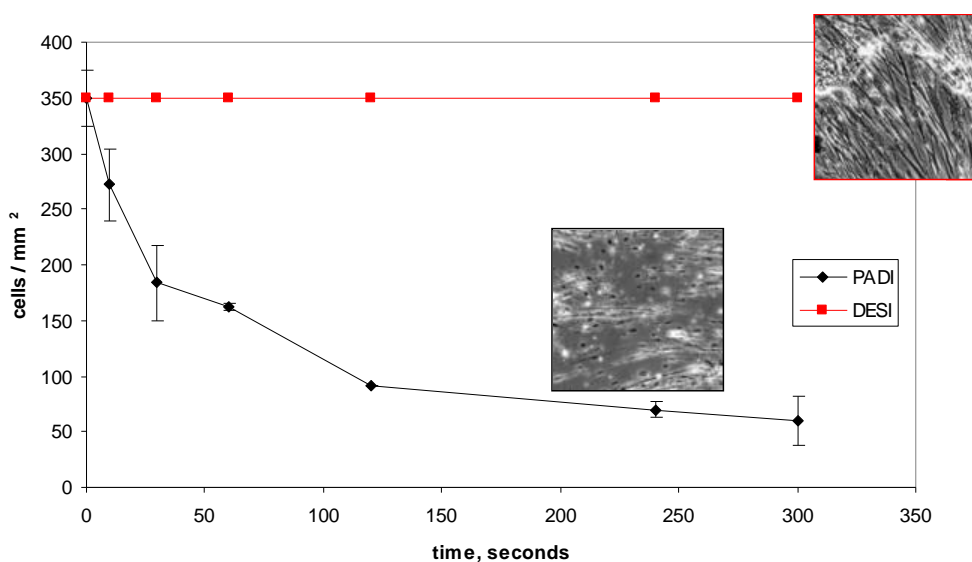
Figure 6.5. Morphological damage to fibroblast cells using DESI and PADI.

For PADI it is also interesting to look at how cell morphological damage changes when the plasma power is modified. A fixed time of 120 seconds was used for this experiment and the same power settings as used for the PADI optimisation were used. Figure 6.6 shows how increasing the power increases the morphological damage to the cells. At a power of 22 W, recommended earlier for optimum signal intensity, which results in a surface temperature of approximately 100 °C as shown in Figure 4.7, the damage is approximately 3 times higher than the lowest power setting of 16 W. From, Figures 4.6 (b) and (c), the intensity of the molecular ion for triethanolamine and hydroxycitronellal drops by approximately 3 and 2 fold respectively over the same power range. Therefore, for these ions the time and plasma power can be traded for a given signal intensity per unit of damage. For other ions where the signal is relatively constant or even increases at lower powers then clearly a lower power setting is better.
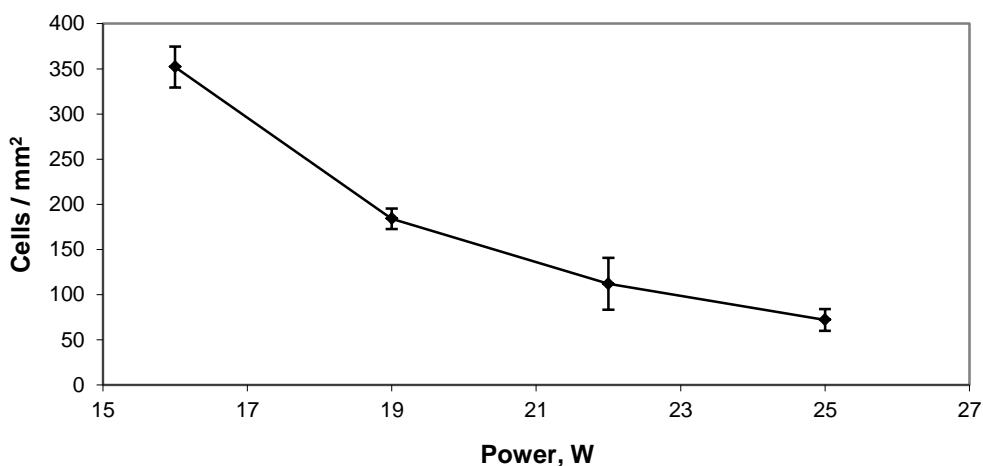
Figure 6.6. Morphological damage to fibroblast cells after a PADI analysis of 120 seconds with different RF power settings

136

It is very important to note that in this study we have only examined the morphological damage of fixed cells. This is an important first step but more extensive studies to measure any biochemical changes or other damage, such as genetic mutation, are required before *in vivo* use on skin.

6.4   Conclusions

DESI analyses of pure PCP components show straightforward mass spectra with molecular ion peaks, however, DESI is not able to detect all components. PADI is able to detect all components, but the mass spectra are sometimes difficult to interpret. Adjustment of the plasma conditions can be used to minimise the level of fragmentation and enhance the molecular ion signal in PADI.

PCPs are complicated mixtures of many components. There is no separation with direct analysis and consequently, the mass spectra are very complex. Even with MS/MS capabilities it can be difficult to identify ions. Elsewhere, it has been shown that with a mass scale calibration accuracy of around 1 ppm [186] and isotope pattern matching [187] that chemical databases such as PubChem [188] can be used to identify unknown substances. There are therefore significant advantages to combining ambient techniques with high performance mass spectrometry when studying such complex mixtures [186].

We have illustrated that DESI and PADI are capable of obtaining useful information regarding the siloxane content of PCPs, such as creams, rapidly

and directly, here deposited on a fibroblast cell surface. This is a first step in determining penetration and concentration in these difficult systems.

The morphological damage done to the fixed fibroblast cells when analysed by ambient mass spectrometry differs depending on the technique used. PADI damages the whole cell structure after 5 seconds whereas DESI is much more gentle with negligible morphological damage observed for a 300 second acquisition. Analysis times for PADI should therefore be limited to less than 5 seconds under these operating conditions to avoid damage to the cell structure.

Chapter 7

Overall conclusions and future outlook

7.1   Conclusions

The work presented in this thesis has further enhanced the metrology base for ambient mass spectrometry. Before any analytical technique can be used to its full advantage, optimisation and characterisation of the source needs to be performed. By carrying out a systematic study to optimise parameters for the plasma assisted desorption ionisation source, PADI, signal intensities were improved to a maximum, with a repeatability of approximately 7%. Figure 7.1 summarises the different parameters that affect the signal intensities of molecular and fragment ions. The plasma power was shown to significantly affect both the absolute and relative intensities of the different characteristic fragment ions from valine, showing the level of fragmentation can be controlled.
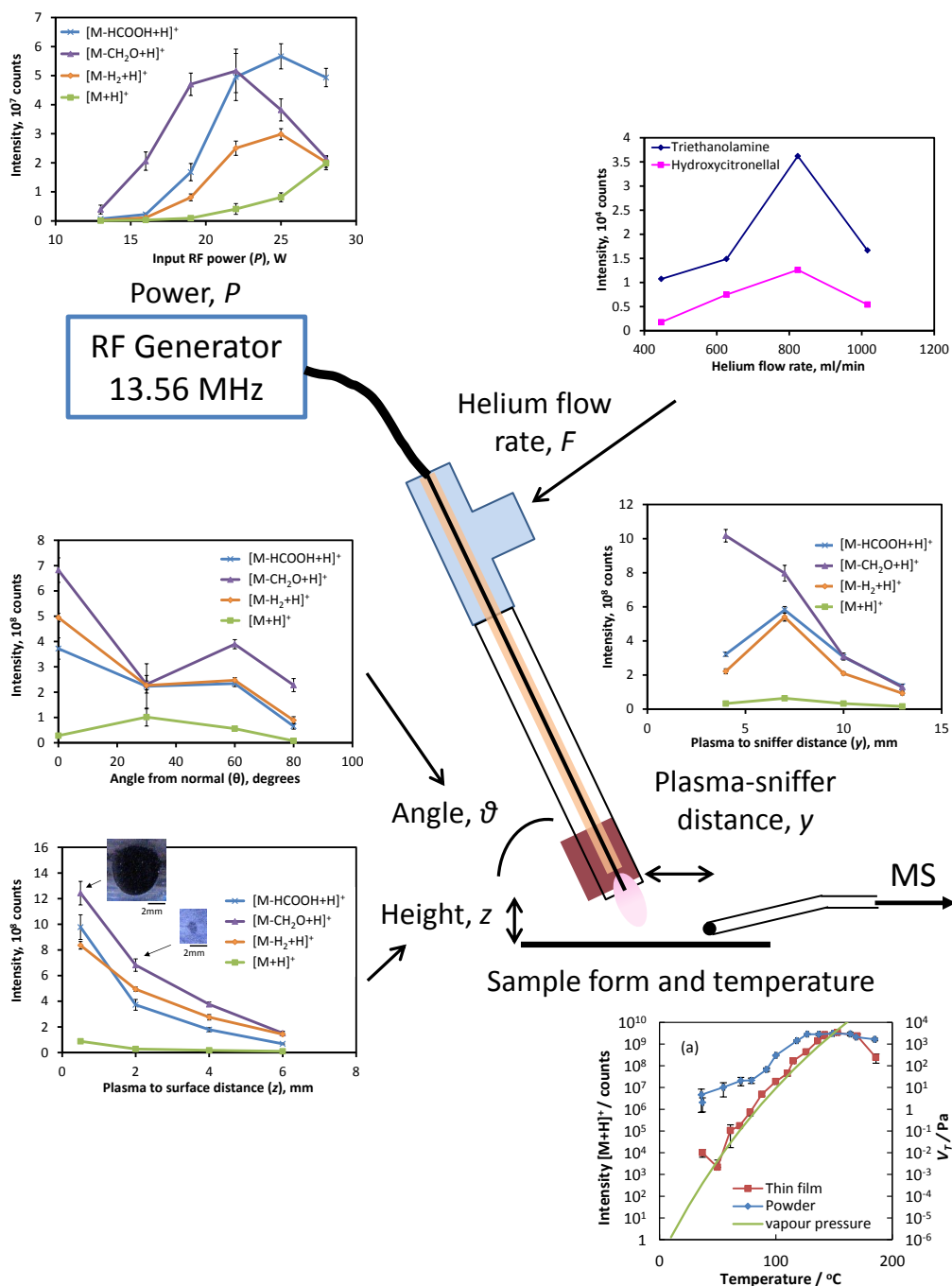
Figure 7.1. Summary of the PADI parameters that affect signal intensities.

The importance of sample temperature when analysing with PADI has been highlighted in two chapters; 4 and 5. For this particular set up we have shown two ways that this can be changed; firstly by increasing the power of the plasma and hence its temperature resulting in thermal desorption of compounds, although at the same time more complex desorption and ionisation

mechanisms occur; and secondly by using a heated sample stage to desorb analytes before ionisation by the plasma. In this second experiment, we have tried to decouple the desorption and ionisation steps by using a plasma power that supplies limited heat to the sample. These results show that volatility plays a large role in the successfulness of PADI analysis, with a vapour pressure of greater than 10^{-4} Pa required for successful analyte detection. Volatile molecules that easily form gas-phase ions are readily ionised by PADI. An example of this has been shown in the analysis of ingredients used in personal care products, namely oils, and also the detection of siloxanes in Chapter 6.

The sample form has also been found to be crucial for PADI analysis: characteristic ions from powders are easily detected but when these samples are prepared as a thin film only the volatile analytes are detected. This is also thought to be due to the ability to generate gas-phase ions.

As well as understanding the limitations of the technique, it is also important to find methods to overcome them. This has been demonstrated by the use of a thermal desorption stage to increase the temperature of analytes and to be able to analyse those which are less volatile, increasing their signal intensities by several orders of magnitude. For example, molecules with low vapour pressure, such as Irganox, can be analysed using this method (Irganox is not detected by DESI as discussed in Chapter 3).

Ambient mass spectrometry sources operate at atmospheric pressure, therefore the mass spectra from these sources exhibit a large background signal

containing adducts formed from atmospheric constituents. These can also provide information about the ionisation pathways; oxygen adducts are frequently observed in the negative ion mode, especially for polymer analysis. This can confirm the mechanisms postulated and discussed in Chapter 1. Interestingly, polymers are easily analysed with PADI providing rich fingerprint spectra unique to each polymer and showing the repeating monomer units. Clearly this is not a simple thermal desorption process and instead we speculate that there is a bond scission process first, analogous to SIMS, followed by thermal desorption. It is certainly evident that larger polymer fragments require higher surface temperatures, which would support this conjecture but it needs to be properly evaluated. It is proposed that a systematic study of a polymer with different molecular weights is conducted. A further study to investigate the capability of PADI for polymer depth profiling, offering a complementary technique to SIMS, is also part of ongoing investigations.

There are a multitude of ambient mass spectrometry sources, at the current count over 30, and this number is always increasing. Although a lot of research has been carried out and reported on the advantages of individual sources, little has been done to examine like-for-like comparisons of different AMS sources. We have performed a study to compare and show the differences and complementarities between DESI and PADI which have very different desorption/ionisation mechanisms. It is interesting to see the similarities between the mass spectra, the molecules that can be detected and the ions that are observed. PADI was able to detect characteristic ions from 13 molecules

commonly used in personal care products; however DESI was only able to detect ions from 9 of them. The PADI mass spectra also showed greater fragmentation compared to DESI. A real world example of an everyday object, skin creams, demonstrates how ambient techniques can be applied to complex samples in their native state. These can be in the form of pastes and liquids as well as the more traditional solid surfaces. This feature would not be possible with vacuum mass spectrometry techniques such as SIMS. As yet, we have not applied these techniques to *in vivo* analysis, however we are able to analyse fixed cells. This has provided a first look at the damage that these techniques can cause to cells and whether they will be suitable for live analysis, which could provide real-time monitoring as the techniques are quick enough and can also analyse any sample shape or form (within reasonable limits).

A comparison to more established techniques is needed to understand the current progress of ambient MS techniques and the advantages they can offer over more traditional vacuum based mass spectrometry. This is exemplified by the comparison of DESI and SIMS, where DESI has advantages in the analysis of larger biomolecules, as well as the simplicity of the mass spectra which are easier to interpret, and also the ease and quickness of analysis using the technique. However, a comparison like this, as well as showing the advantages and major areas of growth for this technique, draws to the attention the areas that DESI needs to improve on, such as sensitivity, repeatability and spatial resolution. We have shown in this thesis that PADI can be used to fill some of the measurement gaps where DESI is not successful, such as the analysis of polymers and some small molecules.

We are currently conducting a study to assess the differences in sensitivity between DESI, PADI and SIMS, as well as comparison with an atmospheric pressure MALDI source on the same Orbitrap™ mass spectrometer as the DESI and PADI. A range of different molecular types and weights will be analysed. This study will provide an exact comparison of the limit of detection and efficiency (counts per volume of analyte consumed) of the four techniques.

7.2   Future outlook

It is envisaged that each ambient mass spectrometry technique will have its own niche area; we have shown in this thesis that this is certainly true for DESI and PADI, they are complementary but also have select areas where they can be utilised to an advantage, such as polymer and volatile molecular analysis by PADI. In Table 7.1, a summary is provided on the different analytes and capabilities of DESI, PADI and SIMS.

Table 7.1. Summary of the analysis capabilities and types of molecule that can be analysed by DESI, PADI and SIMS. Notes: *(a) DESI is not able to analyse some small molecules dependent on their solubility or molecular type, *(b) with thermal desorption PADI is able to analyse small molecules with vapour pressures lower than 10^{-4} Pa.

		DESI	**PADI**	**SIMS**
	Small molecules	✓*(a)	VP $>10^{-4}$ Pa *(b)	✓
Analyte	*Biomolecules*	✓	X	X
	Polymers	X	✓	✓
	Surface MS	✓	✓	✓
Capability	*Imaging MS*	40-150 µm	150 - 1000 µm	< 1 µm
	Depth profiling	X	Potentially	✓

Research must be undertaken to further address the molecular types that plasma sources can successfully analyse, as well as their sensitivity and detection limits. A thorough investigation into the ionisation mechanisms, including studies using a modified (nitrogen or oxygen rich) atmosphere, will provide insight into what analytes the technique will be most successful at detecting. Quantitative analysis is also an important consideration in the future development and relevance of this technology. A few studies have already been undertaken in this area, showing the potential but also the current limitations that need to be overcome. These will be important steps before ambient plasma sources can be fully utilised and implemented into analytical laboratory workflows or for reliable in-field use.

The coupling of DESI or PADI to other desorption techniques will be one of the future directions in this area of research. We have already seen a few studies coupling laser ablation sources with plasma ionisation, as detailed in Chapter 1. The results from this thesis show that plasma techniques are not very successful at desorbing non-volatile molecules however they are successful ionisation sources. The potential to utilise plasmas as a post ionisation source coupled with other desorption processes, such as laser ablation, has great promise. This would enhance sensitivity and also provide the opportunity for mass spectrometry imaging at atmospheric pressure with improved spatial resolution.

Preliminary experiments using a new atmospheric pressure transmission mode laser ablation ion source with an additional plasma post-ionisation source have already been conducted. For these studies an 8 cm cube flatbed DBD source was utilised and placed between the sample and the inlet to the mass spectrometer, as shown in Figure 7.2. Initial results using this source are promising; for the analysis of caffeine, a 10 fold improvement in signal intensity was observed for the molecular ion when using the plasma post-ionisation source compared to results using laser ablation alone. However, a large increase in the background signal was also observed when using the plasma source. It is clear that modification and optimisation of the new sources are needed for them to reach their full potential.
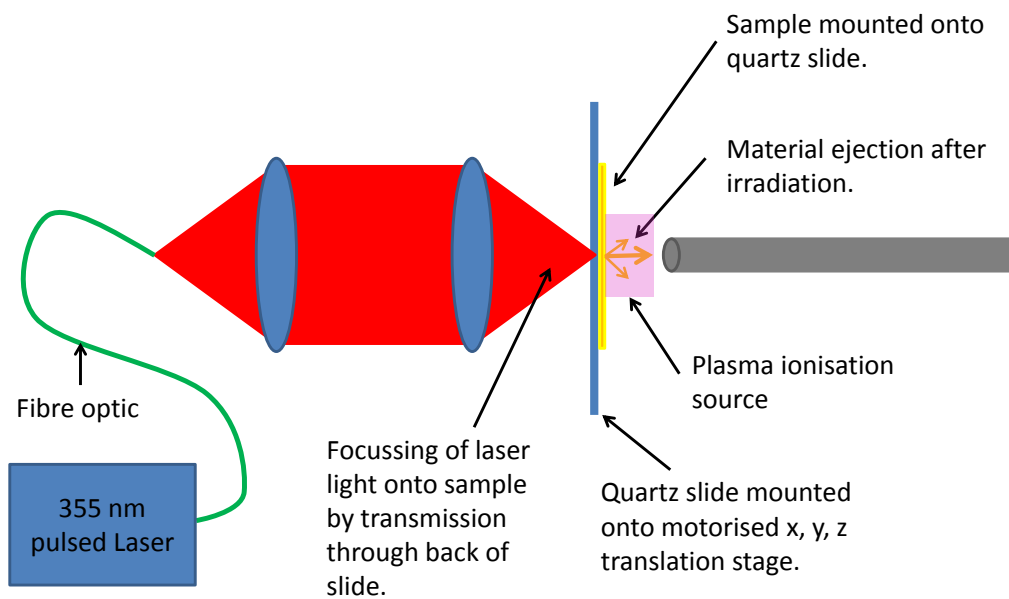
Figure 7.2. Schematic of the new high resolution atmospheric pressure transmission mode laser ablation ion source with additional plasma post-ionisation. Unpublished work courtesy of R. T. Steven, NPL.

References

1. Caprioli, R.M., Farmer, T.B., and Gile, J., *Molecular Imaging of Biological Samples: Localization of Peptides and Proteins Using MALDI-TOF MS.* Analytical Chemistry, 1997. **69**(23): p. 4751-4760.

2. Chaurand, P., Schwartz, S.A., and Caprioli, R.M., *Imaging mass spectrometry: a new tool to investigate the spatial organization of peptides and proteins in mammalian tissue sections.* Curr. Opin. Chem. Biol., 2002. **6**(5): p. 676-681.

3. Cornett, D.S., Reyzer, M.L., Chaurand, P., and Caprioli, R.M., *MALDI imaging mass spectrometry: molecular snapshots of biochemical systems.* Nat. Methods, 2007. **4**(10): p. 828-833.

4. McDonnell, L.A. and Heeren, R.M.A., *Imaging mass spectrometry.* Mass Spectrom. Rev., 2007. **26**(4): p. 606-643.

5. Gilmore, I.S., *SIMS of organics-Advances in 2D and 3D imaging and future outlook.* J. Vac. Sci. Technol. A, 2013. **31**(5): p. 050819.

6. Benninghoven, A., *Surface analysis by Secondary Ion Mass Spectrometry (SIMS).* Surf. Sci., 1994. **299**(1-3): p. 246-260.

7. Takats, Z., Wiseman, J.M., Gologan, B., and Cooks, R.G., *Mass Spectrometry Sampling Under Ambient Conditions with Desorption Electrospray Ionization.* Science, 2004. **306**(5695): p. 471-473.

8. Weston, D.J., *Ambient ionization mass spectrometry: current understanding of mechanistic theory; analytical performance and application areas.* Analyst, 2010. **135**(4): p. 661-668.

9. Cody, R.B., Laramee, J.A., and Durst, H.D., *Versatile new ion source for the analysis of materials in open air under ambient conditions.* Anal. Chem., 2005. **77**(8): p. 2297-2302.

10. Harris, G.A., Galhena, A.S., and Fernandez, F.M., *Ambient Sampling/Ionization Mass Spectrometry: Applications and Current Trends.* Anal. Chem., 2011. **83**(12): p. 4508-4538.

11. Venter, A., Nefliu, M., and Cooks, R.G., *Ambient desorption ionization mass spectrometry.* Trac-Trends Anal. Chem., 2008. **27**(4): p. 284-290.

12. Hu, Q.Z., Noll, R.J., Li, H.Y., Makarov, A., Hardman, M., and Cooks, R.G., *The Orbitrap: a new mass spectrometer.* Journal of Mass Spectrometry, 2005. **40**(4): p. 430-443.

13. Keil, A., Talaty, N., Janfelt, C., Noll, R.J., Gao, L., Ouyang, Z., and Cooks, R.G., *Ambient mass spectrometry with a handheld mass spectrometer at high pressure.* Anal. Chem., 2007. **79**(20): p. 7734-7739.

14. Albert, A., Shelley, J.T., and Engelhard, C., *Plasma-based ambient desorption/ionization mass spectrometry: state-of-the-art in qualitative and quantitative analysis.* Anal. Bioanal. Chem., 2014: p. 1-17.

15. Ding, X. and Duan, Y., *Plasma-based ambient mass spectrometry techniques: The current status and future prospective.* Mass Spectrom. Rev., 2013: p. n/a-n/a.

16. Andrade, F.J., Wetzel, W.C., Chan, G.C.Y., Webb, M.R., Gamez, G., Ray, S.J., and Hieftje, G.M., *A new, versatile, direct-current helium atmospheric-pressure glow discharge.* J. Anal. At. Spectrom., 2006. **21**(11): p. 1175-1184.

17. Andrade, F.J., Shelley, J.T., Wetzel, W.C., Webb, M.R., Gamez, G., Ray, S.J., and Hieftje, G.M., *Atmospheric pressure chemical ionization source. 1. Ionization of compounds in the gas phase.* Anal. Chem., 2008. **80**(8): p. 2646-2653.

18. Na, N., Zhao, M.X., Zhang, S.C., Yang, C.D., and Zhang, X.R., *Development of a dielectric barrier discharge ion source for ambient mass spectrometry.* J. Am. Soc. Mass Spectrom., 2007. **18**(10): p. 1859-1862.

19. Ratcliffe, L.V., Rutten, F.J.M., Barrett, D.A., Whitmore, T., Seymour, D., Greenwood, C., Aranda-Gonzalvo, Y., Robinson, S., and McCoustra, M., *Surface analysis under ambient conditions using plasma-assisted desorption/ionization mass spectrometry.* Anal. Chem., 2007. **79**(16): p. 6094-6101.

20. Harper, J.D., Charipar, N.A., Mulligan, C.C., Zhang, X.R., Cooks, R.G., and Ouyang, Z., *Low-Temperature Plasma Probe for Ambient Desorption Ionization.* Anal. Chem., 2008. **80**(23): p. 9097-9104.

21. Symonds, J.M., Galhena, A.S., Fernandez, F.M., and Orlando, T.M., *Microplasma Discharge Ionization Source for Ambient Mass Spectrometry.* Analytical Chemistry, 2010. **82**(2): p. 621-627.

22. Shelley, J.T., Wiley, J.S., Chan, G.C.Y., Schilling, G.D., Ray, S.J., and Hieftje, G.M., *Characterization of Direct-Current Atmospheric-Pressure Discharges Useful for Ambient Desorption/Ionization Mass Spectrometry.* J. Am. Soc. Mass Spectrom., 2009. **20**(5): p. 837-844.

23. Shelley, J.T., Wiley, J.S., and Hieftje, G.M., *Ultrasensitive Ambient Mass Spectrometric Analysis with a Pin-to-Capillary Flowing Atmospheric-*

Pressure Afterglow Source. Analytical Chemistry, 2011. **83**(14): p. 5741-5748.

24. Pfeuffer, K.P., Schaper, J.N., Shelley, J.T., Ray, S.J., Chan, G.C.Y., Bings, N.H., and Hieftje, G.M., *Halo-Shaped Flowing Atmospheric Pressure Afterglow: A Heavenly Design for Simplified Sample Introduction and Improved Ionization in Ambient Mass Spectrometry.* Analytical Chemistry, 2013. **85**(15): p. 7512-7518.

25. Stoffels, E., Flikweert, A.J., Stoffels, W.W., and Kroesen, G.M.W., *Plasma needle: a non-destructive atmospheric plasma source for fine surface treatment of (bio)materials.* Plasma Sources Sci. Technol., 2002. **11**(4): p. 383-388.

26. Almasian, M.R., Yang, C.D., Xing, Z., Zhang, S.C., and Zhang, X.R., *Development of a graphite low-temperature plasma source with dual-mode in-source fragmentation for ambient mass spectrometry.* Rapid Communications in Mass Spectrometry, 2010. **24**(6): p. 742-748.

27. Nudnova, M.M., Zhu, L., and Zenobi, R., *Active capillary plasma source for ambient mass spectrometry.* Rapid Communications in Mass Spectrometry, 2012. **26**(12): p. 1447-1452.

28. Chan, G.C.Y., Shelley, J.T., Wiley, J.S., Engelhard, C., Jackson, A.U., Cooks, R.G., and Hieftje, G.M., *Elucidation of Reaction Mechanisms Responsible for Afterglow and Reagent-Ion Formation in the Low-Temperature Plasma Probe Ambient Ionization Source.* Anal. Chem., 2011. **83**(10): p. 3675-3686.

29. Gross, J.H., *Direct analysis in real time-a critical review on DART-MS.* Anal. Bioanal. Chem., 2014. **406**(1): p. 63-80.

30. Cody, R.B., *Observation of Molecular Ions and Analysis of Nonpolar Compounds with the Direct Analysis in Real Time Ion Source.* Anal. Chem., 2009. **81**(3): p. 1101-1107.

31. Penning, F.M., *Uber Ionisation durch metastabile Atome.* Naturwissenschaften, 1927. **15**(40): p. 818-818.

32. Raizer, Y.P., *Gas Discharge Physics.* 1991, New York: Springer-Verlag.

33. Song, L.G., Gibson, S.C., Bhandari, D., Cook, K.D., and Bartmess, J.E., *Ionization Mechanism of Positive-Ion Direct Analysis in Real Time: A Transient Microenvironment Concept.* Analytical Chemistry, 2009. **81**(24): p. 10080-10088.

34. Meyer, C., Muller, S., Gilbert-Lopez, B., and Franzke, J., *Impact of homogeneous and filamentary discharge modes on the efficiency of dielectric*

barrier discharge ionization mass spectrometry. Anal. Bioanal. Chem., 2013. **405**(14): p. 4729-4735.

35.   Kratzer, J., Mester, Z., and Sturgeon, R.E., *Comparison of dielectric barrier discharge, atmospheric pressure radiofrequency-driven glow discharge and direct analysis in real time sources for ambient mass spectrometry of acetaminophen.* Spectrochim. Acta, Part B, 2011. **66**(8): p. 594-603.

36.   Olenici-Craciunescu, S.B., Michels, A., Meyer, C., Heming, R., Tombrink, S., Vautz, W., and Franzke, J., *Characterization of a capillary dielectric barrier plasma jet for use as a soft ionization source by optical emission and ion mobility spectrometry.* Spectroc. Acta Pt. B-Atom. Spectr., 2009. **64**(11-12): p. 1253-1258.

37.   Song, L.G., Dykstra, A.B., Yao, H.F., and Bartmess, J.E., *Ionization Mechanism of Negative Ion-Direct Analysis in Real Time: A Comparative Study with Negative Ion-Atmospheric Pressure Photoionization.* J. Am. Soc. Mass Spectrom., 2009. **20**(1): p. 42-50.

38.   Cody, R.B. and Dane, A.J., *Soft Ionization of Saturated Hydrocarbons, Alcohols and Nonpolar Compounds by Negative-Ion Direct Analysis in Real-Time Mass Spectrometry.* J. Am. Soc. Mass Spectrom., 2013. **24**(3): p. 329-334.

39.   Olenici-Craciunescu, S.B., Muller, S., Michels, A., Horvatic, V., Vadla, C., and Franzke, J., *Spatially resolved spectroscopic measurements of a dielectric barrier discharge plasma jet applicable for soft ionization.* Spectroc. Acta Pt. B-Atom. Spectr., 2011. **66**(3-4): p. 268-273.

40.   Xiong, Q., Lu, X., Liu, J., Xian, Y., Xiong, Z., Zou, F., Zou, C., Gong, W., Hu, J., Chen, K., Pei, X., Jiang, Z., and Pan, Y., *Temporal and spatial resolved optical emission behaviors of a cold atmospheric pressure plasma jet.* J. Appl. Phys., 2009. **106**(8): p. 083302.

41.   Heywood, M.S., Taylor, N., and Farnsworth, P.B., *Measurement of Helium Metastable Atom Densities in a Plasma-Based Ambient Ionization Source.* Anal. Chem., 2011. **83**(17): p. 6493-6499.

42.   Shelley, J.T., Chan, G.C.Y., and Hieftje, G.M., *Understanding the Flowing Atmospheric-Pressure Afterglow (FAPA) Ambient Ionization Source through Optical Means.* J. Am. Soc. Mass Spectrom., 2012. **23**(2): p. 407-417.

43.   Chan, G.C.Y., Shelley, J.T., Jackson, A.U., Wiley, J.S., Engelhard, C., Cooks, R.G., and Hieftje, G.M., *Spectroscopic plasma diagnostics on a low-temperature plasma probe for ambient mass spectrometry.* J. Anal. At. Spectrom., 2011. **26**(7): p. 1434-1444.

44. Shelley, J.T., Stindt, A., Riedel, J., and Engelhard, C., *Time-resolved mass-spectral characterization of ion formation from a low-frequency, low-temperature plasma probe ambient ionization source.* J. Anal. At. Spectrom., 2014. **29**(2): p. 359-366.

45. Andrade, F.J., Shelley, J.T., Wetzel, W.C., Webb, M.R., Gamez, G., Ray, S.J., and Hieftje, G.M., *Atmospheric pressure chemical ionization source. 2. Desorption-ionization for the direct analysis of solid compounds.* Anal. Chem., 2008. **80**(8): p. 2654-2663.

46. Radu, I., Bartnikas, R., and Wertheimer, M.R., *Frequency and voltage dependence of glow and pseudoglow discharges in helium under atmospheric pressure.* IEEE Trans. Plasma Sci., 2003. **31**(6): p. 1363-1378.

47. Martens, T., Bogaerts, A., Brok, W.J.M., and Dijk, J.V., *The dominant role of impurities in the composition of high pressure noble gas plasmas.* Appl. Phys. Lett., 2008. **92**(4): p. 041504.

48. Albert, A. and Engelhard, C., *Characteristics of Low-Temperature Plasma Ionization for Ambient Mass Spectrometry Compared to Electrospray Ionization and Atmospheric Pressure Chemical Ionization.* Analytical Chemistry, 2012. **84**(24): p. 10657-10664.

49. Harrison, A.G., *Chemical ionization mass spectrometry, 2nd edition*. Organic Mass Spectrometry. 1992: C.R.C. press. 152-152.

50. Garcia-Reyes, J.F., Harper, J.D., Salazar, G.A., Charipar, N.A., Ouyang, Z., and Cooks, R.G., *Detection of Explosives and Related Compounds by Low-Temperature Plasma Ambient Ionization Mass Spectrometry.* Anal. Chem., 2011. **83**(3): p. 1084-1092.

51. Gillen, G., Mahoney, C., Wight, S., and Lareau, R., *Characterization of high explosive particles using cluster secondary ion mass spectrometry.* Rapid Communications in Mass Spectrometry, 2006. **20**(12): p. 1949-1953.

52. Na, N., Zhang, C., Zhao, M.X., Zhang, S.C., Yang, C.D., Fang, X., and Zhang, X.R., *Direct detection of explosives on solid surfaces by mass spectrometry with an ambient ion source based on dielectric barrier discharge.* Journal of Mass Spectrometry, 2007. **42**(8): p. 1079-1085.

53. Zhang, Y., Ma, X.X., Zhang, S.C., Yang, C.D., Ouyang, Z., and Zhang, X.R., *Direct detection of explosives on solid surfaces by low temperature plasma desorption mass spectrometry.* Analyst, 2009. **134**(1): p. 176-181.

54. Garcia-Reyes, J.F., Mazzoti, F., Harper, J.D., Charipar, N.A., Oradu, S., Ouyang, Z., Sindona, G., and Cooks, R.G., *Direct olive oil analysis by low-*

temperature plasma (LTP) ambient ionization mass spectrometry. Rapid Commun. Mass Spectrom., 2009. **23**(19): p. 3057-3062.

55.   Shelley, J.T. and Hieftje, G.M., *Ionization matrix effects in plasma-based ambient mass spectrometry sources.* J. Anal. At. Spectrom., 2010. **25**(3): p. 345-350.

56.   Liu, Y.Y., Lin, Z.Q., Zhang, S.C., Yang, C.D., and Zhang, X.R., *Rapid screening of active ingredients in drugs by mass spectrometry with low-temperature plasma probe.* Anal. Bioanal. Chem., 2009. **395**(3): p. 591-599.

57.   Zhan, X.F., Zhao, Z.J., Yuan, X., Wang, Q.H., Li, D.D., Xie, H., Li, X.M., Zhou, M.G., and Duan, Y.X., *Microwave-Induced Plasma Desorption/Ionization Source for Ambient Mass Spectrometry.* Anal. Chem., 2013. **85**(9): p. 4512-4519.

58.   Brewer, T.M. and Verkouteren, J.R., *Atmospheric identification of active ingredients in over-the-counter pharmaceuticals and drugs of abuse by atmospheric pressure glow discharge mass spectrometry (APGD-MS).* Rapid Commun. Mass Spectrom., 2011. **25**(17): p. 2407-2417.

59.   Martinez-Jarquin, S. and Winkler, R., *Design of a low-temperature plasma (LTP) probe with adjustable output temperature and variable beam diameter for the direct detection of organic molecules.* Rapid Communications in Mass Spectrometry, 2013. **27**(5): p. 629-634.

60.   Dalgleish, J.K., Wleklinski, M., Shelley, J.T., Mulligan, C.C., Ouyang, Z., and Cooks, R.G., *Arrays of low-temperature plasma probes for ambient ionization mass spectrometry.* Rapid Communications in Mass Spectrometry, 2013. **27**(1): p. 135-142.

61.   Usmanov, D.T., Ninomiya, S., and Hiraoka, K., *Flash Desorption/Mass Spectrometry for the Analysis of Less- and Nonvolatile Samples Using a Linearly Driven Heated Metal Filament.* J. Am. Soc. Mass Spectrom., 2013. **24**(11): p. 1727-1735.

62.   Jackson, A.U., Garcia-Reyes, J.F., Harper, J.D., Wiley, J.S., Molina-Diaz, A., Ouyang, Z., and Cooks, R.G., *Analysis of drugs of abuse in biofluids by low temperature plasma (LTP) ionization mass spectrometry.* Analyst, 2010. **135**(5): p. 927-933.

63.   Benassi, M., Berisha, A., Romao, W., Babayev, E., Rompp, A., and Spengler, B., *Petroleum crude oil analysis using low-temperature plasma mass spectrometry.* Rapid Commun. Mass Spectrom., 2013. **27**(7): p. 825-834.

64.   Chen, W.D., Hou, K.Y., Xiong, X.C., Jiang, Y., Zhao, W.D., Hua, L., Chen, P., Xie, Y.Y., Wang, Z.X., and Li, H.Y., *Non-contact halogen lamp heating*

assisted LTP ionization miniature rectilinear ion trap: a platform for rapid, on-site explosives analysis. Analyst, 2013. **138**(17): p. 5068-5073.

65.   Huang, G.M., Zheng, O.Y., and Cooks, R.G., *High-throughput trace melamine analysis in complex mixtures.* Chemical Communications, 2009(5): p. 556-558.

66.   Liu, Y.Y., Ma, X.X., Lin, Z.Q., He, M.J., Han, G.J., Yang, C.D., Xing, Z., Zhang, S.C., and Zhang, X.R., *Imaging Mass Spectrometry with a Low-Temperature Plasma Probe for the Analysis of Works of Art.* Angew. Chem.-Int. Edit., 2010. **49**(26): p. 4435-4437.

67.   Campbell, D.I., Dalgleish, J.K., Cotte-Rodriguez, I., Maeno, S., and Cooks, R.G., *Chemical analysis and chemical imaging of fragrances and volatile compounds by low-temperature plasma ionization mass spectrometry.* Rapid Commun. Mass Spectrom., 2013. **27**(16): p. 1828-1836.

68.   Shiea, J., Huang, M.Z., Hsu, H.J., Lee, C.Y., Yuan, C.H., Beech, I., and Sunner, J., *Electrospray-assisted laser desorption/ionization mass spectrometry for direct ambient analysis of solids.* Rapid Communications in Mass Spectrometry, 2005. **19**(24): p. 3701-3704.

69.   Nemes, P. and Vertes, A., *Laser ablation electrospray ionization for atmospheric pressure, in vivo, and imaging mass spectrometry.* Analytical Chemistry, 2007. **79**(21): p. 8098-8106.

70.   Galhena, A.S., Harris, G.A., Nyadong, L., Murray, K.K., and Fernandez, F.M., *Small Molecule Ambient Mass Spectrometry Imaging by Infrared Laser Ablation Metastable-Induced Chemical Ionization.* Analytical Chemistry, 2010. **82**(6): p. 2178-2181.

71.   He, X.N., Xie, Z.Q., Gao, Y., Hu, W., Guo, L.B., Jiang, L., and Lu, Y.F., *Mass spectrometry of solid samples in open air using combined laser ionization and ambient metastable ionization.* Spectroc. Acta Pt. B-Atom. Spectr., 2012. **67**: p. 64-73.

72.   Zhang, J.L., Zhou, Z.G., Yang, J.W., Zhang, W., Bai, Y., and Liu, H.W., *Thin Layer Chromatography/Plasma Assisted Multiwavelength Laser Desorption Ionization Mass Spectrometry for Facile Separation and Selective Identification of Low Molecular Weight Compounds.* Analytical Chemistry, 2012. **84**(3): p. 1496-1503.

73.   Zhang, J., Li, Z., Zhang, C., Feng, B., Zhou, Z., Bai, Y., and Liu, H., *Graphite-Coated Paper as Substrate for High Sensitivity Analysis in Ambient Surface-Assisted Laser Desorption/Ionization Mass Spectrometry.* Analytical Chemistry, 2012. **84**(7): p. 3296-3301.

74. Feng, B.S., Zhang, J.L., Chang, C.L., Li, L.P., Li, M., Xiong, X.C., Guo, C.G., Tang, F., Bai, Y., and Liu, H.W., *Ambient Mass Spectrometry Imaging: Plasma Assisted Laser Desorption Ionization Mass Spectrometry Imaging and Its Applications.* Analytical Chemistry, 2014. **86**(9): p. 4164-4169.

75. Gilbert-Lopez, B., Schilling, M., Ahlmann, N., Michels, A., Hayen, H., Molina-Diaz, A., Garcia-Reyes, J.F., and Franzke, J., *Ambient Diode Laser Desorption Dielectric Barrier Discharge Ionization Mass Spectrometry of Nonvolatile Chemicals.* Anal. Chem., 2013. **85**(6): p. 3174-3182.

76. Bregy, L., Sinues, P.M.L., Nudnova, M.M., and Zenobi, R., *Real-time breath analysis with active capillary plasma ionization-ambient mass spectrometry.* J. Breath Res., 2014. **8**(2): p. 8.

77. Gong, X.Y., Xiong, X.C., Peng, Y.E., Yang, C.D., Zhang, S.C., Fang, X., and Zhang, X.R., *Low-temperature plasma ionization source for the online detection of indoor volatile organic compounds.* Talanta, 2011. **85**(5): p. 2458-2462.

78. Bowfield, A., Barrett, D.A., Alexander, M.R., Ortori, C.A., Rutten, F.M., Salter, T.L., Gilmore, I.S., and Bradley, J.W., *Surface analysis using a new plasma assisted desorption/ionisation source for mass spectrometry in ambient air.* Rev. Sci. Instrum., 2012. **83**(6): p. 063503.

79. Jecklin, M.C., Gamez, G., and Zenobi, R., *Fast polymer fingerprinting using flowing afterglow atmospheric pressure glow discharge mass spectrometry.* Analyst, 2009. **134**(8): p. 1629-1636.

80. Wiley, J.S., Garcia-Reyes, J.F., Harper, J.D., Charipar, N.A., Ouyang, Z., and Cooks, R.G., *Screening of agrochemicals in foodstuffs using low-temperature plasma (LTP) ambient ionization mass spectrometry.* Analyst, 2010. **135**(5): p. 971-979.

81. Soparawalla, S., Tadjimukhamedov, F.K., Wiley, J.S., Ouyang, Z., and Cooks, R.G., *In situ analysis of agrochemical residues on fruit using ambient ionization on a handheld mass spectrometer.* Analyst, 2011. **136**(21): p. 4392-4396.

82. Jecklin, M.C., Gamez, G., Touboul, D., and Zenobi, R., *Atmospheric pressure glow discharge desorption mass spectrometry for rapid screening of pesticides in food.* Rapid Communications in Mass Spectrometry, 2008. **22**(18): p. 2791-2798.

83. Wang, H., Sun, W.J., Zhang, J.S., Yang, X.H., Lin, T., and Ding, L., *Desorption corona beam ionization source for mass spectrometry.* Analyst, 2010. **135**(4): p. 688-695.

84.   Huang, G.M., Xu, W., Visbal-Onufrak, M.A., Ouyang, Z., and Cooks, R.G., *Direct analysis of melamine in complex matrices using a handheld mass spectrometer.* Analyst, 2010. **135**(4): p. 705-711.

85.   Stein, M.J., Lo, E., Castner, D.G., and Ratner, B.D., *Plasma Pencil Atmospheric Mass Spectrometry Detection of Positive Ions from Micronutrients Emitted from Surfaces.* Analytical Chemistry, 2012. **84**(3): p. 1572-1578.

86.   Zhang, J.I., Costa, A.B., Tao, W.A., and Cooks, R.G., *Direct detection of fatty acid ethyl esters using low temperature plasma (LTP) ambient ionization mass spectrometry for rapid bacterial differentiation.* Analyst, 2011. **136**(15): p. 3091-3097.

87.   Zhang, J.I., Tao, W.A., and Cooks, R.G., *Facile Determination of Double Bond Position in Unsaturated Fatty Acids and Esters by Low Temperature Plasma Ionization Mass Spectrometry.* Analytical Chemistry, 2011. **83**(12): p. 4738-4744.

88.   Benassi, M., Garcia-Reyes, J.F., and Spengler, B., *Ambient ion/molecule reactions in low-temperature plasmas (LTP): reactive LTP mass spectrometry.* Rapid Communications in Mass Spectrometry, 2013. **27**(7): p. 795-804.

89.   Ma, X.X., Zhang, S.C., Lin, Z.Q., Liu, Y.Y., Xing, Z., Yang, C.D., and Zhang, X.R., *Real-time monitoring of chemical reactions by mass spectrometry utilizing a low-temperature plasma probe.* Analyst, 2009. **134**(9): p. 1863-1867.

90.   Na, N., Xia, Y., Zhu, Z.L., Zhang, X.R., and Cooks, R.G., *Birch Reduction of Benzene in a Low-Temperature Plasma.* Angew. Chem.-Int. Edit., 2009. **48**(11): p. 2017-2019.

91.   Norgaard, A.W., Vibenholt, A., Benassi, M., Clausen, P.A., and Wolkoff, P., *Study of Ozone-Initiated Limonene Reaction Products by Low Temperature Plasma Ionization Mass Spectrometry.* J. Am. Soc. Mass Spectrom., 2013. **24**(7): p. 1090-1096.

92.   Vortmann, B., Nowak, S., and Engelhard, C., *Rapid Characterization of Lithium Ion Battery Electrolytes and Thermal Aging Products by Low-Temperature Plasma Ambient Ionization High-Resolution Mass Spectrometry.* Analytical Chemistry, 2013. **85**(6): p. 3433-3438.

93.   Schaper, J.N., Pfeuffer, K.P., Shelley, J.T., Bings, N.H., and Hieftje, G.M., *Drop-on-Demand Sample Introduction System Coupled with the Flowing Atmospheric-Pressure Afterglow for Direct Molecular Analysis of Complex*

Liquid Microvolume Samples. Analytical Chemistry, 2012. **84**(21): p. 9246-9252.

94.   Hiraoka, K., Ninomiya, S., Chen, L.C., Iwama, T., Mandal, M.K., Suzuki, H., Ariyada, O., Furuya, H., and Takekawa, K., *Development of double cylindrical dielectric barrier discharge ion source.* Analyst, 2011. **136**(6): p. 1210-1215.

95.   Wang, H., Wu, Y.N., Guo, B., Sun, W.J., Ding, L., and Chen, B., *Quantification of low-polar small molecules using room temperature ionic liquids matrix-assisted desorption corona beam ionization.* Analyst, 2012. **137**(17): p. 3982-3988.

96.   Li, L.P., Feng, B.S., Yang, J.W., Chang, C.L., Bai, Y., and Liu, H.W., *Applications of ambient mass spectrometry in high-throughput screening.* Analyst, 2013. **138**(11): p. 3097-3103.

97.   Bowfield, A., Bunch, J., Salter, T.L., Steven, R.T., Gilmore, I.S., Barrett, D.A., Alexander, M.R., McKay, K., and Bradley, J.W., *Characterisation of a micro-plasma for ambient mass spectrometry imaging.* Analyst, 2014. **139**(21): p. 5430-5438.

98.   Shelley, J.T., Ray, S.J., and Hieftje, G.M., *Laser Ablation Coupled to a Flowing Atmospheric Pressure Afterglow for Ambient Mass Spectral Imaging.* Analytical Chemistry, 2008. **80**(21): p. 8308-8313.

99.   Bennett, R.V., Morzan, E.M., Huckaby, J.O., Monge, M.E., Christensen, H.I., and Fernandez, F.M., *Robotic plasma probe ionization mass spectrometry (RoPPI-MS) of non-planar surfaces.* Analyst, 2014. **139**(11): p. 2658-2662.

100.   Li, L.F., Chen, T.C., Ren, Y., Hendricks, P.I., Cooks, R.G., and Ouyang, Z., *Mini 12, Miniature Mass Spectrometer for Clinical and Other Applications-Introduction and Characterization.* Analytical Chemistry, 2014. **86**(6): p. 2909-2916.

101.   Wiley, J.S., Shelley, J.T., and Cooks, R.G., *Handheld Low-Temperature Plasma Probe for Portable "Point-and-Shoot" Ambient Ionization Mass Spectrometry.* Analytical Chemistry, 2013. **85**(14): p. 6545-6552.

102.   Hendricks, P.I., Dalgleish, J.K., Shelley, J.T., Kirleis, M.A., McNicholas, M.T., Li, L., Chen, T.-C., Chen, C.-H., Duncan, J.S., Boudreau, F., Noll, R.J., Denton, J.P., Roach, T.A., Ouyang, Z., and Cooks, R.G., *Autonomous in Situ Analysis and Real-Time Chemical Detection Using a Backpack Miniature Mass Spectrometer: Concept, Instrumentation Development, and Performance.* Analytical Chemistry, 2014. **86**(6): p. 2900-2908.

103. Hoffmann, E. and Stroobant, V., *Mass Spectrometry: Principles and Applications*. Third ed. 2007, Chichester, UK: Wiley.

104. Hager, J.W., *A new linear ion trap mass spectrometer.* Rapid Communications in Mass Spectrometry, 2002. **16**(6): p. 512-526.

105. Makarov, A., *Electrostatic Axially Harmonic Orbital Trapping: A High-Performance Technique of Mass Analysis.* Analytical Chemistry, 2000. **72**(6): p. 1156-1162.

106. Kingdon, K.H., *A Method for the Neutralization of Electron Space Charge by Positive Ionization at Very Low Gas Pressures.* Physical Review, 1923. **21**(4): p. 408-418.

107. Michalski, A., Damoc, E., Lange, O., Denisov, E., Nolting, D., Müller, M., Viner, R., Schwartz, J., Remes, P., Belford, M., Dunyach, J.-J., Cox, J., Horning, S., Mann, M., and Makarov, A., *Ultra High Resolution Linear Ion Trap Orbitrap Mass Spectrometer (Orbitrap Elite) Facilitates Top Down LC MS/MS and Versatile Peptide Fragmentation Modes.* Mol. Cell. Proteomics, 2012. **11**(3): p. O111.013698.

108. Makarov, A., Denisov, E., and Lange, O., *Performance Evaluation of a High-field Orbitrap Mass Analyzer.* J. Am. Soc. Mass Spectrom., 2009. **20**(8): p. 1391-1396.

109. Olsen, J.V., Schwartz, J.C., Griep-Raming, J., Nielsen, M.L., Damoc, E., Denisov, E., Lange, O., Remes, P., Taylor, D., Splendore, M., Wouters, E.R., Senko, M., Makarov, A., Mann, M., and Horning, S., *A Dual Pressure Linear Ion Trap Orbitrap Instrument with Very High Sequencing Speed.* Mol. Cell. Proteomics, 2009. **8**(12): p. 2759-2769.

110. Makarov, A.A. *Theory and Practice of the Orbitrap Mass Analyzer*. in *54th ASMS Conference on Mass Spectrometry and Allied Topics*. 2006. Seattle.

111. Makarov, A., Denisov, E., Kholomeev, A., Balschun, W., Lange, O., Strupat, K., and Horning, S., *Performance Evaluation of a Hybrid Linear Ion Trap/Orbitrap Mass Spectrometer.* Analytical Chemistry, 2006. **78**(7): p. 2113-2120.

112. Hardman, M. and Makarov, A.A., *Interfacing the orbitrap mass analyzer to an electrospray ion source.* Analytical Chemistry, 2003. **75**(7): p. 1699-1705.

113. Michalski, A., Damoc, E., Hauschild, J.-P., Lange, O., Wieghaus, A., Makarov, A., Nagaraj, N., Cox, J., Mann, M., and Horning, S., *Mass Spectrometry-based Proteomics Using Q Exactive, a High-performance Benchtop Quadrupole Orbitrap Mass Spectrometer.* Mol. Cell. Proteomics, 2011. **10**(9): p. M111.011015.

114. Conrads, H. and Schmidt, M., *Plasma generation and plasma sources*. Plasma Sources Sci. Technol., 2000. **9**(4): p. 441-454.

115. Lieberman, M.A. and Lichtenburg, A.J., *Principles of Plasma Discharges and Materials Processing*. 2 ed. 2005: Wiley.

116. Becker, K.H., Kersten, H., Hopwood, J., and Lopez, J.L., *Microplasmas: scientific challenges & technological opportunities*. The European Physical Journal D, 2010. **60**(3): p. 437-439.

117. Schutze, A., Jeong, J.Y., Babayan, S.E., Park, J., Selwyn, G.S., and Hicks, R.F., *The atmospheric-pressure plasma jet: A review and comparison to other plasma sources*. IEEE Trans. Plasma Sci., 1998. **26**(6): p. 1685-1694.

118. Tendero, C., Tixier, C., Tristant, P., Desmaison, J., and Leprince, P., *Atmospheric pressure plasmas: A review*. Spectrochimica Acta Part B: Atomic Spectroscopy, 2006. **61**(1): p. 2-30.

119. Sladek, R.E.J. and Stoffels, E., *Deactivation of Escherichia coli by the plasma needle*. J. Phys. D-Appl. Phys., 2005. **38**(11): p. 1716-1721.

120. Talaty, N., Takats, Z., and Cooks, R.G., *Rapid in situ detection of alkaloids in plant tissue under ambient conditions using desorption electrospray ionization*. Analyst, 2005. **130**(12): p. 1624-1633.

121. Wiseman, J.M., Puolitaival, S.M., Takats, Z., Cooks, R.G., and Caprioli, R.M., *Mass spectrometric profiling of intact biological tissue by using desorption electrospray ionization*. Angew. Chem.-Int. Edit., 2005. **44**(43): p. 7094-7097.

122. Takats, Z., Cotte-Rodriguez, I., Talaty, N., Chen, H.W., and Cooks, R.G., *Direct, trace level detection of explosives on ambient surfaces by desorption electrospray ionization mass spectrometry*. Chemical Communications, 2005(15): p. 1950-1952.

123. Monge, M.E., Harris, G.A., Dwivedi, P., and Fernandez, F.M., *Mass Spectrometry: Recent Advances in Direct Open Air Surface Sampling/Ionization*. Chem. Rev., 2013. **113**(4): p. 2269-2308.

124. Venter, A., Sojka, P.E., and Cooks, R.G., *Droplet dynamics and ionization mechanisms in desorption electrospray ionization mass spectrometry*. Analytical Chemistry, 2006. **78**(24): p. 8549-8555.

125. Costa, A.B. and Cooks, R.G., *Simulated splashes: Elucidating the mechanism of desorption electrospray ionization mass spectrometry*. Chem. Phys. Lett., 2008. **464**(1-3): p. 1-8.

126.   Costa, A.B. and Cooks, R.G., *Simulation of atmospheric transport and droplet-thin film collisions in desorption electrospray ionization.* Chemical Communications, 2007(38): p. 3915-3917.

127.   Green, F.M., Stokes, P., Hopley, C., Seah, M.P., Gilmore, I.S., and O'Connor, G., *Developing Repeatable Measurements for Reliable Analysis of Molecules at Surfaces Using Desorption Electrospray Ionization.* Analytical Chemistry, 2009. **81**(6): p. 2286-2293.

128.   Takats, Z., Wiseman, J.M., and Cooks, R.G., *Ambient mass spectrometry using desorption electrospray ionization (DESI): instrumentation, mechanisms and applications in forensics, chemistry, and biology.* Journal of Mass Spectrometry, 2005. **40**(10): p. 1261-1275.

129.   Green, F.M., Salter, T.L., Gilmore, I.S., Stokes, P., and O'Connor, G., *The effect of electrospray solvent composition on desorption electrospray ionisation (DESI) efficiency and spatial resolution.* Analyst, 2010. **135**(4): p. 731-737.

130.   Vickerman, J.C. and Gilmore, I.S., eds. *Surface Analysis - The Principal Techniques, 2nd Edition*. 2009, Wiley: Chichester, UK. 113-206.

131.   Cooks, R.G., Ouyang, Z., Takats, Z., and Wiseman, J.M., *Ambient mass spectrometry.* Science, 2006. **311**(5767): p. 1566-1570.

132.   Cotte-Rodriguez, I., Takats, Z., Talaty, N., Chen, H.W., and Cooks, R.G., *Desorption electrospray ionization of explosives on surfaces: Sensitivity and selectivity enhancement by reactive desorption electrospray ionization.* Anal. Chem., 2005. **77**(21): p. 6755-6764.

133.   Justes, D.R., Talaty, N., Cotte-Rodriguez, I., and Cooks, R.G., *Detection of explosives on skin using ambient ionization mass spectrometry.* Chem. Commun., 2007(21): p. 2142-2144.

134.   Cotte-Rodriguez, I., Hernandez-Soto, H., Chen, H., and Cooks, R.G., *In situ trace detection of peroxide explosives by desorption electrospray ionization and desorption atmospheric pressure chemical ionization.* Analytical Chemistry, 2008. **80**(5): p. 1512-1519.

135.   Green, F.M., Salter, T.L., Stokes, P., Gilmore, I.S., and O'Connor, G., *Ambient mass spectrometry: advances and applications in forensics.* Surf. Interface Anal., 2010. **42**(5): p. 347-357.

136.   Nyadong, L., Late, S., Green, M.D., Banga, A., and Fernandez, F.M., *Direct quantitation of active ingredients in solid artesunate antimalarials by noncovalent complex forming reactive desorption electrospray ionization mass spectrometry.* J. Am. Soc. Mass Spectrom., 2008. **19**(3): p. 380-388.

137.   Chen, H., Li, M., Zhang, Y.P., Yang, X., Lian, J.J., and Chen, J.M., *Rapid analysis of SVOC in aerosols by desorption electrospray ionization mass spectrometry.* J. Am. Soc. Mass Spectrom., 2008. **19**(3): p. 450-454.

138.   Manicke, N.E., Wiseman, J.M., Ifa, D.R., and Cooks, R.G., *Desorption electrospray ionization (DESI) mass Spectrometry and tandem mass spectrometry (MS/MS) of phospholipids and sphingolipids: Ionization, adduct formation, and fragmentation.* J. Am. Soc. Mass Spectrom., 2008. **19**(4): p. 531-543.

139.   Shin, Y.S., Drolet, B., Mayer, R., Dolence, K., and Basile, F., *Desorption electrospray ionization-mass spectrometry of proteins.* Analytical Chemistry, 2007. **79**(9): p. 3514-3518.

140.   Ifa, D.R., Wiseman, J.M., Song, Q.Y., and Cooks, R.G., *Development of capabilities for imaging mass spectrometry under ambient conditions with desorption electrospray ionization (DESI).* Int. J. Mass Spectrom., 2007. **259**(1-3): p. 8-15.

141.   Kertesz, V. and Van Berkel, G.J., *Improved imaging resolution in desorption electrospray ionization mass spectrometry.* Rapid Communications in Mass Spectrometry, 2008. **22**(17): p. 2639-2644.

142.   Gilmore, I.S. and Seah, M.P., *Static SIMS: towards unfragmented mass spectra - the G-SIMS procedure.* Applied Surface Science, 2000. **161**(3-4): p. 465-480.

143.   Gilmore, I.S. and Seah, M.P., *Static SIMS: A study of damage using polymers.* Surf. Interface Anal., 1996. **24**(11): p. 746-762.

144.   Green, F.M., Kollmer, F., Niehuis, E., Gilmore, I.S., and Seah, M.P., *Imaging G-SIMS: a novel bismuth-manganese source emitter.* Rapid Communications in Mass Spectrometry, 2008. **22**(16): p. 2602-2608.

145.   Gilmore, I.S. and Seah, M.P., *Organic molecule characterization - G-SIMS.* Applied Surface Science, 2004. **231**: p. 224-229.

146.   Green, F.M., Seah, M.P., Gilmore, I.S., Salter, T.L., and Spencer, S.J., *Analysis of thin films and molecular orientation using cluster SIMS.* Surf. Interface Anal., 2011. **43**(9): p. 1224-1230.

147.   Szakal, C. and Brewer, T.M., *Analysis and Mechanisms of Cyclotrimethylenetrinitramine Ion Formation in Desorption Electrospray Ionization.* Analytical Chemistry, 2009. **81**(13): p. 5257-5266.

148.   Nefliu, M., Cooks, R.G., and Moore, C., *Enhanced desorption ionization using oxidizing electrosprays.* J. Am. Soc. Mass Spectrom., 2006. **17**(8): p. 1091-1095.

149. Kauppila, T.J., Wiseman, J.M., Ketola, R.A., Kotiaho, T., Cooks, R.G., and Kostiainen, R., *Desorption electrospray ionization mass spectrometry for the analysis of pharmaceuticals and metabolites.* Rapid Communications in Mass Spectrometry, 2006. **20**(3): p. 387-392.

150. Mahoney, C.M., *Cluster secondary ion mass spectrometry of polymers and related materials.* Mass Spectrom. Rev., 2010. **29**(2): p. 247-293.

151. Nefliu, M., Venter, A., and Cooks, R.G., *Desorption electrospray ionization and electrosonic spray ionization for solid- and solution-phase analysis of industrial polymers.* Chem. Commun., 2006(8): p. 888-890.

152. Rothenbacher, T. and Schwack, W., *Rapid and nondestructive analysis of phthalic acid esters in toys made of poly(vinyl chloride) by direct analysis in real time single-quadrupole mass spectrometry.* Rapid Commun. Mass Spectrom., 2009. **23**(17): p. 2829-2835.

153. Beck, A.J., Gonzalvo, Y.A., Pilkington, A., Yerokhin, A., and Matthews, A., *Positive Ion Mass Spectrometry during an Atmospheric Pressure Plasma Treatment of Polymers.* Plasma Process. Polym., 2009. **6**(8): p. 521-529.

154. Tuccitto, N., Lobo, L., Tempez, A., Delfanti, I., Chapon, P., Canulescu, S., Bordel, N., Michler, J., and Licciardello, A., *Pulsed radiofrequency glow discharge time-of-flight mass spectrometry for molecular depth profiling of polymer-based films.* Rapid Commun. Mass Spectrom., 2009. **23**(5): p. 549-556.

155. Lobo, L., Tuccitto, N., Bordel, N., Pereiro, R., Pisonero, J., Licciardello, A., Tempez, A., Chapon, P., and Sanz-Medel, A., *Polymer screening by radiofrequency glow discharge time-of-flight mass spectrometry.* Anal. Bioanal. Chem., 2010. **396**(8): p. 2863-2869.

156. Salter, T.L., Green, F.M., Faruqui, N., and Gilmore, I.S., *Analysis of personal care products on model skin surfaces using DESI and PADI ambient mass spectrometry.* Analyst, 2011. **136**(16): p. 3274-3280.

157. Keenan, M.R. and Kotula, P.G., *Accounting for Poisson noise in the multivariate analysis of ToF-SIMS spectrum images.* Surf. Interface Anal., 2004. **36**(3): p. 203-212.

158. Chen, H.W., Zheng, J., Zhang, X., Luo, M.B., Wang, Z.C., and Qiao, X.L., *Surface desorption atmospheric pressure chemical ionization mass spectrometry for direct ambient sample analysis without toxic chemical contamination.* Journal of Mass Spectrometry, 2007. **42**(8): p. 1045-1056.

159. Dalgleish, J.K., Wleklinski, M., Shelley, J.T., Mulligan, C.C., Ouyang, Z., and Cooks, R.G., *Development and characterization of bundled arrays of low-*

temperature plasma probes for use as improved ambient ionization sources Proceedings of the 60th ASMS Conference on Mass Spectrometry and Allied Topics **2012**.

160. Shick, C.R., DePalma, P.A., and Marcus, R.K., *Radio frequency glow discharge mass spectrometry for the characterization of bulk polymers.* Anal. Chem., 1996. **68**(13): p. 2113-2121.

161. Nilles, J.M., Connell, T.R., and Durst, H.D., *Thermal separation to facilitate Direct Analysis in Real Time (DART) of mixtures.* Analyst, 2010. **135**(5): p. 883-886.

162. Krechmer, J., Tice, J., Crawford, E., and Musselman, B., *Increasing the rate of sample vaporization in an open air desorption ionization source by using a heated metal screen as a sample holder.* Rapid Communications in Mass Spectrometry, 2011. **25**(17): p. 2384-2388.

163. Saha, S., Chen, L.C., Mandal, M.K., and Hiraoka, K., *Leidenfrost Phenomenon-assisted Thermal Desorption (LPTD) and Its Application to Open Ion Sources at Atmospheric Pressure Mass Spectrometry.* J. Am. Soc. Mass Spectrom., 2013. **24**(3): p. 341-347.

164. Wright, J.P., Heywood, M.S., Thurston, G.K., and Farnsworth, P.B., *The Effects of Added Hydrogen on a Helium Atmospheric-Pressure Plasma Jet Ambient Desorption/Ionization Source.* J. Am. Soc. Mass Spectrom., 2013. **24**(3): p. 335-340.

165. Chan, M.N., Nah, T., and Wilson, K.R., *Real time in situ chemical characterization of sub-micron organic aerosols using Direct Analysis in Real Time mass spectrometry (DART-MS): the effect of aerosol size and volatility.* Analyst, 2013. **138**(13): p. 3749-3757.

166. Nah, T., Chan, M., Leone, S.R., and Wilson, K.R., *Real Time in Situ Chemical Characterization of Submicrometer Organic Particles Using Direct Analysis in Real Time-Mass Spectrometry.* Anal. Chem., 2013. **85**(4): p. 2087-2095.

167. Bruns, E.A., Greaves, J., and Finlayson-Pitts, B.J., *Measurement of Vapor Pressures and Heats of Sublimation of Dicarboxylic Acids Using Atmospheric Solids Analysis Probe Mass Spectrometry.* J. Phys. Chem. A, 2012. **116**(24): p. 5900-5909.

168. Salter, T.L., Gilmore, I.S., Bowfield, A., Olabanji, O.T., and Bradley, J.W., *Ambient Surface Mass Spectrometry Using Plasma-Assisted Desorption Ionization: Effects and Optimization of Analytical Parameters for Signal Intensities of Molecules and Polymers.* Anal. Chem., 2013. **85**(3): p. 1675-1682.

169.   Atkins, P.W., *Physical Chemistry*. 6 ed. 1999, Oxford: Oxford University Press.

170.   Svec, H.J. and Clyde, D.D., *Vapor Pressures of Some a-Amino Acids.* J. Chem. Eng. Data, 1965. **10**(2): p. 151-152.

171.   Wu, C.P., Ifa, D.R., Manicke, N.E., and Cooks, R.G., *Rapid, Direct Analysis of Cholesterol by Charge Labeling in Reactive Desorption Electrospray Ionization.* Anal. Chem., 2009. **81**(18): p. 7618-7624.

172.   Wang, R., Moody, R.P., Koniecki, D., and Zhu, J.P., *Low molecular weight cyclic volatile methylsiloxanes in cosmetic products sold in Canada: Implication for dermal exposure.* Environ. Int., 2009. **35**(6): p. 900-904.

173.   Shen, H.Y., Jiang, H.L., Mao, H.L., Pan, G., Zhou, L., and Cao, Y.F., *Simultaneous determination of seven phthallates and four parabens in cosmetic products using HPLC-DAD and GC-MS methods.* J. Sep. Sci., 2007. **30**(1): p. 48-54.

174.   Facino, R.M., Carini, M., Aldini, G., Marinello, C., Traldi, P., and Seraglia, R., *Analaysis of cosmetic products by gas chromatography mass spectrometry and fast-atom bombardment mass spectrometry: When a combined approach is successful.* Rapid Communications in Mass Spectrometry, 1997. **11**(12): p. 1329-1334.

175.   Cotte-Rodriguez, I., Mulligan, C.C., and Cooks, G., *Non-proximate detection of small and large molecules by desorption electrospray ionization and desorption atmospheric pressure chemical ionization mass spectrometry: Instrumentation and applications in forensics, chemistry, and biology.* Anal. Chem., 2007. **79**(18): p. 7069-7077.

176.   Martinez-Lozano, P. and de la Mora, J.F., *On-line Detection of Human Skin Vapors.* J. Am. Soc. Mass Spectrom., 2009. **20**(6): p. 1060-1063.

177.   Chen, H.W. and Zenobi, R., *Neutral desorption sampling of biological surfaces for rapid chemical characterization by extractive electrospray ionization mass spectrometry.* Nat. Protoc., 2008. **3**(9): p. 1467-1475.

178.   Chen, H.W., Hu, B., Hu, Y., Huan, Y.F., Zhou, Z.Q., and Qiao, X.F., *Neutral Desorption Using a Sealed Enclosure to Sample Explosives on Human Skin for Rapid Detection by EESI-MS.* J. Am. Soc. Mass Spectrom., 2009. **20**(4): p. 719-722.

179.   Teichmann, A., Jacobi, U., Waibler, E., Sterry, W., and Lademann, J., *An in vivo model to evaluate the efficacy of barrier creams on the level of skin penetration of chemicals.* Contact Dermatitis, 2006. **54**(1): p. 5-13.

180. Rieger, T., Teichmann, A., Richter, H., Schanzer, S., Sterry, W., and Lademann, J., *Evaluation of barrier creams - introduction and comparison of 3 in vivo methods.* Contact Dermatitis, 2007. **56**(6): p. 347-354.

181. Pershing, L.K., Bakhtian, S., Poncelet, C.E., Corlett, J.L., and Shah, V.P., *Comparison of skin stripping, in vitro release, and skin blanching response methods to measure dose response and similarity of triamcinolone acetonide cream strengths from two manufactured sources.* J. Pharm. Sci., 2002. **91**(5): p. 1312-1323.

182. Nohynek, G.J., Antignac, E., Re, T., and Toutain, H., *Safety assessment of personal care products/cosmetics and their ingredients.* Toxicol. Appl. Pharmacol., 2010. **243**(2): p. 239-259.

183. Schlosser, A. and Volkmer-Engert, R., *Volatile polydimethylcyclosiloxanes in the ambient laboratory air identified as source of extreme background signals in nanoelectrospray mass spectrometry.* Journal of Mass Spectrometry, 2003. **38**(5): p. 523-525.

184. Horii, Y. and Kannan, K., *Survey of organosilicone compounds, including cyclic and linear siloxanes, in personal-care and household products.* Arch. Environ. Contam. Toxicol., 2008. **55**(4): p. 701-710.

185. Xing, Z., Wang, J.A., Han, G.J., Kuermaiti, B., Zhang, S.C., and Zhang, X.R., *Depth Profiling of Nanometer Coatings by Low Temperature Plasma Probe Combined with Inductively Coupled Plasma Mass Spectrometry.* Analytical Chemistry, 2010. **82**(13): p. 5872-5877.

186. Green, F.M., Gilmore, I.S., and Seah, M.P., *Mass Spectrometry and Informatics: Distribution of Molecules in the PubChem Database and General Requirements for Mass Accuracy in Surface Analysis.* Analytical Chemistry, 2011. **83**(9): p. 3239-3243.

187. Kind, T. and Fiehn, O., *Metabolomic database annotations via query of elemental compositions: Mass accuracy is insufficient even at less than 1 ppm.* BMC Bioinformatics, 2006. **7**: p. 234.

188. PubChem, N.I.o.H. https://pubchem.ncbi.nlm.nih.gov/ 2011.